1996

An experimental study of particle cracking in metal-matrix composites.

Bingjie Wang
University of Alabama at Birmingham

AN EXPERIMENTAL STUDY OF PARTICLE CRACKING IN METAL MATRIX COMPOSITES

by

BINGJIE WANG

A DISSERTATION

Submitted in partial fulfillment of the requirements for the degree of Doctor of Philosophy in the Department of Materials Science and Engineering in the Graduate School, The University of Alabama at Birmingham

BIRMINGHAM, ALABAMA

1996

UMI Number: 9700031

ABSTRACT OF DISSERTATION
GRADUATE SCHOOL, UNIVERSITY OF ALABAMA AT BIRMINGHAM

Degree Doctor of Philosophy Major Subject Materials Engineering

Name of Candidate Bingjie Wang

Title An Experimental Study of Particle Cracking in Metal Matrix Composites

Particle cracking is one of the key elements in the fracture process of particulate-reinforced metal-matrix composites (MMCs). The first two sections of this dissertation focus on the investigation of the effects of matrix properties and reinforcement size on SiC particle cracking behavior during tensile deformation in Al- and Cu-based MMCs. The third section of this research studied the sputter coating of ceramic reinforcement particles and the effect of this Cu coating on interfacial bonding.

The influence of matrix properties and reinforcement size on particle cracking was examined in aluminum and copper matrix composites reinforced with 9 vol pct of either 23, 63, or 142 μm SiC particulate. Two fracture features, new surface area created by particle cracking (S_V) and the number fraction of cracked particles (F_{No}), were quantitatively measured in the sample interior and were found to be approximately linear as a function of strain. The number fraction of cracked particles was affected by particle size and matrix yield strength for both matrix systems. The composites reinforced with large particles or with high matrix yield strength exhibited a higher percentage of cracked particles. The slope of S_V was not significantly affected by particle size but was strongly dependent on matrix yield strength for both matrix systems and increases approximately linearly with yield strength. A comparison of the results from two matrix systems indicates that particles crack during elastic deformation and that the matrix Young's modulus affect the particle cracking behavior. The higher the matrix Young's modulus, the fewer the cracked particles (both S_V and F_{No}) for a given stress and particle size. These results suggest that matrix Young's modulus may have a significant effect on particle fracture in the case of low plastic deformations.

Coatings applied to the reinforcement phase will change the composition near the interface and may yield the desired interface properties. A technique for uniformly sputter coating ceramic reinforcement particles was developed and used to coat large SiC particles with copper. Although the copper coating did not significantly improve the interfacial bonding in copper matrix composites, the success in coating reinforcement particles suggests that this approach may be useful in other composite systems.

Abstract Approved by: **Committee Chairman** ____________________

Program Director ____________________

Date 7/1/96 ____ **Dean of Graduate School** ____________________

ACKNOWLEDGEMENTS

My sincere gratitude is extended to Dr. Gregg M. Janowski, my advisor, for his invaluable guidance, motivation, and, especially, his patience throughout this research.

I also wish to thank my committee for their time and suggestions during this study. The help of my fellow graduate students and staff of the Department of Materials and Mechanical Engineering is greatly appreciated.

The financial support of the Alabama NSF-EPSCoR Composites Program is gratefully acknowledged.

Finally, I would like to thank my husband and my son for their love, patience, and support. I would also like to express my deepest gratitude to my parents and the rest of my family for their continued love and encouragement.

TABLE OF CONTENTS

TABLE OF CONTENTS (Continued)

LIST OF TABLES

LIST OF FIGURES

Figure | Page

GENERAL EXPERIMENTAL PROCEDURE

SiC PARTICLE CRACKING IN POWDER METALLURGY PROCESSED ALUMINUM MATRIX COMPOSITE MATERIALS

THE EFFECTS OF MATRIX PROPERTIES ON REINFORCEMENT FRACTURE IN MMCS

LIST OF FIGURES (Continued)

LIST OF FIGURES (Continued)

LIST OF FIGURES (Continued)

GENERAL INTRODUCTION

Metal matrix composites (MMCs) can combine the toughness of metals with the strength and stiffness of ceramic reinforcements. Their superior mechanical properties (such as high specific modulus, high specific yield strength, and good wear resistance) at room temperature and elevated temperature have led to limited commercial application. For example, the combustion bowl edges of diesel pistons have been made from SiC whisker-reinforced Al-Si alloys, and engine and gear box parts in a racing car have been made from SiC particle-reinforced Al-Cu alloys.[1]

The development of metal matrix composites has been largely driven by the need for new structural and functional materials in the aerospace and, increasingly, automotive industries. Early work was primarily focused on continuous fiber reinforced composites. However, the cost of continuous fibers, complex fabrication procedures, and non-isotropic properties restricted the commercial applications of these composites. This led to the development of discontinuously-reinforced composites, in which reinforcements can be short fibers, whiskers, or particulate. The cost of whiskers is much less than continuous fibers, and the cost of particulate is even less. Discontinuously-reinforced composites can be fabricated using conventional techniques such as powder metallurgy and casting, with or without secondary processing such as extrusion and rolling. Finally, discontinuously reinforced composites exhibit relatively isotropic mechanical properties compared to continuously-reinforced composites and significantly improved mechanical properties compared to the unreinforced matrix. Cost is a particularly critical factor in utilizing these materials in the automotive industry.

The most common discontinuous MMC has been SiC-reinforced aluminum. Aluminum alloys have been chosen as the matrix due to their low density, wide range in alloys, heat treatment capability, and processing flexibility. SiC has been chosen as the reinforcement because of its chemical compatibility with aluminum, good wettability, generally good bonding with aluminum, and low cost.[1,2]

One of the technical challenges in utilizing discontinuously-reinforced composites, including SiC/Al, is their tendency to possess low ductility and fracture toughness, which may offset the gains in modulus and strength. Thus, it is necessary to better understand the deformation and fracture behavior of MMCs in order to improve their properties and to place them in wider use.

LITERATURE REVIEW

The fracture behavior of SiC-reinforced aluminum matrix composites has been widely investigated.[3-24] Since reinforcement size, reinforcement morphology, reinforcement volume fraction, matrix composition, and composite processing have been varied in these investigations, it is difficult to unambiguously describe the failure mechanisms in SiC-reinforced aluminum matrix composites. However, the ductile failure process is active in these MMCs.[7,8,12-16,24-29] It is, therefore, necessary to determine how the addition of SiC particles affects ductile failure and how microstructural factors (reinforcement size, shape, distribution, and morphology) and "mechanical" factors (matrix strength, interface bonding, *etc.*) influence this process.

Unreinforced aluminum alloys typically fail by the ductile rupture mechanism, which consists of void nucleation, void growth, and void link-up (coalescence). The factors that control this process in unreinforced Al alloys are the number and size of constituent (intermetallic) phases and the alloy flow stress. When large constituent phases are present, they serve as sites for void nucleation, which causes premature failure and, therefore, are deleterious to toughness and ductility. Thus, large constituent phases should be avoided, especially in high strength alloys. An effective method to control constituent phases is improving alloy cleanliness. For example, alloy 7475 and alloy 7075 have the same general chemistry, differing only in iron and silicon content, which are undesirable in these aluminum alloys. As a result, even though the strength is similar, alloy 7475 has enhanced toughness and fatigue resistance due to reduced Fe and Si levels.[30]

The addition of relatively high volume fractions (> 10%) of large (>20 μm), brittle SiC particles would be expected to significantly reduce the ductility and toughness of the matrix material. Studies have shown that the fracture toughness of SiC reinforced aluminum composites are in the range of 7 to 25 $MPa \cdot m^{1/2}$, compared to values of 25 to 75 $MPa \cdot m^{1/2}$ for unreinforced aluminum matrix alloys.[31] The overall tensile elongation of composites was usually less than 10%, with typical values being about 2% for peak-aged composite materials.[3-6] Elongations of unreinforced aluminum alloys after similar heat treatments were about 10% to 20%.[32]

In spite of the low macroscopic ductility exhibited in composite materials, fractography shows that the fracture surfaces have a dimpled morphology, which is an important characteristic of ductile failure. Two sizes of dimples are typically observed.[7,8,12-16,24-29] The large dimples were similar in size and shape to their associated reinforcement particles. Smaller dimples (between the reinforcement particles), which were nucleated by dispersoids, inclusions, oxides, and very fine SiC particles, were similar to dimples formed in the unreinforced materials.[33]

The ductile rupture process of the composites and unreinforced matrices differ in several ways. First, cracking and/or debonding of SiC particles was added to cracking and/or debonding of constituent phases as sites for void nucleation. Secondly, the void growth and coalescence processes were short circuited by the further nucleation of voids associated with cracked and/or debonded reinforcement particles,[4,12,14,34] which is a major reason for low ductility in composites. It is apparent that the ductility could be improved if rapid crack growth was inhibited by decreasing the nucleation of voids at or near cracked particles and slowing the void growth and coalescence process in the matrix.

Studies have shown that MMC ductility was significantly improved by using a superimposed hydrostatic pressure during the tensile testing.[5,9,12,18] It was initially thought that superimposed hydrostatic pressure significantly inhibited the void growth and coalescence since the void nucleation associated with SiC cracking was unlikely to have been prevented at the levels of pressure that were employed.[18] However, further quantitative investigation indicated that the number of fractured particles decreased due to the superimposed hydrostatic pressure with a concomitant increase in tensile ductility.[5,35]

Factors Affecting Active Failure Mechanisms in Composites

The incorporation of SiC reinforcement into aluminum alloys introduces several more possible elements into the rupture process, most of which specifically affect void nucleation. These factors include reinforcement cracking, reinforcement/matrix interface debonding, and reinforcement cluster failure. The dominant factor will vary with microstructural parameters such as reinforcement distribution, size, morphology, volume fraction, and matrix microstructure; reinforcement distribution and matrix microstructure are strongly influenced by processing. Other parameters include interfacial bond strength and the relative sizes of the reinforcement and constituent phase(s). These parameters will be addressed below.

(1) The fracture behavior is sensitive to the reinforcement distribution, which is largely determined during the primary processing stage but can be modified somewhat by secondary processing. It is not surprising that areas of clustered reinforcement are preferential regions to initiate fracture since particle/particle bonding is weak or totally absent, and the matrix within the clusters is in a high level of triaxial stress due to the constraint of the surrounding particles. This issue has been examined in detail by Hunt *et al.* and Lewandowski *et al.*[3,9,13,18] A study of a 7000 series alloy reinforced with 20 vol.% of 16 μm SiC particulate, fabricated by P/M (hot pressing) followed by extrusion, revealed that clustered areas were preferred sites for fracture initiation.[13] The ductility of 6061 reinforced with 10 and 20 vol.% < 10 μm SiC particles, fabricated by molten metal mixing followed by extrusion, was mainly limited by damage initiation within the clusters in form of particle cracking and/or decohesion of the matrix between the particles.[3] Other work [19] on 6061 reinforced with 15 vol.% SiC whiskers, fabricated by squeeze infiltration, found a similar result by using *in situ* SEM, a technique of dynamic fracture observation.

Improved fabrication as well as secondary processing can achieve a more uniformed reinforcement distribution and, therefore, a better ductility of the composite. Particle clustering can largely be overcome by the proper selection of matrix particle size in P/M processed materials.[32] During casting, particle distribution can be improved by proper control of wetting and buoyancy effects as well as by high solidification rates.[36] Secondary processing such as extrusion can modify the particle distribution by separating the clusters and also can change the particle size distribution by cracking the particles.[13] Particle or whisker alignment also results from deformation of the composite.

(2) Particle size and aspect ratio affect the probability of particle cracking. Studies have shown that SiC particle fracture has most often been observed in the large particles as well as those with the longest reinforcement direction parallel to the loading direction, whereas composites reinforced with small particles were more likely to fail in the matrix.[3-5,7-10,26-28,34] The greater likelihood of cracking the larger particles has been attributed to the increased probability of finding a critical-sized defect.[37] The effect of the aspect ratio is due to load transfer from the matrix being more efficient for high aspect ratio particles.[38] Flom and Arsenault [7] found that a particle size of 20 μm was the transition between matrix failure and particle cracking in a P/M processed 1100 aluminum matrix composite. Llorca [4,34] found that the transition particle size was 5 μm for a spray

codeposited 2618 aluminum matrix composite. These results suggest that the transition particle size between matrix failure and particle cracking mechanisms depends upon the particle characteristics, particle distribution, matrix strength, and, possibly, composite processing.

(3) Intermetallic particle cracking can be a dominant failure mechanism when the intermetallic particles are larger and weaker than the SiC particles. The relative sizes of reinforcement and intermetallic particles depend upon the size of reinforcement that was used, the matrix composition, and the composite processing.

It is well known that proper microstructural control can improve the combination of strength and toughness. For example, rapid solidification has been successful in refining the constituent phases in aluminum alloys. However, these benefits are lost if consolidation is carried out above the solidus temperature since large intermetallic phases form. This effect is particularly pronounced in composite materials reinforced with whiskers or small particles in which the reinforcements are smaller than the intermetallic phases. An investigation of 2124 reinforced with 15 vol.% of SiC whiskers using *in-situ* SEM provided detailed information on fracture initiation and propagation process.[15] The observations indicated that voids initiated at cracked coarse Mn-containing intermetallic particles. Growth and coalescence of the voids led to failure. In addition, the fracture of intermetallic particles caused local stress concentrations, which affected neighboring reinforcements and led to either whisker cracking or interface debonding. Other investigators demonstrated similar results.[7,14,21,39] It should be noted that there is one thing in common in these studies: the composite material was SiC whiskers or fine SiC particles in a 2124 matrix. In this alloy, the coarse Mn-containing intermetallic particles are formed during processing; SiC whiskers or fine SiC particles are small compared to the coarse intermetallic particles. Therefore, matrix failure by nucleation and growth of voids due to coarse particle cracking is, not surprisingly, a dominant failure mechanism in these composites.

Age-hardening precipitates can also affect the fracture process of a composite material. A 7000 series alloy reinforced with 20 vol.% of 16 μm SiC particulate in under-aged (UA) and over-aged (OA) conditions with equivalent strengths has been studied in detail.[12,13] The UA materials exhibited SiC particle fracture and matrix failure, while OA materials exhibited near-interface and matrix failure. It was believed that the precipitates in OA materials either directly weakened the interfacial bonding or depleted solute near the interface, thereby leading to weaker regions adjacent to the particle.[12] Work on a 6061 matrix composite showed a similar result.[19] However, 2124 reinforced with 20 vol.% of SiC particles did not exhibit a heat treatment effect on the fracture micromechanism.[14] These seemingly contradictory results are likely due to differences in matrix composition and, therefore, the microstructural evolution of the alloys.

(4) Reinforcement morphology also plays a role in composite fracture since it influences the level and state of matrix stress. Due to the different thermal expansion coefficients of the reinforcement and matrix, the residual stress state of the matrix is a combination of tension and compression, but the average stress is tensile.[40] As a composite is deformed, the reinforcement raises the stress level in the matrix around particles due to the generation of geometrically necessary dislocations, which maintain continuity at the interface. If the reinforcement has sharp corners, the stress levels in matrix will be significantly higher than if the reinforcements are rounded. The irregular, sharp corners of the reinforcement are severe stress concentrations, thereby causing intense localized plastic flow even at low macroscopic stresses. This process can lead to premature damage in the form of void initiation at corners or at whisker ends, which are normal to the loading direction.[14,15,21]

From the above review, the mechanisms of SiC/Al composite failure can be loosely divided into reinforcement failure and matrix failure. The category of reinforcement failure can be further divided based upon the microstructural element which leads to fracture:

(1) A strong reinforcement/matrix interface is present, and load can be transferred to the reinforcement without interface decohesion occurring. If the stress applied on the reinforcement exceeds the failure stress of the reinforcement,

the reinforcement cracks and acts as a failure initiation site.

(2) The matrix is highly stressed and particles are weakly bonded within the clustered areas. Clustering results in very large voids forming at low strains.

(3) A weak reinforcement/matrix interface exists due to interfacial oxide particles, intermetallic particles, poor bonding, and/or age hardening precipitates. Interface debonding can act as a void initiation site.

The category of matrix failure can also be further divided:

(1) If coarse, brittle intermetallic particles exist in the composite, void initiation will favor intermetallic particle cracking. The voids associated with cracked intermetallic particles grow, coalesce, and the composite eventually fractures.

(2) The sharp corners of reinforcement and whisker ends are sites of severe stress concentration, which leads to void initiation at corners or at whisker ends.

Although all of these failure mechanisms may coexist, particle cracking is the dominant failure mechanism in many commercial SiC particle reinforced aluminum matrix composites. In these materials, a strong particle/matrix interface bond exists, coarse intermetallic particles are smaller than the SiC particles, and a homogeneous particle distribution is present.The importance of reinforcement fracture on mechanical properties such as modulus, work hardening rate, and flow stress has also been examined recently.[3-5,9,10,22,41-46]

PRESENT STUDY

Few systematic studies on the quantitative link between microstructural fracture features and MMC deformation and fracture behavior have been reported in the literature, [3-5,24] despite the important implications on mechanical properties. Unfortunately, it has been shown that these results are not strictly valid due to the measurements being carried out on the surface of a specimen, which is under plane stress and does not represent the interior plane strain condition of specimens.[47] Thus, the present study will yield quantitatively correct results by measuring the cracked particles on the interior of the specimen.

The objective of the present work is to quantitatively investigate particle cracking behavior during deformation and failure in SiC particle reinforced Al-based and Cu-based composites. In this study, composite materials were fabricated using P/M without secondary processing. An effective method of measuring local tensile strain has been developed. The effects of matrix Young's modulus, matrix yield strength, and particle size on particle cracking behavior have been examined. This systematic, quantitative study of particle cracking in MMCs is an important step in better understanding MMC deformation and failure. The results of this study can then be applied to composite material design and processing in order to minimize the deleterious effects of reinforcement fracture on ductility, fatigue, and fracture toughness.

Materials

Matrix materials used in this study are aluminum alloy 201 (the main system of study) and copper alloys (a model system). The aluminum alloy was alloy 201 (Al-4.4 wt.% Cu-0.5 wt.% Mg-0.8 wt.% Si), which is approximately equivalent to the cast and wrought alloy 2014. Alloy 201 is a high strength, age hardenable alloy. Copper alloys with compositions Cu-7 wt.% Al-2 wt.% Mg-2 wt.%Si (Cu7) and Cu-8 wt.% Al-2 wt.% Mg-2 wt.%Si (Cu8) were developed for this study to achieve strong bonding with SiC particles and as-sintered high density. The properties of alloy 201 and the copper alloys are list in Table I.

Table I: The Mechanical Properties of Matrix Alloys

Materials		σ_y(MPa)	E (GPa)
Alloy 201	Solutionized	125	72.4* [48]
	1 hr. Aged	193	
	14 Hr. Aged	299	
Copper	Cu7	203	105** [49]
	Cu8	269	

* This value is from tensile elastic modulus of alloy 2014.
** This value is from tensile elastic modulus of C95600.

Copper alloys are ideal matrix alloys to investigate the effects of matrix properties (such as Young's modulus and a broader range of yield strength) on the fracture process in MMCs. Not only do copper alloys have a significantly higherYoung's modulus (approximate 105 GPa) than do aluminum alloys (approximate 70 GPa), but they can also be fabricated by P/M. The yield strength and, to some extent, the ultimate tensile strength of copper alloys can be varied either by changing the alloy composition or by thermal treatment. From an application point of view, there is also interest in the development of copper-based alloys with high strength and high conductivity for applications in electronic and thermal systems.[50-53] Copper is attractive in its high electrical and thermal conductivity. It has excellent resistance to corrosion and is highly ductile. However, copper has fairly low strength and high density. These disadvantages can be overcome by either dispersion of the oxide particles or addition of ceramic or carbon reinforcements in the copper matrix. Carbon reinforcements were used in early copper matrix composites due to their high thermal conductivity, whereas the ceramic reinforcements become more attractive due to their high oxidation resistance. A particularly attractive ceramic reinforcement is silicon carbide, which is also widely used in aluminum matrix composites as a reinforcement.

Processing

In this study, matrix alloys and 9 vol.% of 23 μm, 63 μm, or 142 μm SiC particulate reinforced metal matrix composite materials were fabricated by P/M methods, which include powder mixing, cold compacting, and sintering. P/M processing is one of the main composite manufacturing and offers the greatest flexibility in terms of the size, volume fraction, and type of matrix and reinforcement which may be used. The particle distribution is more easily controlled during the P/M processing than during casting. The reason is that the particle distribution in the matrix is influenced by particle distribution in the powder mixture and matrix powder size in P/M,[32] whereas it is influenced by particle distribution in the melt and solidification dynamics during casting.[36] Secondary processing (such as hot isostatic pressing, hot rolling, and extruding) were not utilized, which avoided particle alignment and minimized SiC particle cracking during the processing.

Measurements

Quantitative evaluation of particle cracking behavior during the composite deformation and fracture process has been undertaken. One of the microstructural fracture features, new surface area created by particle cracking per unit volume, employed in this research is a global parameter. It is independent of particle size and, therefore, makes comparisons of data from composites with different particle sizes meaningful. Another microstructural parameter, number frequency of cracked particles, is also employed, which is dependent on particle size. This parameter can show not only total frequency of cracked particles but also the frequencies of different numbers of cracks in a single particle. Also, crack frequency was used in prior work,[3-5,11] which allows the results of the present study to be compared with previous results.

GENERAL EXPERIMENTAL PROCEDURE

MATRIX ALLOY SELECTION AND DEVELOPMENT

The aluminum alloy used in this study was the commercial alloy 201 (Al-4.4 wt.% Cu-0.5 wt.% Mg-0.8 wt.% Si), which is approximately equivalent to the composition of the cast and wrought alloy 2014. Alloy 201 is a high strength, age hardenable alloy. Thus, a variety of alloy yield strengths can be achieved by solutionizing followed with different aging times and temperatures. In addition, most commercial aluminum particulate composites are based on precipitation hardening matrices such as 2xxx series and 6xxx series alloys, which make comparisons possible. It was shown that reinforcement/matrix interface in SiC-reinforced aluminum matrix composites fabricated as in this study was strong.[7,23]

Copper-based alloys and procedures used in this study were developed to give strong bonding with SiC particles and high density (>95% theoretical density). Preliminary results showed that SiC-reinforced copper without additives produced by solid state sintering did not achieve strong interfacial bonding. Liquid phase sintering was considered because of faster sintering, and, more importantly, it was hypothesized that interaction between liquid metal and reinforcement would lead to improvement in wetting and, therefore, interfacial bonding.

The considerations for additives included that (1) they are soluble in copper; (2) they have low melting point or produce low melting point alloys with copper or other alloying elements; (3) they change surface energy of the liquid or form reaction products, which improve SiC wetting. Al, Si, and Mg were chosen as additives. Al, Mg are low melting point elements (compared to Cu). Al-Cu, Mg-Cu, Al-Mg, and Al-Si will form low melting point eutectics below the sintering temperature. In addition, it is well documented that Mg improves wetting between liquid Al alloy and ceramic reinforcements (such as SiC and Al_2O_3) by forming MgO and $MgAl_2O_4$ at the interface.[23,54-56]

The cast alloy C95600 (Cu-2 wt.% Si-7 wt.% Al) combined with Mg was the initial alloy choice. The amount of magnesium was determined based upon the solubility of magnesium in copper and, eventually, the resulting interfacial bonding. The fracture surfaces showed that many SiC particles cracked and few particles debonded, which is evidence of strong interfacial bonding, when matrix is Cu-7 wt.% Al-2 wt.% Mg-2 wt.%Si. The amount of aluminum was found to directly affect matrix yield strength and ductility. The matrix yield strength increases and ductility decreases as the amount of aluminum increases. A copper alloy with the composition Cu-8 wt.% Al-2 wt.% Mg-2 wt.%Si was developed to achieve a higher matrix yield strength without sacrificing the interfacial bonding and density. The as-sintered density of copper matrix composites can be approximately 95% of theoretical density.

SPECIMEN PREPARATION

Aluminum Alloy and Aluminum Matrix Composites

The aluminum matrix alloys and aluminum matrix composite materials were fabricated by press and sinter P/M methods. The matrix alloys were prepared by blending elemental Al, Cu, Mg, and Si powders to attain alloy 201 (Al-4.4 wt.% Cu-0.5 wt.% Mg-0.8 wt.% Si). The powders for the aluminum matrix composite materials were produced by blending 9 vol.% of SiC particles (nominally 23 μm, 63 μm, and 142 μm in diameter) with the premixed aluminum matrix powder. The characteristics of the metal and ceramic powders are listed in Table I. The mixed powders were compacted in a standard powder tensile test specimen die with zinc stearate die wall lubricant using a mechanical press and 386 MPa (28 TSI) pressure for the matrix alloy and 441 MPa (32 TSI) for the composites to obtain a green density of 96%-97% of the theoretical values. The specimen configuration was the Metal Powder Industries Federation Standard 10 molded tensile bar.

The sintering of aluminum matrix and aluminum matrix composites consists of degassing followed by sintering. The specimens were degassed at 400 °C ± 3 °C for 30 minutes under a low vacuum (between 1 and 10^{-1} Pa (10^{-2} and 10^{-3} torr)). The degassing removed the die wall lubricant as well as allowed the absorbed moisture and trapped gas to escape. Sintering was at 600 °C ± 3 °C for 1 hour in a high purity argon or nitrogen atmosphere. The degassing and sintering were carried out in a tube furnace, which was evacuated and heated up after loading a basket (which contained the specimens) and replacing the endcap. The heating rate was 5 °C per minute from room temperature to 400 °C. After the degassing was completed, the furnace setpoint was stepped to the sintering temperature. At this time, the vacuum pump was turned off, and the tube was back-filled with gas. The samples were removed from the

Table II: Characteristics of Powders Used For Aluminum Matrix and Aluminum Matrix Composites

Aluminum ALCAN grade MD 101	100% -100 mesh (less than 150 µm) particle size 80% -325 mesh (less than 45 µm) particle size purity 99.3%
Copper ALCAN	-635 mesh (less than 20 µm) particle size purity 99.57%
Magnesium Johnson Matthey Electronics	-325 mesh (less than 45 µm) particle size 99.8% Mg for metallic elements
Silicon Johnson Matthey Electronics	-325 mesh (less than 45 µm) particle size 99.5% Si for metallic elements
Silicon Carbide Leco Corp.	400 grit (mean size 23 µm) 240 grit (mean size 63 µm) 120 grit (mean size 142 µm)

furnace hot zone after sintering and cooled in a N_2 or Ar atmosphere until their temperature was less than 200 °C. The actual furnace temperature was determined by monitoring an internal thermocouple immediately above the samples (and inside the tube).

The aluminum matrix composite materials had greater than 97% of their theoretical density. The density of the specimens was determined by the water immersion method. The SiC particles were well dispersed and randomly oriented in the matrix.

Copper Alloy and Copper Matrix Composites

The copper matrix alloys and copper matrix composite materials were also fabricated by P/M methods. The matrix alloys were prepared by blending elemental Cu (50% NA-FFL and 50% NA-SSM), Al, Mg, and Si powders to attain the composition Cu-7 wt.% Al-2 wt.% Mg-2 wt.% Si and by blending elemental Cu (100% NA-FFL), Al, Mg, and Si powders to attain the composition Cu-8 wt.% Al-2 wt.% Mg-2 wt.% Si. The powders for the copper matrix composite materials were produced by blending 9 vol.% of SiC particles (nominally 23 µm, 63 µm, and 142 µm in diameter) with the premixed copper matrix powder. The characteristics of the metal powders and ceramic powders are listed in Table II. The mixed powders were then cold compacted in a standard powder tensile test specimen die with zinc stearate die wall lubricant using a mechanical press and 524 MPa (38 TSI) for the copper matrix alloy and 552 MPa (40 TSI) for the composites to obtain green densities that were

Table III: Characteristics of Powders Used for Copper Matrix and Copper Matrix Composites

Aluminum ALCAN grade MD 101	-400 mesh (less than 38 µm) particle size purity 99.3%
Copper Norddeutsche Affinerie NA-FFL	≥90% -40 µm particle size ≤10% +40 µm particle size purity ≥99.7%
NA-SSM	37-43% -40 µm particle size 29-37% +40 µm particle size 23-29% +80 µm particle size purity ≥99.8%
Magnesium Johnson Matthey Electronics	-400 mesh (less than 38 µm) particle size 99.8% Mg for metallic elements
Silicon Johnson Matthey Electronics	-325 mesh (less than 45 µm) particle size 99.5% Si for metallic elements
Silicon Carbide Leco Corp.:	400 grit (mean size 23 µm) 240 grit (mean size 63 µm) 400 grit (mean size 142 µm)

92% of their theoretical values. The specimen configuration was the Metal Powder Industries Federation Standard 10 molded tensile bar.

The copper matrix and copper matrix composites were sintered at 800 °C ± 3 °C for 1 hour under high vacuum (between 10^{-2} and 10^{-4} Pa (10^{-4} and 10^{-6} torr)). A basket (which contained the specimens) was placed in a tube furnace before the heating. The furnace was heated using a heating rate of 8 °C per minute after the vacuum of the furnace reached 7×10^{-3} Pa (5×10^{-5} torr). After holding for 1 hour at the sintering temperature, the furnace was cooled using a rate of 8 °C per minute. The samples were cooled under the vacuum until their temperature was less than 100 °C. The actual furnace temperature was determined by monitoring an internal thermocouple immediately above the samples (and inside the tube).

The copper matrix composite materials were about 95% of their theoretical density. The density of the specimens was determined by the water immersion method. The SiC particles were well dispersed and randomly oriented in the matrix.

HEAT TREATMENT

The aluminum alloy and aluminum matrix composite specimens were solutionized and aged in air after sintering. The solutionizing treatment was at 510 °C ± 3 °C for 45 minutes, followed by a cold water quench. The aging treatments were at 160 °C ± 3 °C for 1 hour (under-aged) and 14 hours (peak-aged) immediately following the solutionizing treatment.

STRAIN MEASUREMENT

The tensile specimens were ground with 240 grit SiC paper to remove the surface oxides. Microhardness indentations, nominally 0.5 mm apart, were made in the central portion of the tensile bar parallel to the tensile axis along the entire gage length (Figure 1) using a Vickers Hardness Tester and a load of 200 g. The distance between the indentations was

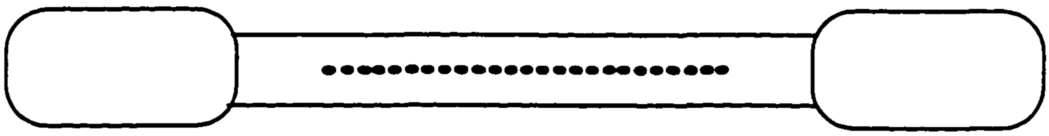

Fig. 1-A sketch of tensile test specimen and microhardness indentations, which are nominally 0.5 mm apart over the entire gage length.

measured twice (with less than 1% relative measuring error) both before and after tensile testing using a Zeiss Image Analysis System and an optical microscope with a magnification of 100. The average distance values, $\bar{X}_{after}$ and $\bar{X}_{before}$, were used to determine the local plastic tensile strain over the 0.5 mm interval along tensile axis. The axial engineering strains, which are same on the surface and in the sample interior, were calculated using the equation:

$$e = \frac{\bar{X}_{after} - \bar{X}_{before}}{\bar{X}_{before}} \quad [1]$$

There are other strains on the specimen surface that are not a cause of particle cracking in the sample interior. Therefore, these strains were not measured in this study.

TENSILE TESTING

Uniaxial tensile tests were carried out using a servo-hydraulic testing machine and an initial strain rate of 3×10^{-4}/s. The 0.1% offset yield strength, ultimate tensile strength, and elongation-to-failure were calculated from load versus time plots.

OPTICAL AND SCANNING ELECTRON MICROSCOPY SAMPLE PREPARATION

The fractured aluminum matrix composite and copper matrix composite specimens were sectioned longitudinally using a low speed saw, mounted, and ground sequentially with 240, 320, 400, and 600 grit SiC paper using Leco AP60 auto grinder/polisher with low downward applied pressure (≈0 lbs force on meter). Polishing was done using 15-, 6-, 1-, and 0.1-µm diamond paste on a nylon polishing cloth with low pressure and short times (approximately 5-10 minutes for each step). Final polishing for the aluminum matrix composites used 0.3 μm Al_2O_3 on a Leco Alphagam polishing cloth.

PHASE IDENTIFICATION

SEM/EDS and x-ray diffraction were utilized to characterize the copper matrix. The compositions of the copper matrix after sintering were qualitively analyzed using SEM/EDS. X-ray diffraction was used to identify the constituent phases. The equilibrium phases for alloys of this study, taken from the Cu-Al-Si ternary system [57] at different temperatures, are listed in Table IV. X-ray diffraction patterns were consistent with the predicted phases. The lattice parameter of FCC Cu was determined by linear extrapolation of lattice-constant data versus the Nelson-Riley-Taylor-Sinclair function.

Table IV:Equilibrium Phases of Cu-Al-Si System at Different Temperatures for Alloys of This Study

	400°C	750°C	955°C
Cu-7Al-2Si	Cu + Cu_3Al(β)	Cu + Cu_5Si(κ)	Cu_3Al(β)
Cu-8Al-2Si	Cu_3Al(β)	Cu + Cu_5Si(κ) + Al_4Cu_9(γ)	Cu_3Al(β)

MEASUREMENT OF NEW SURFACE AREA CREATED BY PARTICLE CRACK PER VOLUME S_V

The new surface area created by particle cracking per unit volume, S_V, was determined as a function of position along the tensile axis of the longitudinal section of the specimens after tensile testing using an optical microscope.

This method eliminates questions regarding differences in cracking behavior of particles on the surface versus particles within the bulk.[28, 47] The value of S_V was determined by measuring the number of intersections between test lines and new surfaces of cracked particles per unit length, P_L. The test lines were from a 11 X 11 grid, which was contained within the microscope eyepiece; only the lines parallel to the tensile axis were used as test lines. For cracks of identical orientation, $S_V = P_L/\cos\theta$, where θ is the angle between the test line and crack surface normal. In this case, most particle crack surfaces were found to be normal to the tensile axis, and the test lines were placed normal to the cracked surface (Figure 2). Therefore, θ was equal to 90°, and S_V was equal to P_L.

Different magnifications were employed for the measurement of the three particle sizes in order to minimize the counting errors while using a reasonable number of test line placements to achieve relatively narrow confidence intervals for S_V measurement. At least 20 placements (or fields) were measured for each position (and, therefore, strain) along the gage length. For some specimens, several planes of polish were necessary to obtain the required 20 placements for each position. It should be noted that the test lines were placed at least 1 mm away from the surface for each position (Figure 2), which eliminated the surface effects on particle cracking. In all cases, the same distance along the gage length (0.2 mm) was examined for each position so that

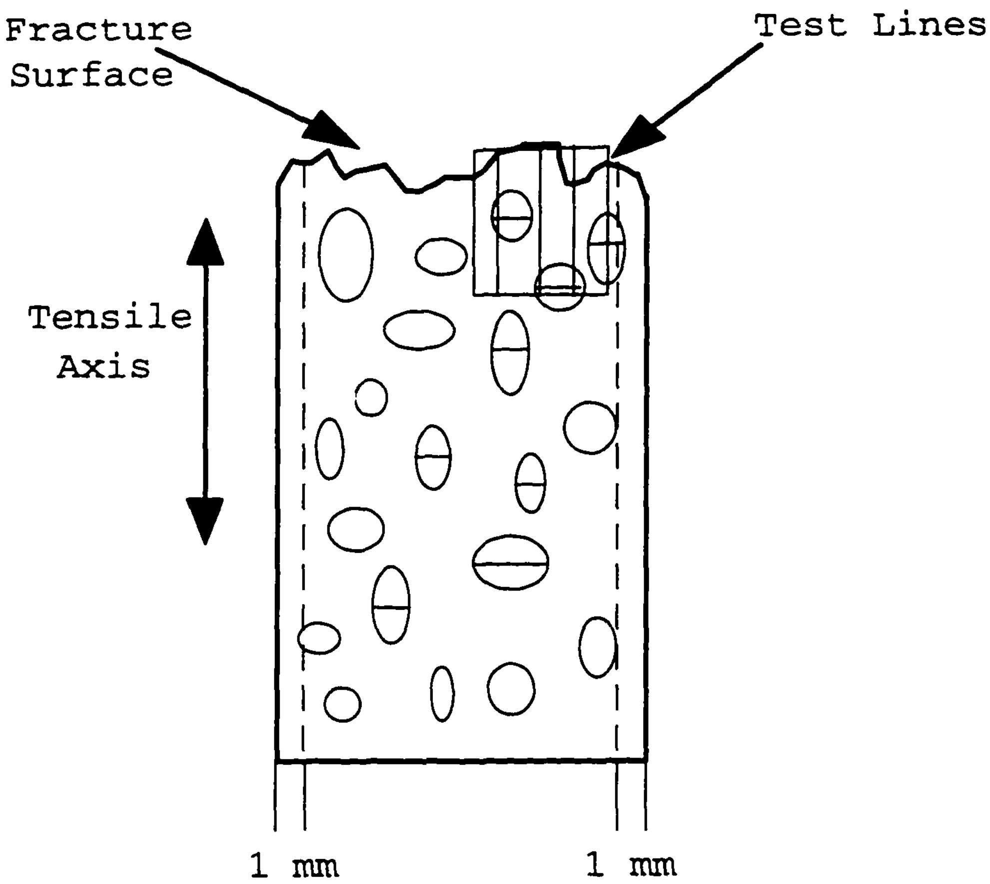

Fig. 2-A sketch of the S_v measurement approach on a tensile test specimen longitudinal section after testing. Test lines were placed at least 1 mm away from surface for each position.

the measured value of S_V was averaged over the same test length range, which assured that measurements were comparable for all three particle sizes.

MEASUREMENT OF NUMBER FREQUENCY OF CRACKED PARTICLES

The number frequency of cracked particles, F_{No}, was determined as a function of position along the tensile axis of the longitudinal section of the specimens after tensile testing using an optical microscope. The test grid was contained within the microscope eyepiece. The value of F_{No} was determined by measuring both the number of cracked particles and the total number of particles in a test field. The ratio of the number of cracked particles to the total number of particles is the value of F_{No}. The number frequency in an area is equal to the number frequency in the volume if the particles have a narrow size distribution.

Different magnifications were employed for different particle size measurements, as in the case of the S_V measurements. The values of F_{No} were obtained at the same positions as S_V measurements. At least 20 placements (or fields) were measured for each position (and, therefore, strain) along the gage length. For some specimens, several planes of polish were necessary to obtain the required 20 placements for each position.

The number frequency of cracked particles was employed instead of the volume frequency of cracked particles, which is the ratio of the number of points on cracked particles to the number of points on all particles in a test grid. The number frequency has the advantage of yielding better counting statistics. However, both measurements show similar results due to relatively narrow size distribution of the SiC particles.

FITTING METHODS

Power law regression was used to fit strain as a function of position. Separate regressions were used for each side of the fracture surface, and the origins were set at the fracture surface. Since S_V and F_{No} are related to local plastic strain and, therefore, position, combined plots of S_V as a function of strain and F_{No} as a function of strain were obtained using the assumption that the fracture surfaces are planar. (This analysis assumes that the outside position, where strain was measured, and the inside position, where S_V and F_{No} were measured, are in correspondence.) This correlation was achieved by measuring S_V and F_{No} and calculating the local strain at those measured positions using the power law regression equation. The calculated strain and the measured S_V and F_{No} were then used to produce plots of S_V as a function of strain and F_{No} as a function of strain. In general, both S_V and F_{No} increase with increasing strain.

A best fit linear regression was used, which was confirmed to be a statistically valid fit by testing the correlation coefficient with a 0.05 level of significance, to fit both S_V and F_{No} as a function of local strain. The 95% confidence intervals of the slopes and y-intersects of these best fit lines were calculated so that envelopes, which indicate error bounds, were obtained. The upper bound lines were calculated using the maximum slopes and intercepts, and the lower bound lines were calculated using the minimum slopes and intercepts. The method outlined in reference [58] was used for this analysis. Best fit lines with their error bounds will be shown in the cases of S_V as a function of strain, and only best fit lines will be shown in the cases of F_{No} as a function of strain.

The uniaxial stress-strain curve of particle reinforced MMC can be described by a Ramberg-Osgood relationship in the form of [59]:

$$\bar{\varepsilon} = \frac{\bar{\sigma}}{\bar{E}} + \alpha\left(\frac{\sigma_0}{E}\right)\left(\frac{\bar{\sigma}}{\bar{\sigma}_N}\right)^{\frac{1}{n}} \qquad [2]$$

and a matrix material can be represented by another Ramberg-Osgood relationship:

$$\varepsilon = \frac{\sigma}{E} + \alpha\left(\frac{\sigma_0}{E}\right)\left(\frac{\sigma}{\sigma_0}\right)^{\frac{1}{n}} \qquad [3]$$

where $\bar{\varepsilon}$ is composite strain, $\bar{\sigma}$ is composite stress, $\bar{E}$ is the composite Young's modulus (which is estimated by Halpin-Tsai equation [2]), α is constant (equal to 3/7), σ_0 is the matrix yield stress, E is the matrix Young's modulus, $\bar{\sigma}_N$ is the asymptotic reference stress of composite, and n is strain-hardening exponent.

The experimental tensile stress-strain curves were fitted using Eq. [2] to extend the stress-strain curve beyond composite fracture. First, the matrix stress-strain curves were fitted using Eq. [3] to obtain n, σ_0, and α. Then, σ_0 and α were directly substituted into Eq. [2]. In order to obtain the most accurate representation of the composite stress-strain curve, n and $\bar{\sigma}_N$ in Eq. [2] were chosen based on n from the matrix fitting and composite yield stress, respectively.

SiC PARTICLE CRACKING IN POWDER METALLURGY PROCESSED ALUMINUM MATRIX COMPOSITE MATERIALS

B. WANG, G.M. JANOWSKI, and B.P. PATTERSON

Metallurgical and Materials Transactions A, volume 26A,

September 1995, pp. 2457

ABSTRACT

Particle cracking is one of the key elements in the fracture process of particulate-reinforced metal-matrix composite materials. The present study quantitatively examined the amount of new surface area created by particle cracking and the number fraction of cracked particles in a series of SiC-reinforced aluminum-matrix composite materials. These composite materials were fabricated by liquid-phase sintering and contained 9 vol.% of 23, 63, or 142 μm SiC. The matrix properties were varied by heat treating to either an under-aged or peak-aged condition. In general, the new surface area created by particle cracking (S_V) and the number fraction of cracked particles (F_{No}) were linearly dependent on the local strain along the tensile specimen. Multiple cracks were frequently observed in the composites containing large particles. It was found that the new surface area created by particle cracking per unit strain was higher for the case of high-strength matrices and was not systematically affected by particle size within the range studied. The number fraction of cracked particles was affected by both particle size and matrix strength. A higher number fraction of particles cracked in the composites reinforced with large particles and with high matrix yield strengths. These results are interpreted in terms of the size of the particle defects, which is a function of particle size, and the critical flaw size necessary to

crack a given particle, which is a function of the stress on the particle. The new surface area created by cracking and the fraction of cracked particles were related and are in good agreement for the large and medium sized particles.

INTRODUCTION

Aluminum matrices reinforced with ceramic particulate additions such as SiC have been of considerable interest for a number of years. In addition to their potential for superior mechanical properties (such as high specific elastic modulus, high specific yield strength, and good wear resistance), this type of metal matrix composite (MMC) material can be produced with relatively isotropic properties using conventional fabrication techniques. However, the addition of ceramic particulate to aluminum alloys can reduce tensile ductility and fracture toughness to unacceptably low levels. This poor damage tolerance can limit the use of these materials in structural applications.

The fracture behavior of a variety of aluminum-matrix, SiC-reinforced composite materials has been studied.[1-21] Due to variations in particle size, particle morphology, particle volume fraction, matrix composition, heat treatment, composite processing, and their combined effects, it is difficult to unambiguously categorize the fracture process in Al/SiC composite materials. However, the presence of SiC reinforcement is typically detrimental to the fracture behavior of a composite material due to the addition of reinforcement fracture, reinforcement/matrix interface decohesion, and matrix failure and/or reinforcement decohesion and/or reinforcement fracture within the clusters to the failure mechanisms of the unreinforced aluminum alloy. (The dominant fracture mechanism contributes most to the deformation and fracture process of a material, even though many failure mechanisms can coexist and are influenced by each other.) For example, SiC particulate cracking has a major influence on the ductility and toughness of SiC/Al composite materials when the particles are well distributed and strongly bonded, particularly for large SiC particles.[1-3,5-9] However, composite fabrication method (such as powder metallurgy, casting, and spray forming) can affect SiC particle distribution and particle/matrix interface bond strength, which in turn affects composite material ductility and toughness.[1-3] Reinforcement particle size also is key in determining the probability of particle cracking and, therefore, the effect of particle cracking on ductility and toughness.[5-9] Thus, it has been shown that composite fabrication process, reinforcement particle size, and matrix microstructure are major elements in controlling the failure mechanism of composite materials.

Quantitative microscopy has been applied to examine the effects of composite fabrication method, reinforcement particle size, and matrix strength on particle fracture in Al/SiC composite materials.[1-3] Lloyd[1] found that the ductility of 6061 reinforced with 10 vol.% and 20 vol.% <10 μm SiC particulate, fabricated by molten metal mixing, was mainly limited by particle decohesion and/or cracking and/or matrix failure within particle clusters rather than particle cracking. It was suggested that the particle clusters were preferential regions to initiate fracture since the particle/particle bonding is weak or totally absent, and the matrix within the clusters was in a high level of triaxial stress due to the constraints of surrounding particles. However, quantitative measurements of particle cracking showed that the number of cracked SiC particles increased with increasing strain and stress. Llorca *et al.*[2] found that the failure of 2618 aluminum alloy reinforced with strongly bonded, well-dispersed 15 vol.% SiC particulate, fabricated by spray codeposition, was controlled by particle cracking. Particle size and aspect ratio affected the probability of particle cracking; large and elongated particles were likely to fail at low applied stress. Other studies have shown that SiC particle fracture has been observed in the large particles as well as those with high aspect ratios along the tensile axis, whereas composites reinforced with small particles were more likely to suffer matrix failure.[5-9] However, the transition particle size between matrix failure and particle cracking mechanisms depends upon the particular composite and matrix condition.[2,3,5-9] Matrix microstructure, which can be controlled by heat treatment, has also been shown to affect the fracture process.[3,10,11] SiC particle cracking was predominant in the under-aged materials, while failure in the matrix and near the interface was observed more frequently in the over-aged materials. Quantitative measurements of SiC particulate fracture were done on 7XXX series aluminum alloy reinforced with 15 vol.% 5 μm and 13 μm SiC particulate, fabricated by a P/M process followed by extrusion.[3] The results showed that the number of cracked SiC particles increases as plastic strain increases for different heat treatments and that, the larger the particle size, the higher the percentage of cracked particle at a given strain for both under-aged and over-aged materials, which is consistent with previous research.[1,2]

The objective of the present work is to investigate particle fracture behavior in aluminum matrix composite materials reinforced with large SiC particles (larger than 20 μm), fabricated by powder metallurgy process without secondary extrusion processing. The lack of extrusion or rolling largely eliminates the particle fracture and particle alignment, which typically occur during secondary processing and differ from much of the prior research. The quantitative parameters, the new surface area created by particle cracking per unit volume,

S_V, and the number frequency of cracked particles will be measured as a function of the local plastic strain, matrix yield strength, and SiC particle size.

EXPERIMENTAL PROCEDURE

The composite materials used in this study were fabricated by press and sinter powder metallurgy (P/M). The matrix powder was prepared by blending elemental Al, Cu, Mg, and Si powders to attain the composition Al-4.4 wt.% Cu-0.5 wt.% Mg-0.8 wt.%Si (alloy 201). The composite powder was prepared by blending 9 vol.% SiC particles (nominally 23 μm, 63 μm, or 142 μm) with premixed matrix powder. The nomenclature for this composite is $201/SiC/9_p$. The powders were compacted in a molded tensile bar die with zinc stearate die wall lubricant using a mechanical press and 486 MPa of pressure. The specimens were degassed at 400 °C ± 3 °C for 30 minutes and sintered at 600 °C ± 3 °C for 1 hour in a high purity argon atmosphere. The composite materials had greater than 97% of their theoretical densities. In general, the SiC particles were well-dispersed and nearly randomly oriented. The specimens were solutionized and aged in air after sintering. The solutionizing treatment was 510 °C ± 3 °C for 45 minutes, followed by a cold water quench. The aging treatments were carried out immediately after the solutionizing treatment at 160 °C ± 3 °C for 1 hour (under-aged) and 14 hours (peak-aged).

The local plastic strains were determined by measuring the distance between microhardness indentations with less than 1% relative measuring error before and after tensile testing using an image processing system and an optical microscope. The microhardness indentations were placed along the gage length of the tensile specimen and were nominally 0.5 mm apart. The tensile tests were carried out using a servo-hydraulic testing machine and an initial strain rate of 2.67×10^{-4}/s.

The new surface area per unit volume, S_V, and the number frequency of cracked particles, F_{No}, were determined as a function of position along the tensile axis of longitudinal sections of the specimens after testing using an optical microscope. This method eliminates questions regarding differences in cracking behavior of particles on the surface versus particles within the bulk. S_V was determined by measuring the number of test lines crossing the cracked surface per unit length, P_L[1]. F_{No} was determined by measuring both the number of cracked particles and the total number of particles in a test field. The ratio of the number of cracked particles to the total number of particles is F_{No}. Different magnifications were employed for the measurement of the three

---

[1] The value of S_V is equal to P_L when the test line is normal to the feature being measured, as was the case in these measurements.

particle sizes in order to minimize the counting errors while using a reasonable number of placements. Magnifications of 125, 250, and 500 were utilized for composites reinforced with 142, 63, and 23 µm particle sizes, respectively. More than 20 placements (or fields) were measured for each position (and, therefore, strain) along the gage length. For some specimens, several layers of polishing were necessary to obtain 20 placements for each position. There were approximately 400, 220, and 150 particles within the measured area of each position for the materials containing 23 µm, 63 µm, and 142 µm SiC particles, respectively. In all cases, approximately the same distance along the gage length was examined for each position so that the S_V and F_{No} were averaged over the same test length range, which assured that the measurements were comparable for all three particle sizes. As will be discussed below, the frequency measurements and the surface area measurements are related by the number of particles per volume and average area per crack.

Power law regression was used to fit strain as a function of position. Separate regressions were used for each side of the fracture surface, and the origins were set at the fracture surface. Since S_V and F_{No} are related to local strain and, therefore, position, combined plots of S_V as a function of strain and F_{No} as a function of strain were obtained using the assumption that the fracture surfaces are planar. A best fit linear regression was used to fit both S_V and F_{No} as a function of local strain. The 95% confidence intervals of the slopes and y-intersects of these best fit lines were calculated so that envelopes, which indicate error bounds, were obtained.

RESULTS

Microstructure

Typical micrographs of alloy 201 and alloy 201 reinforced with 9 vol.% SiC after tensile testing are shown in Figure 1; the tensile axes are vertical in these figures. The SiC particles were relatively well distributed in the matrix for all three particle sizes. The composite materials had greater than 97% of their theoretical densities. The porosity that existed was mainly associated with particle clusters. Constituent phases were present at the grain boundaries in the unreinforced matrix and at grain boundaries and particle/matrix interfaces in the composite materials. The SiC particles were angular, irregular, and nearly-equiaxed. (Few particles with a two-dimensional aspect ratio greater than 2 were observed.) A comparison of the relative sizes of these particles can be seen in Figure 1 since the micrographs were taken at the same magnification.

Particle cracking was observed to varying degrees throughout the gauge length, with more cracks occurring near the fracture surface and most cracks oriented normal to the stress axis. Typical micrographs of regions near the fracture

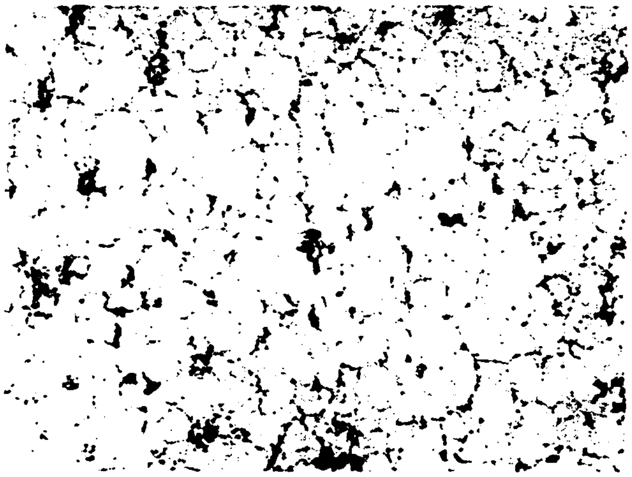

(a)

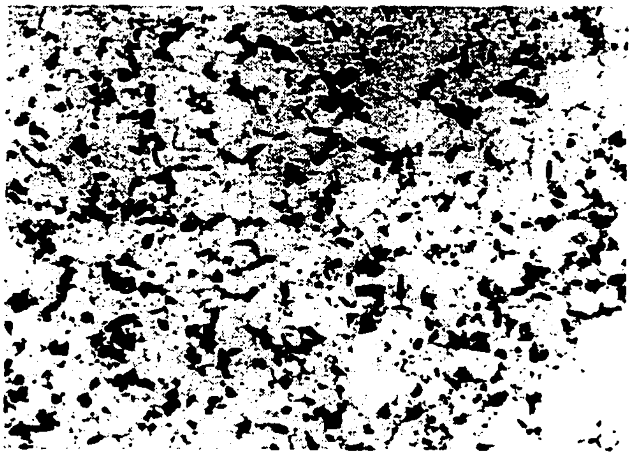

(b)

Fig. 1-Micrographs of the liquid-phase sintered (a) alloy 201 and alloy 201 reinforced with 9 vol.% of (b) 23 μm, (c) 63 μm, and (d) 142 μm SiC particles.

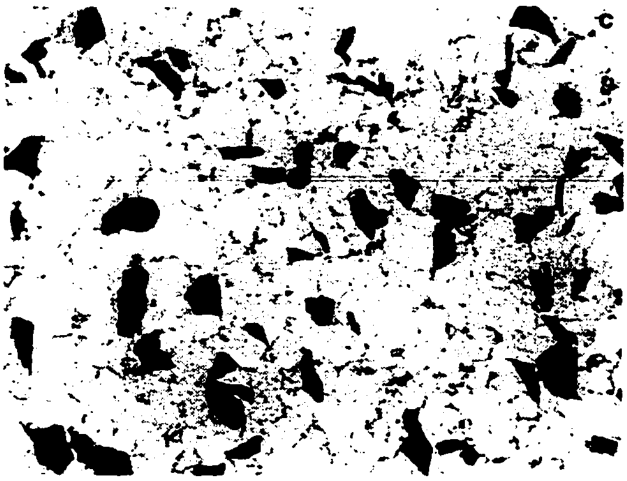

(c)

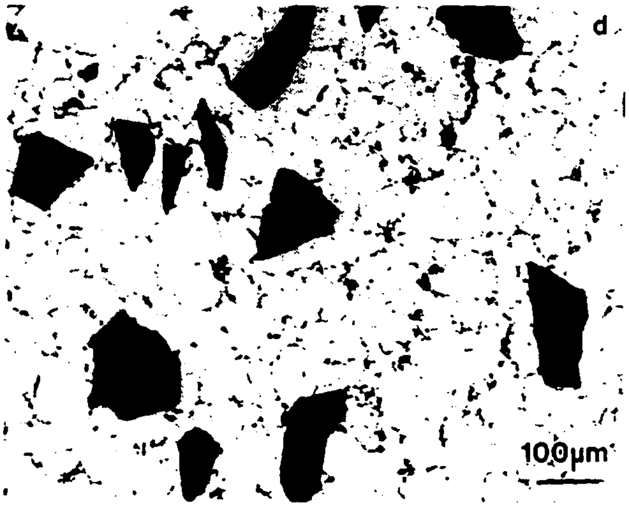

(d)

Fig.1 (continued)

surface are shown in Figures 1c and 1d. Some of the large reinforced particles were multiply cracked, whereas few of the small reinforcement particles were multiply cracked. Fractography reveals that the matrix is dimpled between the particles and fractured SiC particles are clearly visible. A typical SEM micrograph of a fracture surface is shown in Figure 2.

Tensile Properties

The tensile properties of alloy 201 and the alloy 201-based composites reinforced with 23 µm, 63 µm, and 142 µm SiC particles were measured after aging for 1 hour (under-aged) and 14 hours (peak-aged) at 160 °C. The tensile property data are presented in Table I. The ultimate tensile strength (UTS) and elongation to fracture of the composite materials were lower than the matrix alloy for both aging treatments except for the elongation of the under-aged 23 µm SiC composite. The addition of 9 vol.% SiC particles did not significantly affect the 0.1% offset yield strength of composites except in the case of the 23 µm SiC composite aged for 1 hour and 142 µm SiC composite aged for 14 hours. The yield strength, UTS, and elongation of the composite materials were influenced by heat treatment and reinforcement particle size. As expected, both 0.1% offset yield strength and UTS are higher for 14-hour aged composites than for 1-hour aged composites for three particle sizes. The elongations of the 14-hour aged composites are

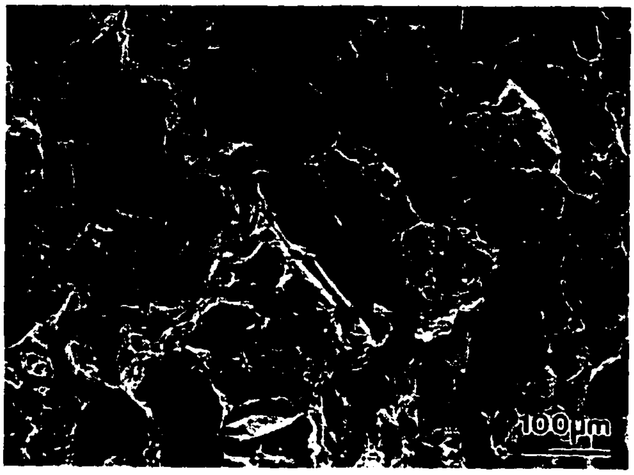

Fig. 2-Micrograph of the fracture surface for alloy 201 reinforced with 142 μm SiC.

Table I: Tensile Properties

Material	Aging Time at 160°C (Hrs.)	0.1% Offset Yield Strength (MPa)	Ultimate Tensile Strength (MPa)	Elongation to Failure (%)
Alloy 201	1	193	275	2.5
	14	299	334	1.3
Alloy 201 + 9 vol.% 23 µm SiC	1	172	236	3.5
	14	297	312	0.3
Alloy 201 + 9 vol.% 63 µm SiC	1	196	240	1.7
	14	283	291	0.3
Alloy 201 + 9 vol.% 142 µm SiC	1	196	217	1.5
	14	260	265	0.3

lower than those of 1-hour aged composites. The composites containing small reinforcement particles exhibited the higher UTS, which is particularly true for 14-hour aged composites, and the higher elongation to failure, which is true for 1-hour aged composites.

Number Frequency of Cracked Particles

The number frequency of cracked particles, F_{No}, as a function of strain for alloy 201 reinforced with 9 vol.% of 23 µm, 63 µm, and 142 µm SiC and aged for 1 hour and 14 hours are shown in Figure 3. For each combination of particle size and aging treatment, F_{No} for each number of cracks per particle (from one crack to more than three cracks) were measured separately as strain varied. The Student t-statistic test

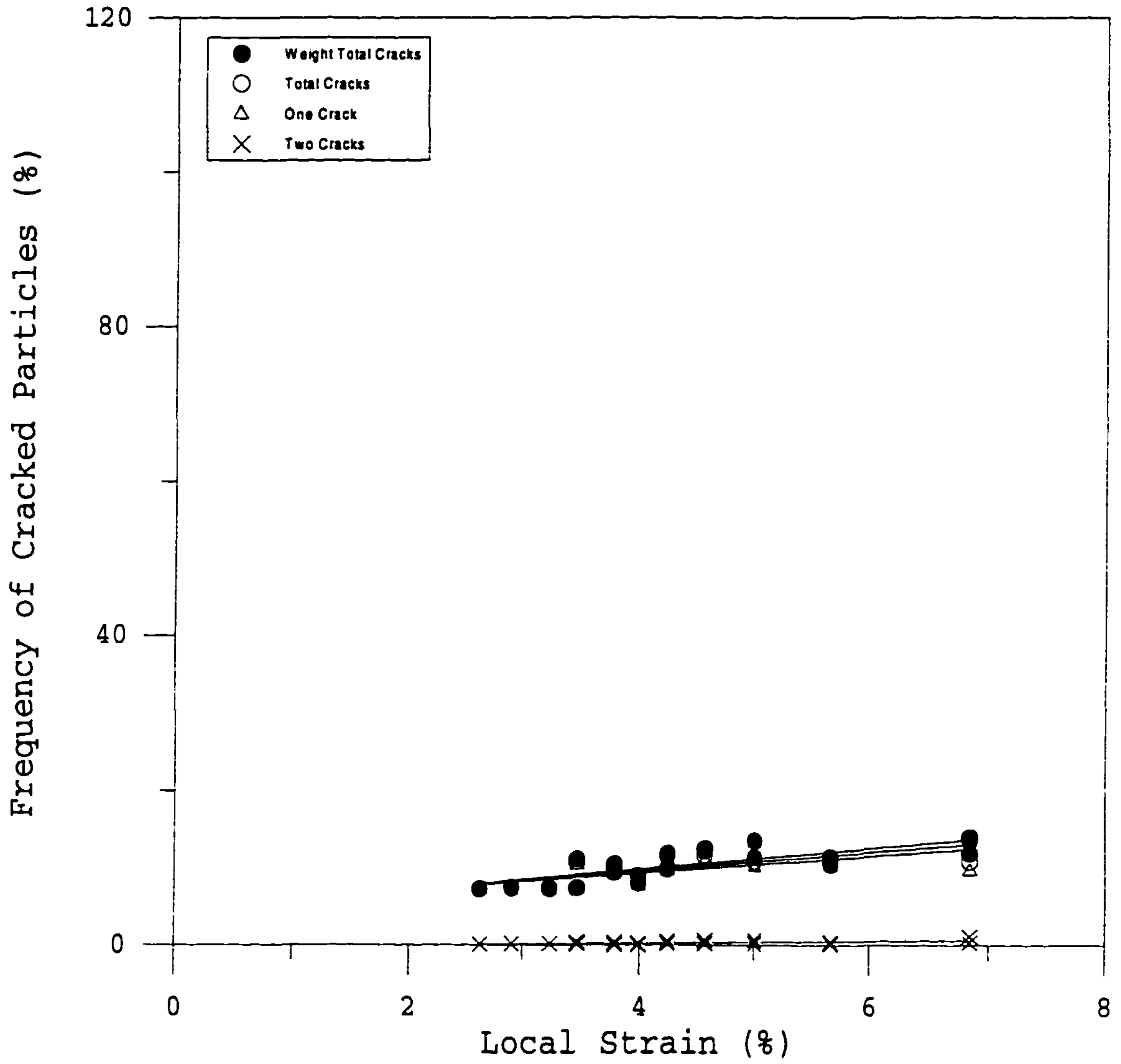

(a)

Fig. 3-F_{No} as a function of strain for alloy 201 reinforced with 9 vol.% of (a) 23 µm, (b) 63 µm, and (c) 142 µm SiC aged for 1 hour and (d) 23 µm, (e) 63 µm, and (f) 142 µm SiC aged for 14 hours at 160 °C.

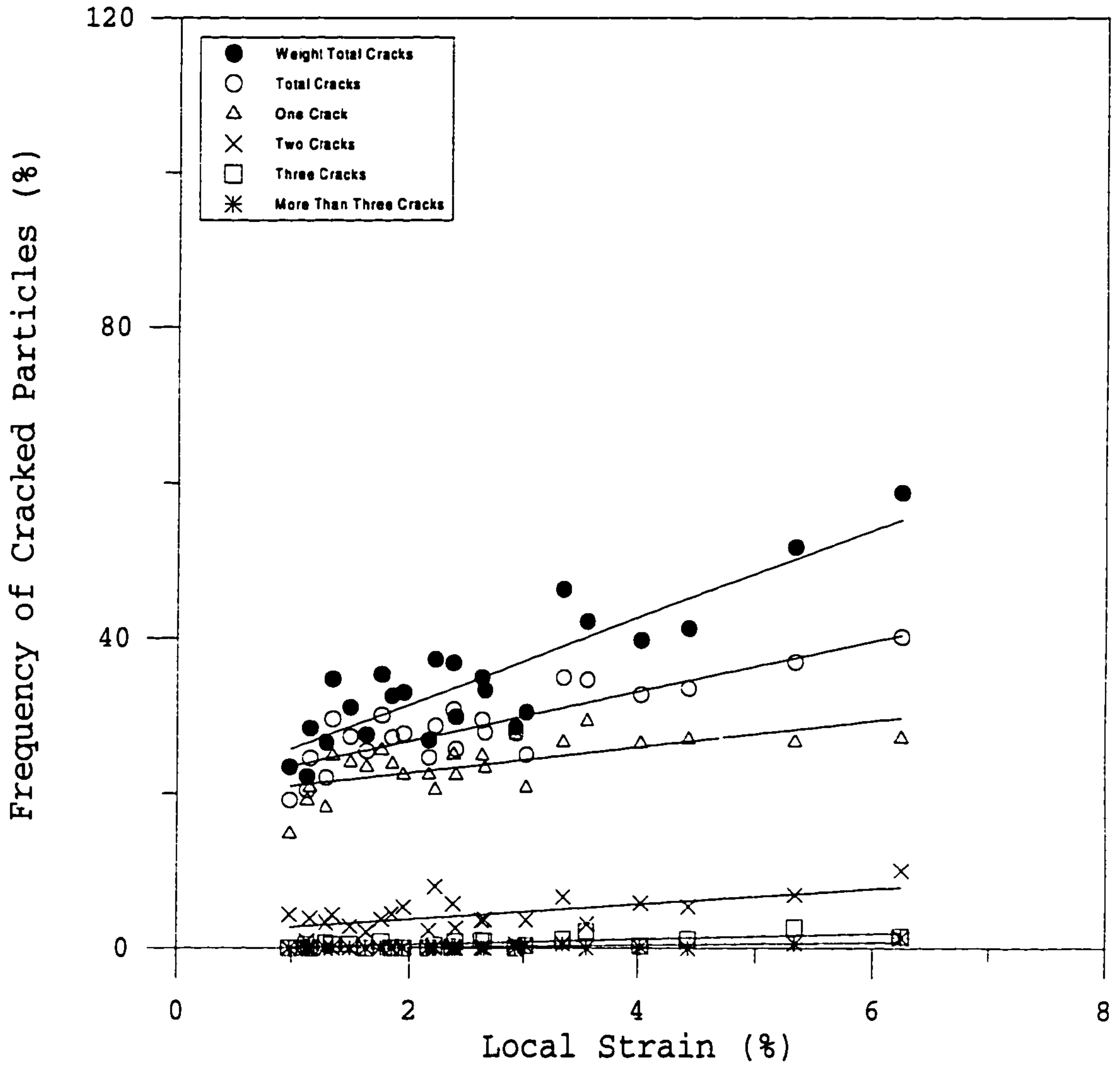

(b)

Fig. 3 (continued)

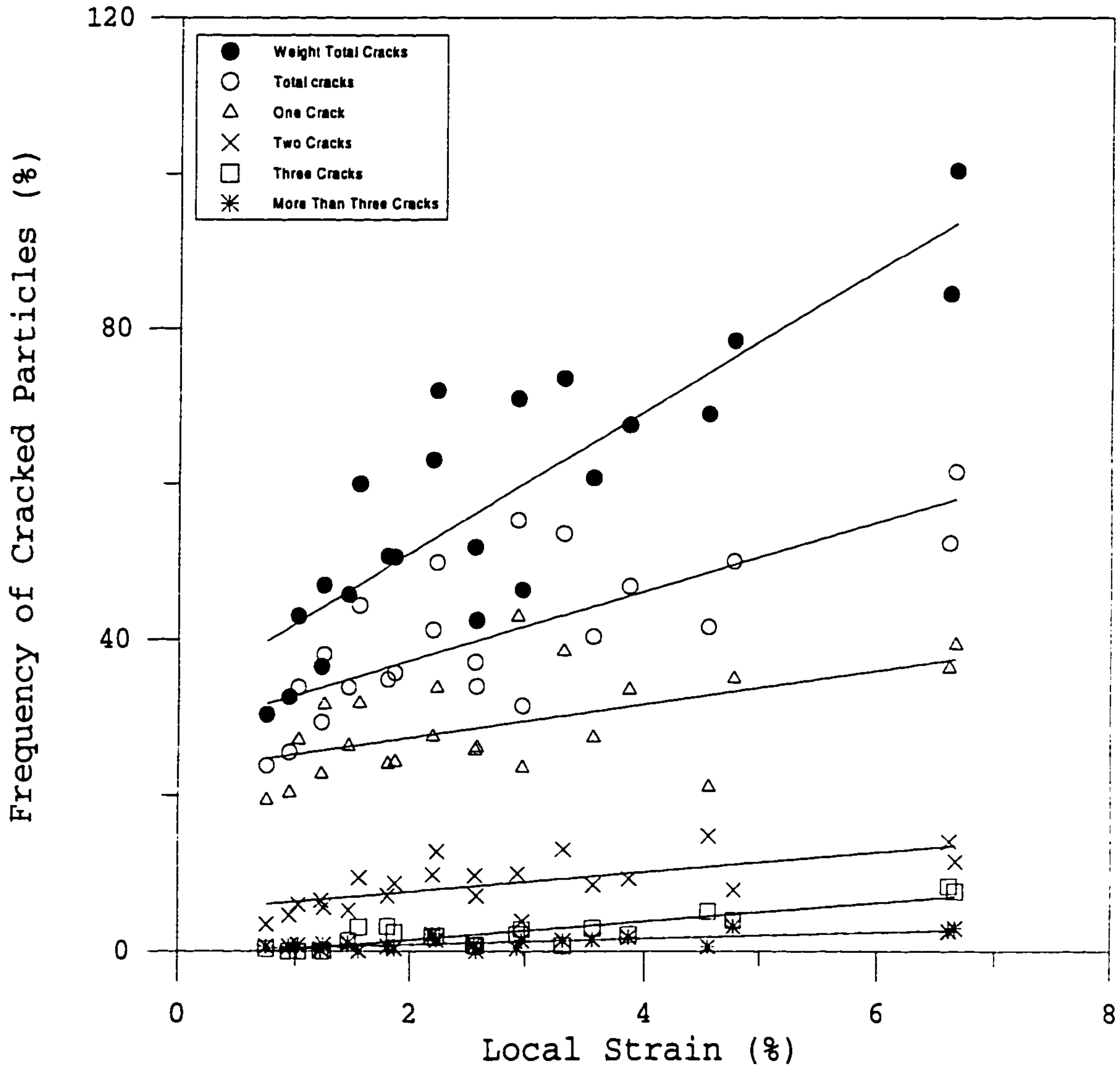

(c)

Fig. 3 (continued)

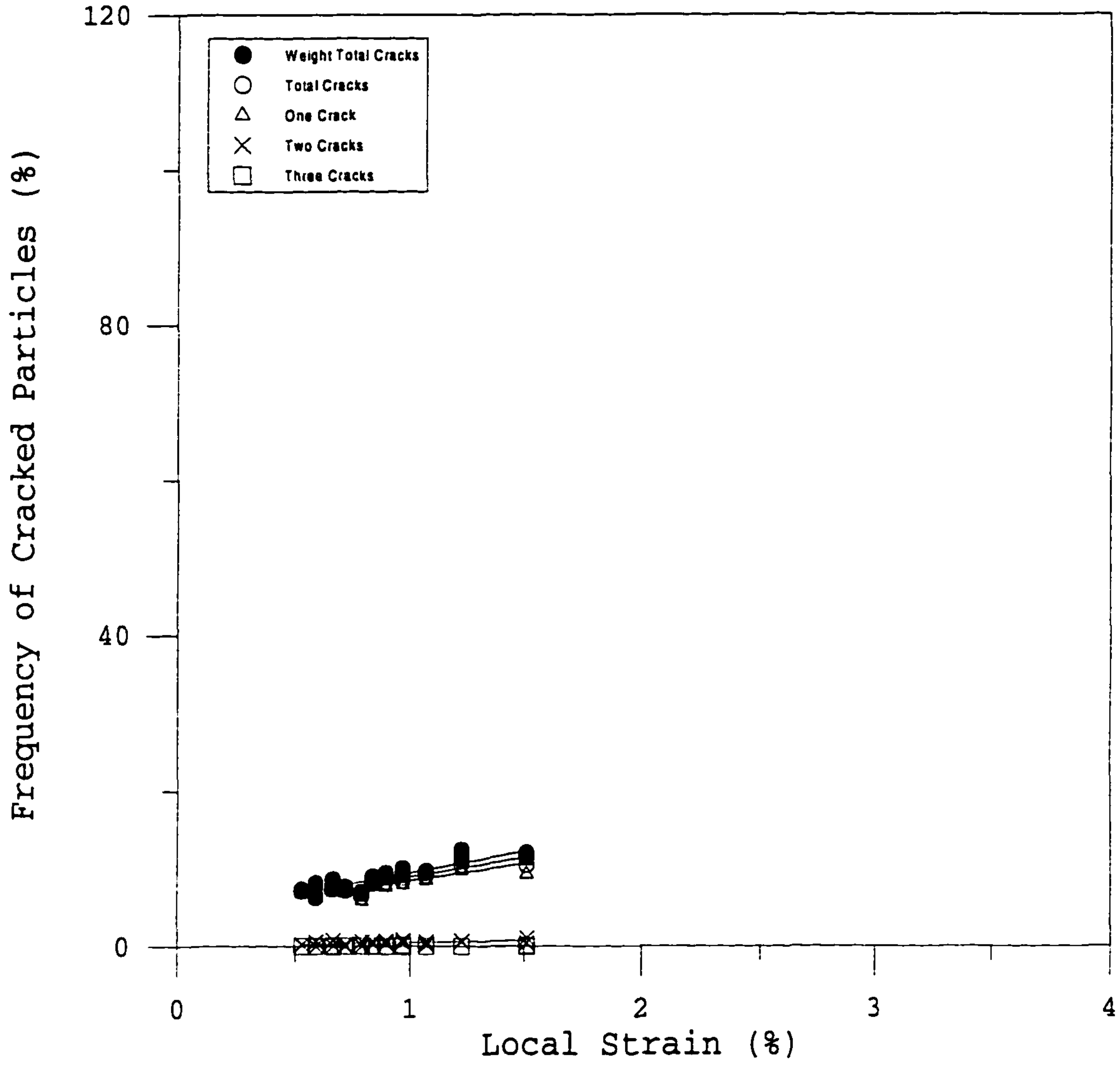

(d)

Fig. 3 (continued)

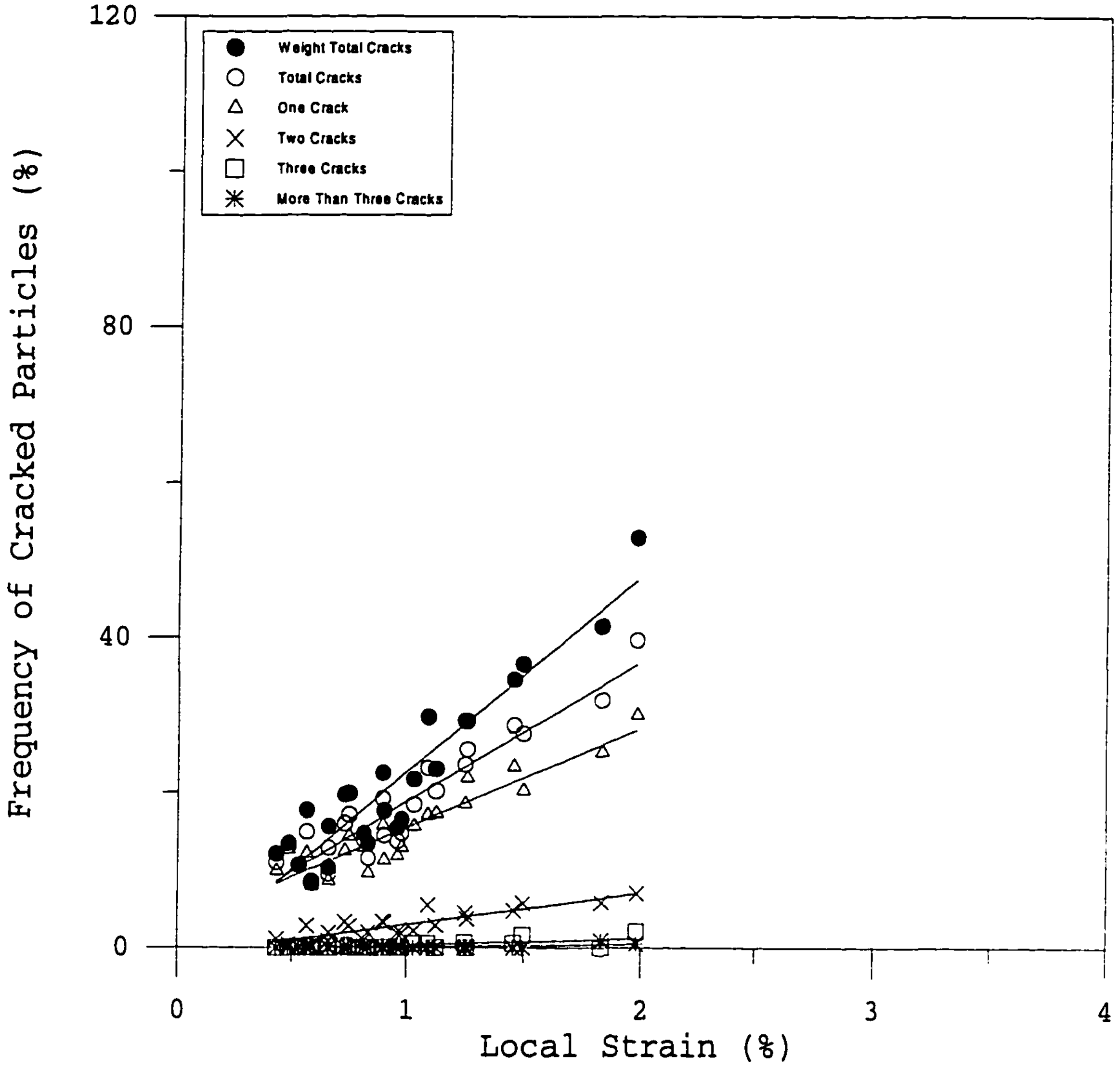

(e)

Fig. 3 (continued)

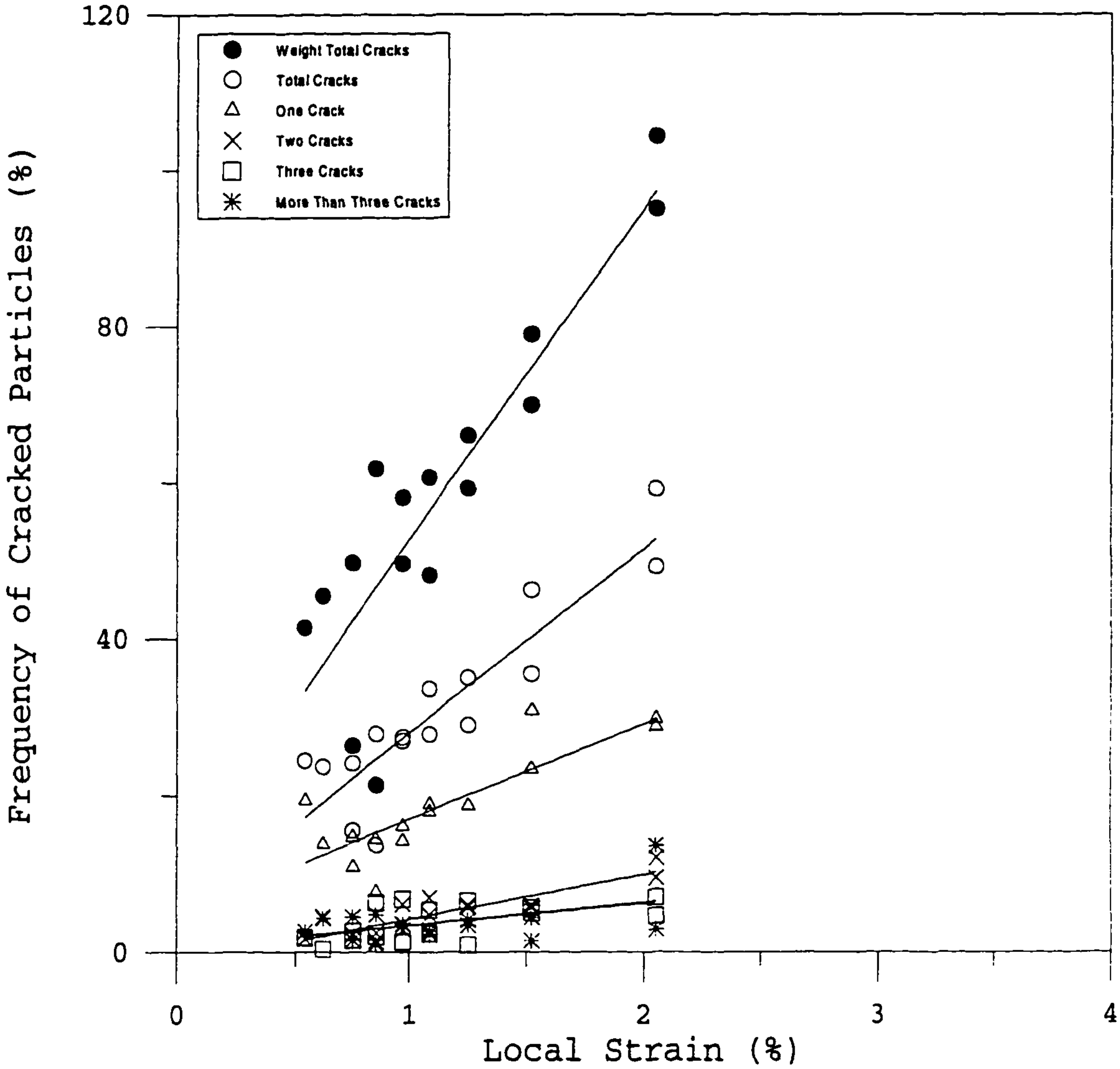

(f)

Fig. 3 (continued)

indicated that a strong correlation between F_{No} and local strain exists since the hypothesis that the slope[2] = 0 can be rejected with a 0.05 level of significance. The F_{No} increases as local strain increases, and a linear regression was used, which is confirmed to be statistically valid fit by testing the correlation coefficient with a 0.05 level of significance. These best fit lines are shown in Figure 3.

It is apparent that increasing the matrix strength through heat treatment increases the number frequency of cracked particles at constant strain and particle size. This change is reflected in increases in the slopes of the best fit lines for each number of cracks (*i.e.*, weighted total cracks[3], total cracks[4], one crack, two cracks, *etc.*), which was confirmed to be statistically significant by using Student *t*-statistics with a 0.05 level of significance. The data contained in Figure 3 also demonstrate that the larger SiC particles are more likely to be cracked than the smaller particles at a given strain and aging treatment. This effect

---

2 The slope is the change in the mean of F_{No} corresponding to a unit increase in the local strain.

3 The "weighted total cracks" is defined as the sum of the F_{No} values for each number of cracks multiplied by the corresponding number of the cracks, in which the effect of the multiple cracks is considered. Therefore, the weighted total cracks can be greater than 100%.

4 "Total cracks" is defined as the sum of the F_{No} values for each number of cracks. The maximum total cracks are equal or less than 100%.

can be clearly seen in these figures by considering the higher percentage of large particles cracked at constant strain and the higher slopes of the best fit lines in larger particle reinforced composites, which is confirmed to be statistically significant by the comparison of slopes for each number of cracks (*i.e.*, weighted total cracks, total cracks, one crack, two cracks, *etc.*) using Student *t*-statistics. In most cases, composites containing large particles exhibited more multiple cracks in each particle than those containing small particles.

S_V Measurements

The results of the new surface area created by particle cracking per volume, S_V, as a function of strain for alloy 201 reinforced with 9 vol.% of 23 µm, 63 µm, and 142 µm SiC aged for 1 hour and 14 hours are shown in Figure 4. S_V increases approximately linearly as local strain increases. A linear regression was used, which was confirmed to be a statistically valid fit by testing the correlation coefficient with a 0.05 level of significance. The slopes and y-intercepts of linear regressions with 95% confidence intervals were calculated and also shown in Figure 4, where the envelopes indicate these error bounds.

The data contained in Figure 4 show that increasing the matrix strength by heat treatment increases the new surface area per volume, S_V, at a given strain and particle size and also increases the slopes of the best fit lines, which is

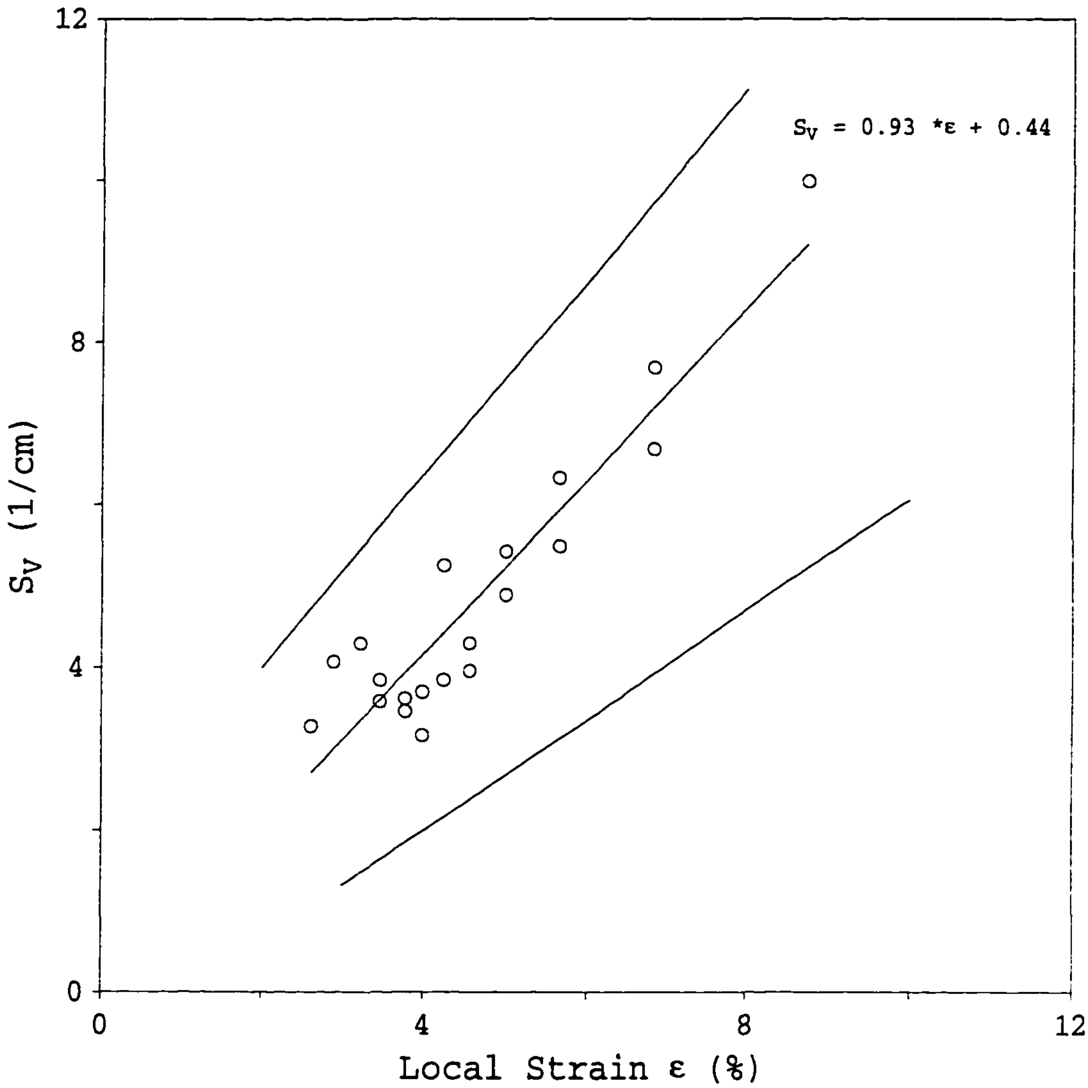

(a)

Fig. 4-S_v as a function of strain for alloy 201 reinforced with 9 vol.% of (a) 23 μm, (b) 63 μm, and (c) 142 μm SiC aged for 1 hour and (d) 23 μm, (e) 63 μm, and (f) 142 μm SiC aged for 14 hours at 160 °C.

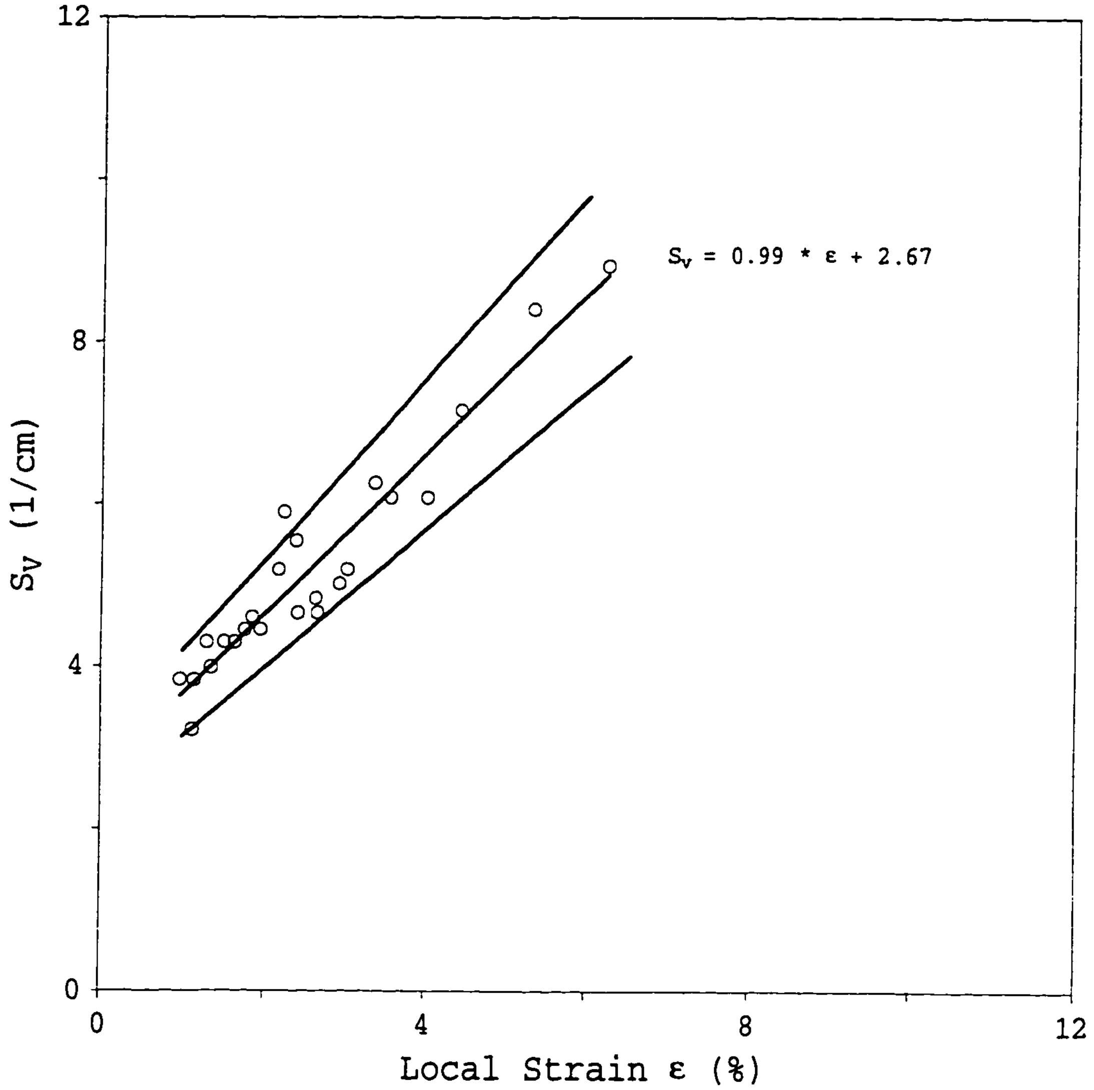

(b)

Fig. 4 (continued)

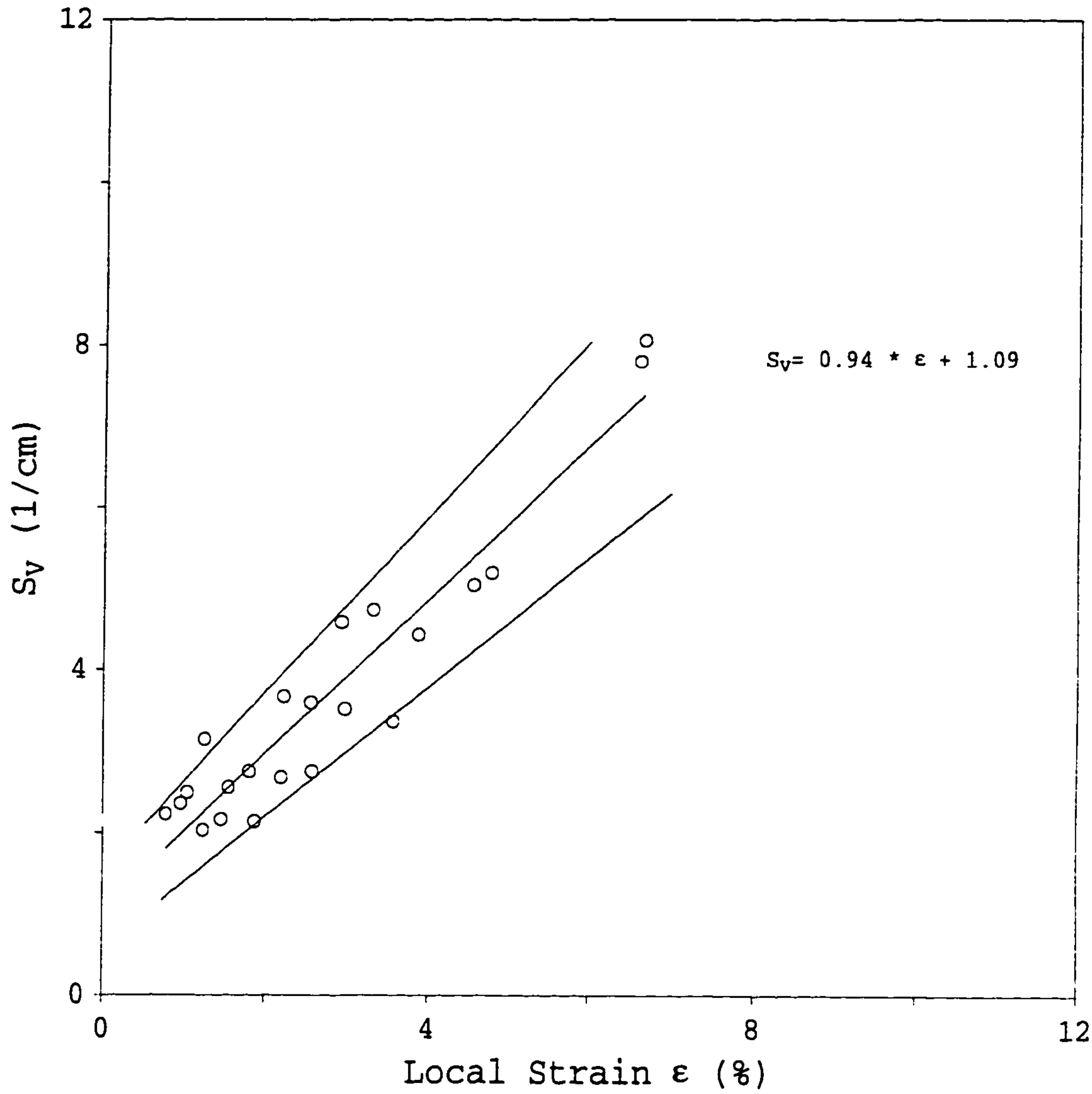

(c)

Fig. 4 (continued)

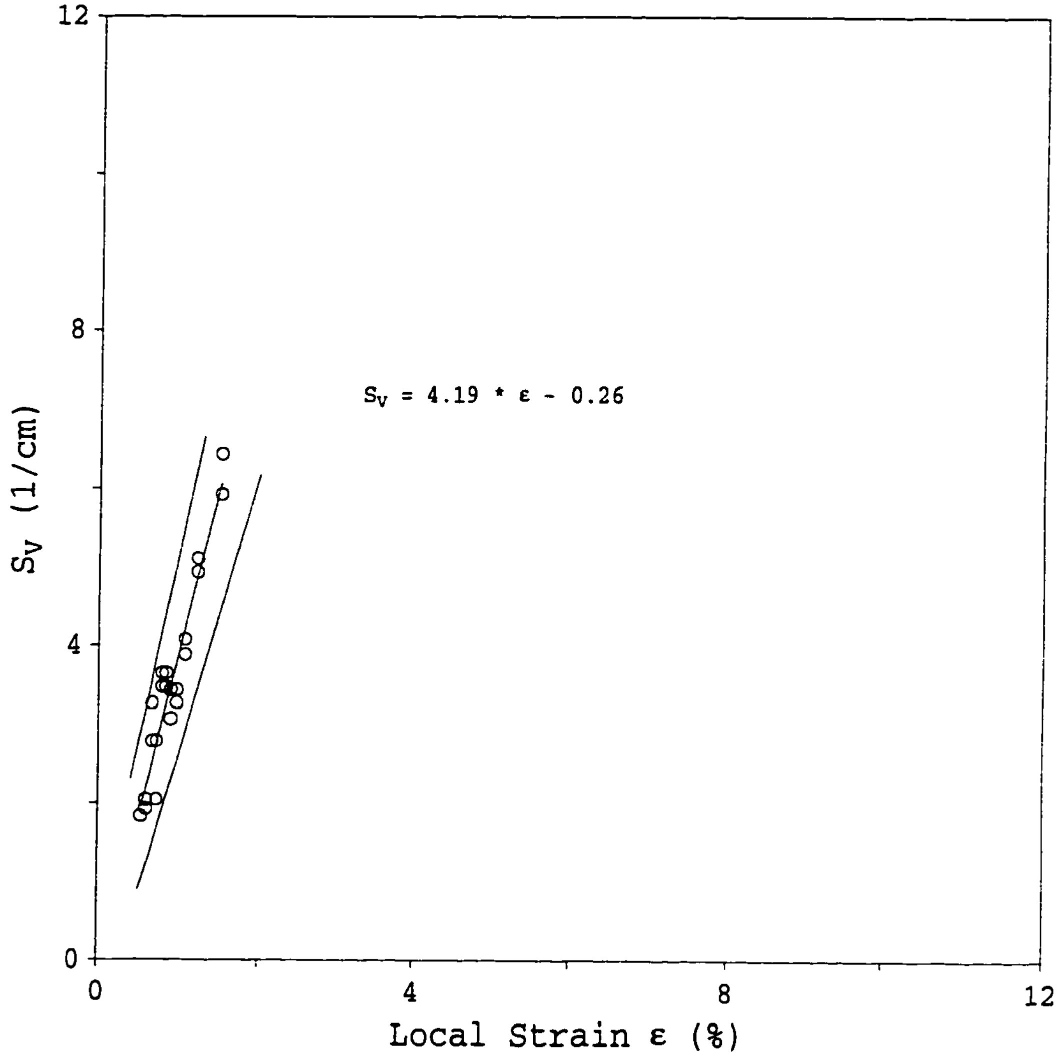

(d)

Fig. 4 (continued)

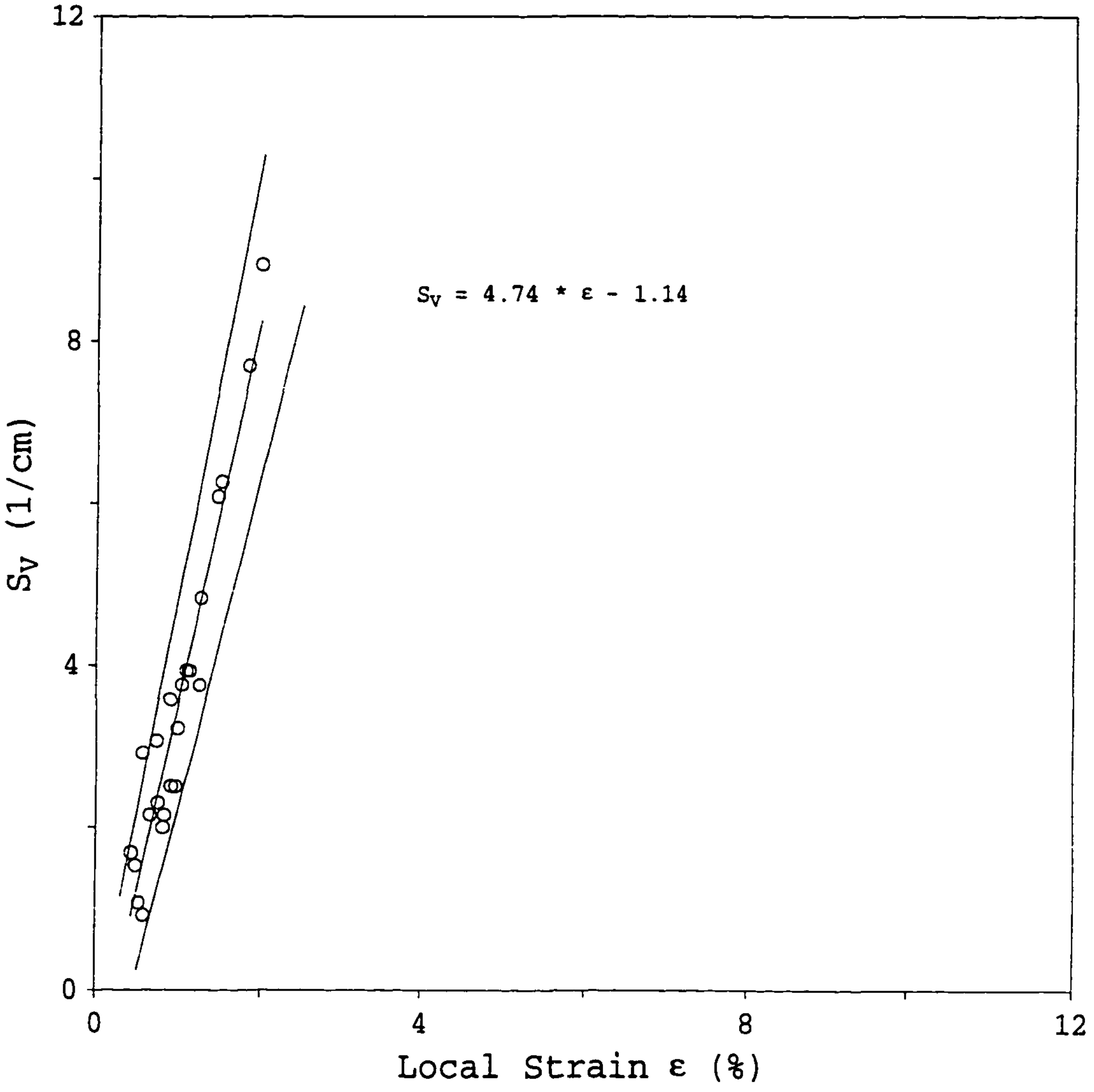

(e)

Fig. 4 (continued)

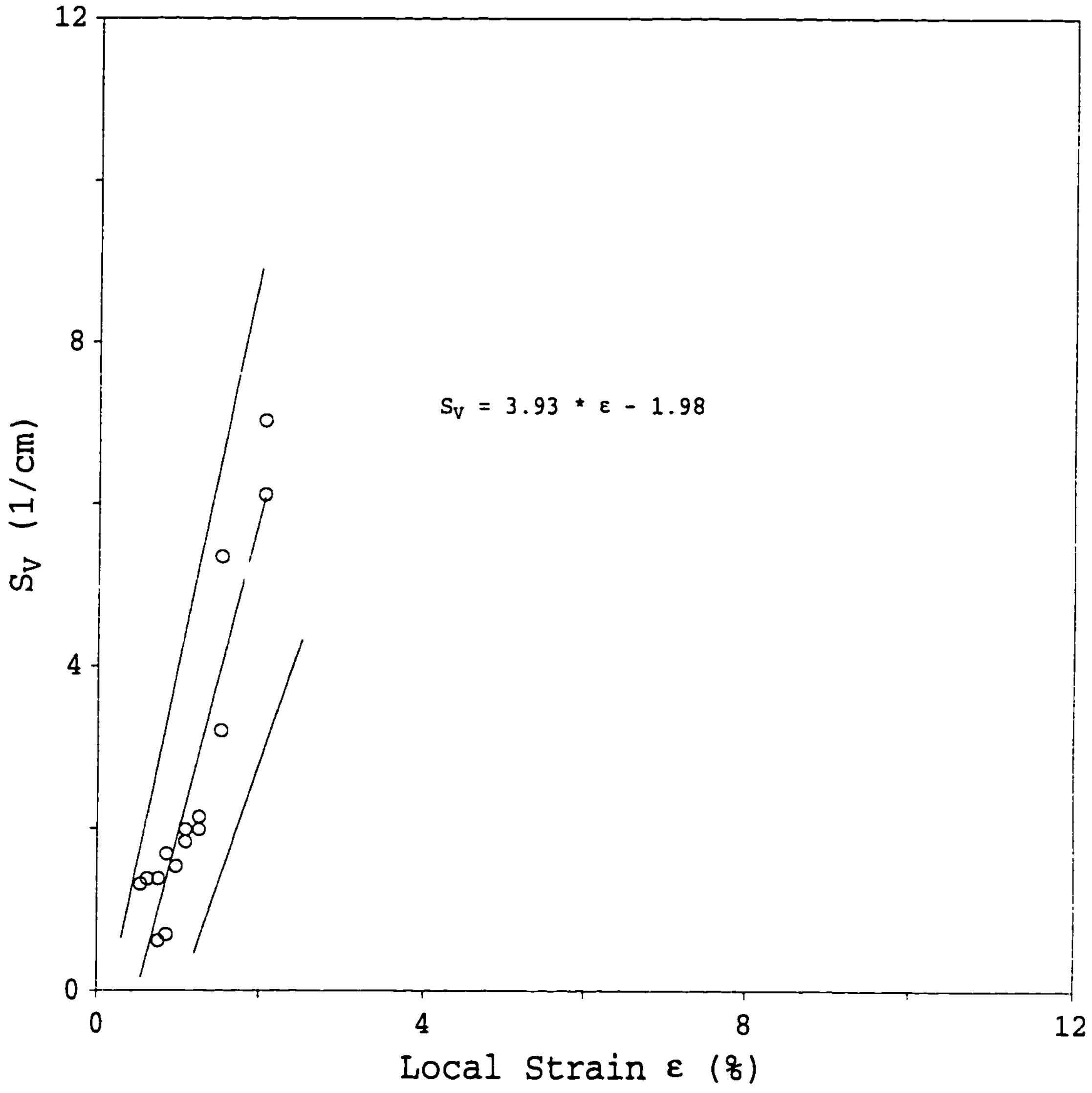

(f)

Fig. 4 (continued)

confirmed to be statistically significant using the Student *t*-statistic test with a 0.05 level of significance. These slopes are summarized in Figure 5. This result is consistent with the effect of heat treatment on the number frequency of cracked particles since the area per crack is proportional to the particle size squared.

Particle size does not appear to affect the slopes of S_V within the limits of the experimental data. The Student *t*-statistic test indicated that there was no significant slope difference among the three particle sizes for under-aged composites. A statistically significant difference between the slopes was observed only for the 142 and 63 μm particle sizes in the peak-aged composites. This result is attributed to the limitations of specimen size and, therefore, measurement statistics. The lack of a clear, consistent picture of S_V increment per unit strain and particle size suggests that this effect is weak if present. The data on particle size and crack surface area is in contrast to the effect of particle size on the number frequency of the cracked particles, where the larger the particle size, the higher the number frequency of the cracked particles. These apparently contradictory observations are the result of the effect of particle size on particle number at a constant volume fraction and the surface area created by each crack.

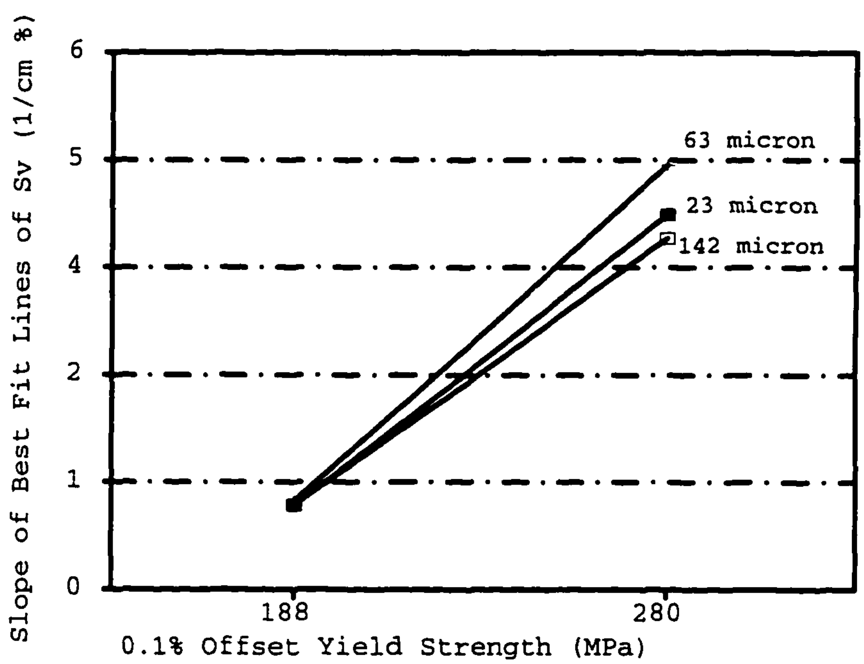

Fig. 5-The effect of particle size and 0.1% offset yield strength on the slope of S_V as a function of strain.

DISCUSSION

The principal goal of this study was to determine the quantitative relationship between composite deformation and particle cracking in aluminum reinforced with SiC particulate. Although several particle cracking studies have been done recently on composite materials processed by molten metal, powder metallurgy, or spray formation and reinforced with small particles,[1-3,9] the need to examine the relationship between microstructural features and composite deformation for composite materials processed by powder metallurgy (without secondary processing, *i.e.*, extrusion, or hot pressing) and reinforced with large particle size remains. The results of the present study indicate that particle cracking is sensitive to controllable parameters such as particle size and matrix microstructure, as will be discussed below.

The fracture of a brittle material is often associated with the presence of surface or internal defects and subsequent crack propagation under a stress. The defects can cause significant stress concentrations and local biaxial or triaxial stresses in the vicinity of the defect; the magnitude of the stress at the crack tip is highly dependant on geometry. The applied stress, defect size, geometry, and fracture toughness are often related by the equation:

$$K_I = Y\sigma\sqrt{\pi a} \qquad [1]$$

where K_I is the stress intensity factor in mode I, σ is the applied stress, a is the depth of penetration of the surface crack, and Y is a constant that depends on the crack opening mode and crack shape. Failure will occur when K_I is equal to K_{IC}, which is a material constant and a measure of fracture toughness.

The critical stress is inversely proportional to the square root of the depth of penetration of the surface crack. By using a value of K_{IC} for SiC of 3.4 $MPa \cdot m^{-1/2}$ [22] and assuming that a is small compared to the size of SiC particles, Y is equal to 1.1; correlations can then be made between stress and the critical defect size, as shown in Table II. It would be expected that these stresses can be exceeded around SiC particles in composite materials since the yield strength of aluminum alloy is approximately 300 MPa and the SiC particle creates a significant stress concentration.

Table II: Calculated Values for Critical Stress as a Function of Defect Size for SiC

Defect Size (μm)	Critical Stress (MPa)
1	1744
5	780
10	551
50	247

The values for stress and defect size were varied in this study by altering the aging treatment and by using three particle sizes, respectively. The former effect is obvious since the stress upon a particle is a function of the macroscopic stress on the specimen. The latter outcome is a consequence of the nature of the defect populations in brittle reinforcements. For example, it has been widely observed that the fracture strength of brittle solids increases as the fiber diameter (or other critical dimension) decreases. This observation has been attributed to the increased likelihood that a larger reinforcement will contain a defect of the critical size. Thus, one would expect that larger SiC particles are more likely to contain a defect of the critical size to cause fracture at a given stress level. It should be emphasized that the SiC particles of this study (and most other similar studies) are commercial grinding media, which are comminuted and sized. Thus, they would be expected to have significant surface flaws and cracks.

Effect of Aging Treatment

The effects of different aging treatments on number frequency of cracked particles as a function of strain have been shown in Figure 3. The slopes of the best fit lines are higher for peak-aged composites, which means that more particles are cracked as strain increases for peak-aged composites. This result indicated that more stress was applied on the particles for peak-aged materials than for under-aged materials, as would be expected. According to Eq. [1], an inversely proportional relationship between applied stress and defect size exists, where the critical defect size decreases as the applied stress increases. Since the critical defect size decreases, the fraction of particles having defects of that critical size increases. Thus, a higher number frequency of cracked particles would be expected in composites with high strength matrix, as has been previously reported.[2, 3]

Aging treatment also affects S_V versus strain behavior; that is, the slopes of the best fit lines are higher for peak-aged composites with three particle sizes, which indicated that more surface areas were created by particle cracking per unit strain. As discussed earlier, the applied stress on the particles is a function of the macroscopic stress on the specimen. Therefore, more stress was expected to be applied on the particles for peak-aged composites than under-aged composites. The critical defect size will decrease as the applied stress increases and the probability of particles having defects of that critical size increases. Thus, more cracked particles would be expected in composites with high strength matrix, and more surface areas were created by particle cracking.

Effect of Particle Size

Particle size effects on the frequency of cracked particles versus strain behavior can be seen by considering both F_{No} values and the slopes of the best fit lines. The larger SiC particles are more likely to be cracked than smaller ones at a given strain and matrix strength and/or as strain increases. This phenomenon can be interpreted given that reinforcement particles have defects. The surface area per particle increases with increasing particle size, and the probability of having a defect of a given size increases. Thus, the probability of a defect of critical flaw size being present increases. The composite materials with larger particles exhibit a higher number frequency of cracked particles at a given strain and stress compared to those with smaller particles.

Particle size does not significantly affect the slopes of S_V versus strain, which indicates the increasing rate of S_V per unit strain. This result can be understood by considering that a necessary condition for crack propagation through a brittle particle is that the strain energy stored in the particle be sufficient to provide the surface energy of the newly created crack surface. In this study, the areas of the newly created particle crack surfaces per unit strain were approximately the same for all particle sizes at a constant matrix strength, which indicates that the same amount of strain energy was released by creating new surfaces regardless of the particle size. Since the higher strength materials have more stored energy at a given strain, more surface area is created in order to release this energy. At this stage, the physical constants that determine the slopes, which are approximately 1 for 1 hour aged and 4 for 14 hour aged materials, are not fully understood. However, it appears that a relationship between the amount of crack surface created and the stored energy of deformation is likely.

Multiple Regression

The significance of the experimental variables (local strain, matrix yield strength, and particle size) on the new surface area created by particle cracking per volume (S_V), number frequency of total cracks (F_T), and number frequency of weighted total cracks (F_W) was determined using the statistical F-test with a 0.05 level of significance. S_V, F_T, and F_W were fit as functions of the experimental variables, the products of each combination of two of these variables, and the products of all three variables. The regression equations were placed in the following form, which separates the equations into strain terms and non-strain terms:

$$S_V = 9.9 - 3.4\times10^{-2}\sigma_y - 8.0\times10^{-5}\sigma_y D + (-7.1 + 4.0\times10^{-2}\sigma_y + 4.0\times10^{-3} D)\,\epsilon$$

$$F_T = 7.5 + 5.8\times10^{-1} D - 2.2\times10^{-3}\sigma_y D + (-2.9\times10^{-1} D + 1.7\times10^{-3}\sigma_y D)\,\epsilon \qquad [2]$$

$$F_W = 2.4 + 6.8\times10^{-1} D - 2.4\times10^{-3}\sigma_y D + (-4.7\times10^{-1} D + 2.8\times10^{-3}\sigma_y D)\,\epsilon$$

where ϵ is the local strain in %, D is the nominal particle diameter in μm, and σ_y is the matrix yield strength in MPa. This analysis indicates the following: (1) the effect of particle size and the product of local strain, particle size, and matrix yield strength on S_V is not statistically significant; and (2) the effects of matrix yield strength, local strain, and the product of local strain and matrix yield strength on both F_T and F_W are not statistically significant.

When the two material variables (matrix yield strength and particle size) are held constant, S_V, F_T, and F_W are linear functions of local strain, which is the same form as that of the experimental data; the slopes of S_V, F_T, and F_W are different functions of matrix yield strength and particle size for all three equations. It should be noted that the effect of particle size on the slope of S_V is very small compared to the effect of matrix yield strength and can be reasonably ignored, although it is statistically significant. Thus, the slope of S_V is only a function of matrix yield strength and increases with increasing matrix yield strength. In the yield strength range of 190 MPa to 280 MPa, the slopes of F_T and F_W increase as strain increases. The effects of particle size on the slopes of F_T and F_W are large, which is in agreement with the experimental data. The slopes are functions of particle size and matrix yield strength and increase as both particle size and matrix yield strength increase. The results of multiple regression for all experimental data are in good agreement with the previous discussion for the effects of individual variables (particle size, local strain, and matrix yield strength) on S_V, F_T, and F_W.

Number Frequency of Weighted Total Cracks and S_V

The new surface area created by particle cracking per unit volume, S_V, and the number frequency of weighted total cracks, F_W, are related by the following equation:

$$S_V = \frac{N_V F_W \overline{A}}{100} \qquad [3]$$

where N_V is the number of cracked particles per unit volume, which is approximately equal to the number of cracked particles per unit area divided by the average particle diameter; F_W is the number frequency of weighted total cracks in %; $\overline{A}$ is the average crack area among all cracks.

The S_V values for a series of local strains were calculated using Eq. [3]. The linear regression was used to fit the calculated S_V as a function of local strain, as was done for measured S_V data. The results of linear regressions for both calculated and measured S_V are shown in Table III. The results for calculated S_V and measured S_V are in an excellent agreement for alloy reinforced with 142 µm and 63 µm SiC and aged for 1 hour and 14 hours; the result of linear regression for calculated S_V and measured S_V are in a poor agreement for alloy reinforced with 23 µm SiC and aged for 1 hour and 14 hours. The poor agreement of the calculated and measured S_V for 23 µm SiC are likely due to the estimations of the number of cracked particles per unit volume, the average crack area $\overline{A}$, variations in local volume fraction, and,

Table III: The Calculated S_V from F_W and the Measured S_V as a Function of Strain Best Fit Slopes with 95% Confidence Intervals

Particle Size (μm)	Aging Time at 160 °C (Hrs.)	Calculated S_V from F_W Slopes of Best Fit Lines with 95% Confidence Intervals (cm^{-1} $\%^{-1}$)		Measured S_V Slopes of Best Fit Lines with 95% Confidence Intervals (cm^{-1} $\%^{-1}$)	
		Best Fit	± Values	Best Fit	± Values
23	1	0.33	0.16	0.93	0.25
	14	1.17	0.32	4.19	0.66
63	1	0.99	0.26	0.99	0.13
	14	4.01	0.82	4.74	0.64
142	1	0.98	0.28	0.94	0.15
	14	4.33	0.95	3.93	0.94

possibly, statistical problems associated with frequency and S_V measurements. Since it is difficult to experimentally measure the average crack area, an assumption was made that the spherical particles were cracked along the diameter. Therefore, the average crack area $\bar{A}$ was set equal to $\pi D^2/4$, where D is the nominal particle diameter. The similarity of the calculated and the measured S_V slopes indicates that the frequency and crack surface area data are in agreement, although the necessary stereological parameters necessary to relate them are not necessarily readily determined.

<u>Multiple Particle Cracking Events</u>

Composite materials containing large particles frequently exhibited multiple cracks in a single particle, while composites containing small particles exhibited few multiply cracked particles. Thus, the probability of observing single cracks and the multiple cracks would be expected to be related in some manner.

In an attempt to understand this relationship, a simple assumption was made that the probability of a particle cracking a second time is identical to the probability of it cracking the first time. Therefore, the probability of particle cracking twice should be equal to a square of the probability of the particle cracking once. (It should be noted that the probability of a particle cracking once means the probability of finding a particle having at least one crack, which is the sum of the observed probability of particles having one crack, two cracks, *etc.*) The probabilities of particles cracking once and twice were calculated using the best fit linear regression equations and are plotted in Figure 6. The logarithmic plot of the probability of particle cracking once versus the probability of particle cracking twice has a linear relationship for under-aged composites with different particle sizes. The best fit line has approximately a slope of 2.6 (Figure 6a). For the peak-aged materials, the logarithmic plot of the probabilities of particle cracking

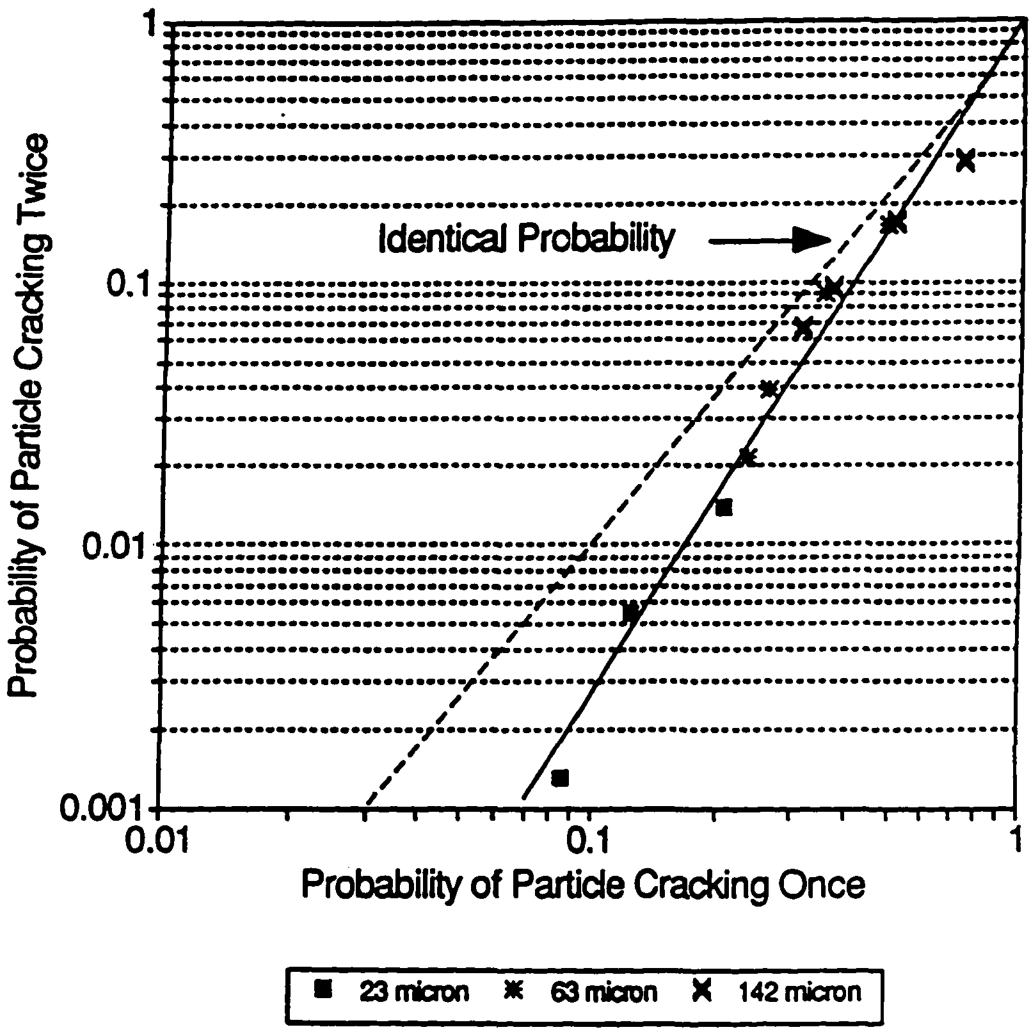

(a)

Fig. 6-The probability of a particle cracking twice as a function of the probability of a particle cracking once for alloy 201 reinforced with 9 vol.% SiC aged for (a) 1 hour and (b) 14 hours.

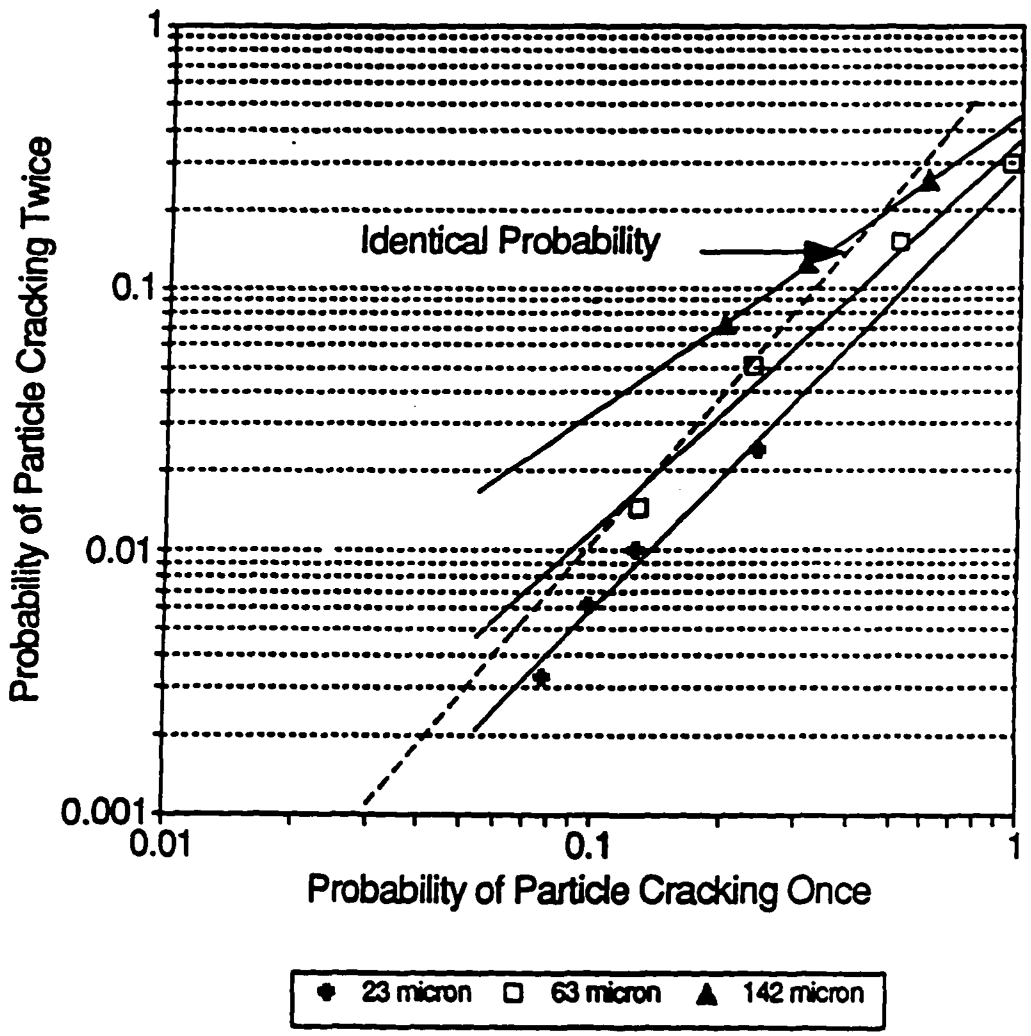

(b)

Fig. 6 (continued)

once and twice has different linear relationships for each particle size. The best fit lines have slopes of approximately 1.1, 1.5, and 1.7 for 142 μm, 63 μm, and 23 μm particle size, respectively (Figure 6b).

Several ideas on multiple particle cracking can be hypothesized based on Figure 6.

(1) Since the probability of particles cracking twice is not equal to a square of the probability of a particle cracking once, the probability of a particle cracking a second time is not identical to the probability of it cracking the first time.

(2) The dashed lines represent an identical probability of a particle cracking the first time and the second time. The data points are below the dashed line, which means particles have less probability of cracking a second time than a first time. Thus, it is more likely that another particle will crack the first time rather than a particle cracking the second time. The necessary conditions for a brittle particle to crack are that the particle has a defect; the defect is oriented properly to the stress axis (which means there is a stress component to propagate the defect); and the defect is of critical size at that stress. After a particle first cracks, the stress in the particle decreases, and the largest properly oriented defect is used. Thus, it would be expected that

probability of a second crack would be less than the probability of the first crack.

(3) Different aging treatments (matrix strength) can cause a different relationship between particles cracking once and cracking twice. In most cases, at a given probability of particles cracking once, the composites with higher matrix strength have the higher probability to crack twice than the composites with lower matrix strength. This result may be due to the higher strength matrix allowing the stress level of cracked particle to increase to a sufficient level to cause a second crack to form.

(4) Particle size affects the relationship between particle cracking once and twice for composites aged for 14 hours. The probability of large particles cracking twice is higher than that for small particles. This result may be due to the larger particles still having a high probability of having a flaw of sufficiently large size to fracture. Only under the severe condition of peak-aging does the effect of particle size appear, since under-aged composites do not exhibit the effect of particle size, which indicates that stress level is a very important factor affecting particle crack behavior. However, more work is needed to better understand the mechanisms of multiple cracking, and effects of matrix strength, particle size, aspect ratio, and probably other factors on multiple cracking.

SUMMARY

A method was developed to quantify particle cracking behavior as a function of strain that does not utilize surface measurements. The new surface area created by particle cracking and the number frequency of cracked particles were found to be approximately linear as a function of local strain along the tensile specimen. The new surface area created by particle cracking per unit strain was not significantly affected by reinforcing particle size but did increase with increasing matrix strength. The number frequency of cracked particles was affected by both reinforcing particle size and matrix strength. The composite materials reinforced with large particles or heat treated to high matrix strength exhibited a higher percentage of cracked particles. These results can be interpreted by considering the roles of stress and defect size on the fracture behavior of the SiC particles. The small particles are less likely to crack since they generally have smaller defects than do the large particles. In addition, the particles in the composites with high matrix strength are more highly stressed and, therefore, are more likely to fracture. The results of multiple regression confirms the effects of local strain, matrix yield strength, and particle size on S_V and number frequency of cracked particles. The number frequency of weighted total cracks (F_W) and the new surface area created by particle cracking (S_V) are related, which was

confirmed by the agreement of the calculated S_V and the measured S_V. Multiple cracks in a single particle were more frequently observed in composite materials reinforced with large particles. It was found that the probability of a particle cracking a second time was less than the probability of it cracking the first time. This relationship was affected by both matrix strength and particle size.

ACKNOWLEDGMENTS

The support of the Alabama NSF-EPSCoR Composites Program is gratefully acknowledged.

REFERENCES

1. D.J. Lloyd: *Acta Metall. Mater.*, 1991, vol. 39, pp. 59-71.

2. J. Llorca, A. Martin, J. Ruiz, and M. Elices: *Metall. Trans. A*, 1993, vol. 24A, pp. 1575-88.

3. P.M. Singh and J. J. Lewandowski: *Metall. Trans. A*, 1993, vol. 24A, pp. 2531-43.

4. Jian Ku Shang, Weikang Yu, and R.O. Ritchie: *Mater. Sci. Eng.*, 1988, vol. A102, pp. 181-92.

5. Y. Flom and R.J. Arsenault: *6th International Conf. on Composite Materials/Second European Conf. on Composite Materials (ICCM VI/ECCM2)*, F.L. Matthews, N.R. Buskell, J.M. Hodgkinson, and J. Morton, eds., Elsevier Applied Science, London and New York, 1987, vol. 2, pp. 2189-98.

6. B.J. Weng, S.T. Chang, and J.S. Shiau: *Scripta Metall.*, 1992, vol. 27, pp. 1127-32.

7. J.J. Lewandowski, D.S. Liu, and C. Liu: *Scripta Metall.*, 1991, vol. 25, pp. 21-26.

8. J. Yang, C. Cady, M.S. Hu, F. Zok, R. Mehrabian, and A.G. Evans: *Acta Metall.*, 1990, vol. 38, pp. 2613-19.

9. Y. Brechet, J.D. Embury, S. Tao, and L. Luo: *Acta Metall. Mater.*, 1991, vol. 39, pp. 1781-86.

10. M. Manoharan and J.J. Lewandowski: *Acta Metall.*, 1990, vol. 38, pp. 489-96.

11. J.J. Lewandowski, C. Liu, and W.H. Hunt, Jr.: *Mater. Sci. Eng.*, 1989, vol. A107, pp. 241-55.

12. C.P. You, A.W. Thompson, and I.M. Bernstein: *Scripta Metall.*, 1987, vol. 21, pp. 181-85.

13. Young-Hwan Kim, Sunghak Lee, and N.J. Kim: *Metall. Trans. A*, 1992, vol. 23A, pp. 2589-96.

14. Zhirui Wang and R.J. Zhang: *Metall. Trans. A*, 1991, vol. 22A, pp. 1585-93.

15. A.K. Vasudevan, O. Richmond, F. Zok, and J.D. Embury: *Mater. Sci. Eng.*, 1989, vol. A107, pp. 63-69.

16. D.S. Liu, M. Manoharan, and J.J. Lewandowski: *Metall. Trans. A*, 1989, vol. 20A, pp. 2409-17.

17. C.S. Lee, Y.H. Kim, T. Lim, and K.S. Han: *Scripta Metall.*, 1991, vol. 25, pp. 613-18.

18. D.L. Davidson: *Metall. Trans. A*, 1991, vol. 22A, pp. 113-23.

19. S.R. Nutt: in *Interfaces in Metal Matrix Composites*, TMS-AIME, Metals Park, OH, 1986, pp. 157-67.

20. W.H. Hunt, Jr., J.R. Brockenbrough, and P.E. Magnusen: *Scripta Metall.*, 1991, vol. 25, pp. 15-20.

21. G.M. Janowski and B.J. Pletka: *Mater. Sci. Eng.*, 1990, vol. A129, pp. 65-76.

22. D.J. Nans, G.B. Batson, and J.L. Lott: *Fracture Mechanics of Ceramics*, Plenum Press, New York, NY, 1974, vol. 2, pp. 489.

THE EFFECTS OF MATRIX PROPERTIES ON REINFORCEMENT FRACTURE IN MMCS

B. WANG and GREGG M. JANOWSKI

Submitted to Metallurgical and Materials Transactions A

ABSTRACT

The influence of matrix properties and reinforcement size on particle cracking behavior during tensile deformation of both aluminum and copper matrix composites has been investigated. These composite systems were fabricated by powder metallurgy methods and reinforced with 9 vol pct of either 23, 63, or 142 μm SiC particulates. Two fracture features, new surface area created by particle cracking (S_V) and the number fraction of cracked particles (F_{No}), were quantitatively measured in the sample interior. They were found to be approximately linearly dependent on the local strain along the tensile specimen within the gage length. The number fraction of cracked particles was affected by reinforcement particle size and matrix yield strength for both composite systems. The composites reinforced with large particles or with high matrix yield strength exhibited a higher percentage of cracked particles. The new surface area created by particle cracking per unit strain was not significantly affected by particle size but was strongly dependent on the matrix yield strength. The investigation of copper matrix composites in addition to aluminum matrix composites (which broadens the range of matrix yield strength) further demonstrates the effect of matrix yield strength on particle cracking behavior. The higher the matrix strength, the higher the slope of S_V for both matrix systems with an

approximately linear relationship. The comparison of two matrix systems indicated that particles cracked during elastic deformation and that matrix Young's modulus affected the particle cracking behavior. The higher the matrix Young's modulus, the fewer the cracked particles (both S_V and F_{No}) for a given stress and particle size. These results suggest that matrix Young's modulus may have a significant effect on particle fracture in the case of low plastic deformation.

INTRODUCTION

Studies of particle-reinforced aluminum matrix composites have shown that composite failure takes place by the nucleation, growth, and coalescence of voids associated with SiC particles.[1-7] The void nucleation rate at or near the particles depends upon the matrix properties, the reinforcement characteristics, and composite processing. Particle cracking, interfacial debonding, and/or failure initiation in the matrix are possible causes of void nucleation. It has been shown that cracking of the large and high-aspect ratio SiC particles is the dominant mechanism for void nucleation in many aluminum matrix composites.[1-6] Similar results have been reported in the high strength aluminum alloys and hypereutectoid spheroidized steels with large second phase particles.[8-11]

Quantitative microscopy has been utilized to examine particle cracking behavior during composite deformation.[1-3, [5,12,13] These investigations used different fabrication methods (powder processing, casting, and spray codeposition with or without secondary processing), different matrix alloys (2XXX, 3XXX, 6XXX, and 7XXX series), and different SiC particle sizes (from 5 µm to 142 µm) and volume fractions (9 to 20 vol pct). The results of these investigations have led to the generalizations that the fraction of cracked particles increases as (1) plastic strain increases, (2) matrix strength increases, and (3) particle size increases. It should be noted that a direct comparison between these results is difficult due to the factors discussed above as well as measurements being carried out either in the interior or on the surface of the specimen.

Particle cracking behavior differs when particles are located on the surface or in the interior of the specimen.[5,14] Several differences contribute to this observation, including stress state and the thermal residual stresses. The surface is in a state of plane stress, whereas large triaxial stresses are developed inside the specimen due to the nearly plane strain condition. Therefore, the large triaxial stresses cause more small particles to crack at low strains inside the specimen.[5] The compressive residual stresses are easily relaxed on the surface, whereas, the compressive stress has to be overcome before the particle can crack inside of the specimen. Finally, polishing reduces the particle size on the surface and decreases the population of surface defects, which would be expected to decrease particle cracking on the surface. Detailed studies[5,14] have shown that the results of *in situ* investigations of surface cracks only correctly describe the micromechanism of crack propagation. However, the quantitative measurements of particle cracking on the surface do not accurately represent the particle cracking behavior of the interior.

The effect of matrix properties (such as yield strength, flow stress, and age-hardening) on particle cracking behavior has been extensively studied. However, these studies were limited to aluminum matrix composites; results from matrices other than aluminum have not been reported. In order to better understand the role of a broader range of matrix properties on particle cracking behavior, a different matrix system is required. Copper alloys are ideal: they have different properties than aluminum alloys (such as Young's modulus, yield strength, and strain hardening exponent), and they can be fabricated by powder metallurgy (P/M), which makes comparisons with the previous results possible.

The present study will investigate the effects of Al-based and Cu-based matrices as well as particle size (in the range of 23 μm to 142 μm) on particle cracking during composite deformation by quantitatively measuring particle cracking as a function of plastic strain. The particle cracking in solutionized 201/SiC/9_p will be quantitatively measured to examine the effect of very low matrix yield strength. In addition, particle cracking behavior of two SiC particle reinforced Cu alloys will be examined. Comparisons with previous results using higher strength Al matrices[1] will be made.

EXPERIMENTAL PROCEDURE

The aluminum matrix composites used in this study are alloy 201 (Al-4.4 wt.% Cu-0.5 wt.% Mg-0.8 wt.%Si) reinforced with 9 vol.% of 23 µm, 63 µm, or 142 µm SiC particulate, which were fabricated by P/M processing. The mixed composite powders were compacted in a molded tensile bar die with zinc stearate die wall lubricant using a mechanical press and 486 MPa of pressure to obtain a green density of 96-97 pct of the theoretical values. The specimens were degassed at 400 °C ± 3 °C for 1 hour under a low vacuum and sintered at 600 °C ± 3 °C for 1 hour in a nitrogen atmosphere. The as-sintered specimens had greater than 97 pct of their theoretical densities. The as-sintered specimens were solutionized at 510 °C ± 3 °C for 45 minutes, followed by a cold water quench and immediately followed by tensile testing.

The copper-based alloys and processing procedure used in this study were developed to achieve strong bonding with SiC particles and high density. The copper alloy Cu-7 wt.% Al-2 wt.% Mg-2 wt.%Si (Cu7) was developed based upon cast alloy

C95600 (Cu-7 wt.% Al-2 wt.% Si). The fracture surfaces showed that many SiC particles cracked and few particles debonded, which is indicative of strong interfacial bonding. Another copper alloy, Cu-8 wt.% Al-2 wt.% Mg-2 wt.%Si (Cu8), was developed to achieve a higher yield strength without sacrificing the interfacial bonding and density.

The copper-based alloys were prepared by blending elemental Cu, Al, Mg, and Si powders to attain the composition Cu-7 wt.% Al-2 wt.% Mg-2 wt.% Si and Cu-8 wt.% Al-2 wt.% Mg-2 wt.% Si. The powders for the copper matrix composite materials were produced by blending 9 vol.% of SiC particles (nominally 23 μm, 63 μm, and 142 μm in diameter) with the premixed copper matrix powder. The mixed composite powders were then cold compacted in a standard powder tensile test specimen die with zinc stearate die wall lubricant using a mechanical press and 552 MPa to obtain a green density of 92 pct of the theoretical values. The specimens were sintered at 800 °C ± 3 °C for 1 hour under a high vacuum (between 10^{-2} and 10^{-4} Pa). The as-sintered composite materials had greater than 95% of their theoretical density. The SiC particles were well dispersed and randomly oriented in the matrix.

The local plastic strains were determined by measuring the distance between microhardness indentations with less than 1% relative measuring error before and after tensile testing using an image processing system and an optical microscope.

The microhardness indentations were placed along the gage length of the tensile specimen and were nominally 0.5 mm apart. The tensile tests were carried out using a servo-hydraulic testing machine and an initial strain rate of 3×10^{-4}/s.

The new surface area per unit volume, S_V, and the number frequency of cracked particles, F_{No}, were determined as a function of position along the tensile axis of longitudinal sections of the specimens after testing using an optical microscope. This method eliminates questions regarding differences in cracking behavior of particles on the surface versus particles within the bulk. S_V was determined by measuring the number of test lines crossing the cracked surface per unit length, P_L[1]. F_{No} was determined by measuring both the number of cracked particles and the total number of particles in a test field. The ratio of the number of cracked particles to the total number of particles is F_{No}. Additional details have been reported previously.[1]

Power law regression was used to fit plastic strain as a function of position. Separate regressions were used for each side of the fracture surface, and the origins were set at the fracture surface. Since S_V and F_{No} are related to local strain

---

1 S_V is equal to P_L when the test line is normal to the feature being measured, as was the case in these maesurement.

and, therefore, position, combined plots of S_V as a function of strain and F_{No} as a function of strain were obtained using the assumption that the fracture surfaces are planar. A best fit linear regression was used, which was confirmed to be a statistically valid fit by testing the correlation coefficient with a 0.05 level of the significance, to fit both S_V and F_{No} as a function of local strain. The 95% confidence intervals of the slopes and y-intersects of these best fit lines were calculated so that error bounds were obtained, which will be shown in the case of S_V as a function of plastic strain.

The uniaxial stress-strain curve of particle reinforced MMC can be described by the Ramberg-Osgood relationship in the form of[15]:

$$\bar{\varepsilon} = \frac{\bar{\sigma}}{\bar{E}} + \alpha \left(\frac{\sigma_0}{E} \right) \left(\frac{\bar{\sigma}}{\bar{\sigma}_N} \right)^{\frac{1}{n}} \qquad [1]$$

and a matrix material can be represented by another Ramberg-Osgood relationship:

$$\varepsilon = \frac{\sigma}{E} + \alpha \left(\frac{\sigma_0}{E} \right) \left(\frac{\sigma}{\sigma_0} \right)^{\frac{1}{n}} \qquad [2]$$

where $\bar{\varepsilon}$ is composite strain, $\bar{\sigma}$ is composite stress, $\bar{E}$ is the composite Young's modulus (which is estimated by Halpin-Tsai equation[16]), α is constant (equal to 3/7), σ_0 is the matrix yield stress, E is the matrix Young's modulus, $\bar{\sigma}_N$ is the asymptotic reference stress of composite, and n is the strain-hardening exponent.

The experimental tensile stress-strain curves were fitted using Eq. [1] to extend the stress-strain curve beyond composite fracture. First, the matrix stress-strain curves were fitted using Eq. [2] to obtain n, σ_0, and α. Then, σ_0 and α were directly substituted into Eq. [1]. In order to obtain the most accurate representation of the composite stress-strain curve, n and $\overline{\sigma}_N$ in Eq. [1] were chosen based on n from the matrix fitting and composite yield stress, respectively.

RESULTS

Microstructure

Typical micrographs of alloy 201 and 7 Cu are shown in Figure 1. Constituent phases and oxide particles lie along the grain boundaries in alloy 201, which were identified as (Fe, Cu)(Al, Cu)$_6$, $CuMg_5Si_4Al_4$, $CuMg_4Al_6$, $CuFeAl_7$, and $MgAl_2O_4$.[17] Equiaxed grains with twins were observed in the Cu-based alloy. Microstructures of Cu7 and Cu8 are essentially the same. X-ray diffraction was used to identify the microconstituents in Cu8. The lattice parameter of the FCC Cu matrix was increased by the addition of Al and Si; a value of 0.3662 nm was measured, compared to a value of 0.3615 nm for pure Cu. The predicted phases[18] Cu_5Si (κ), Cu_3Al (β), and Al_4Cu_9 (γ) were tentatively identified. Magnesium was not observed using SEM/EDS, which is likely due to its low amount

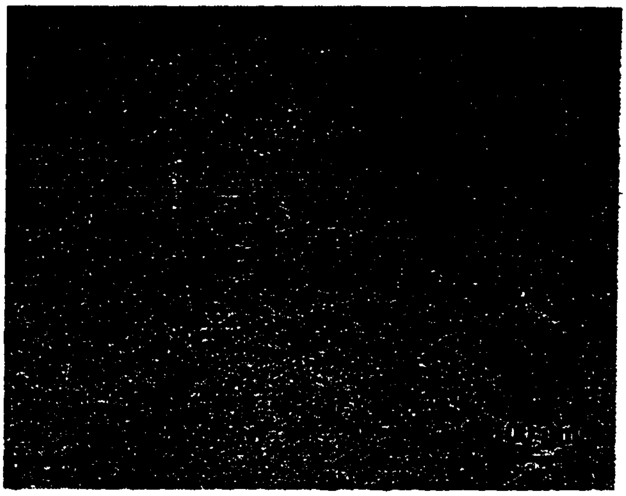

(a)

(b)

Fig. 1-Micrographs of the aluminum and copper matrices (a) alloy 201 and (b) Cu7.

and its high vapor pressure (≈4000 Pa) at sintering temperature. However, Mg additions were critical in obtaining a strong interfacial bond.

Typical micrographs of composites reinforced with 9 vol pct of 23 μm, 63 μm, and 142 μm SiC particles after tensile testing are shown in Figure 2, where the matrix is alloy 201. The tensile axes are horizontal in these micrographs. The particle cracking was evident throughout the gage length, with the highest degree of cracking at the fracture surface. Most cracks were oriented normal to the loading direction, and multiple cracks were observed in composites reinforced with large SiC particles.

Fractography of copper matrix composite showed that the matrix between the SiC particles is dimpled and that large amounts of cracked particles are present, even though some porosity is visible at the interface. This is indicative of strong interfacial bonding between SiC particles and copper-based alloys. A typical micrograph of fracture surface in a copper matrix composite is shown in Figure 3.

Tensile Properties

The tensile properties of alloy 201 and the alloy 201 matrix composites reinforced with 23 μm, 63 μm, and 142 μm SiC particles were measured immediately after solutionizing. The tensile property data (together with data from age-hardened alloy 201 and its composites[1]) are presented in Table I. The

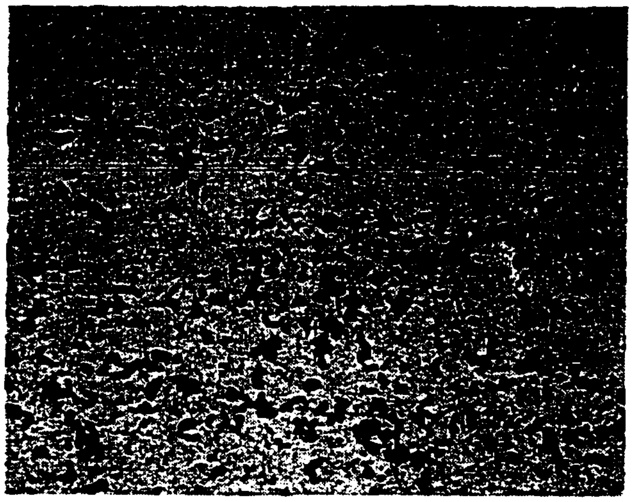

(a)

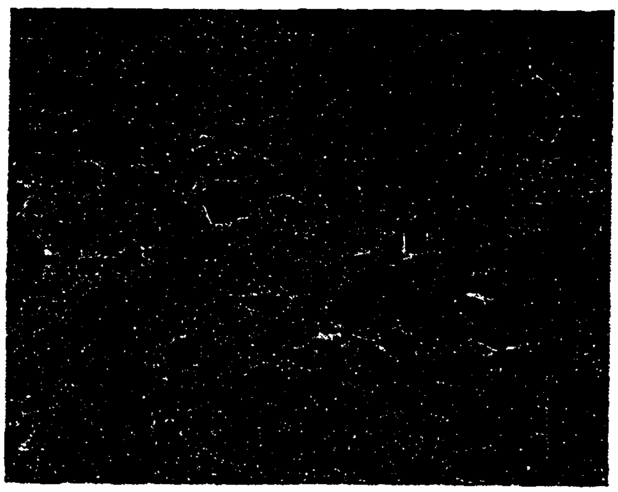

(b)

Fig. 2-Micrographs of alloy 201 reinforced with 9 vol pct of (a) 23 µm, (b) 63 µm, and (c) 142 µm SiC particles.

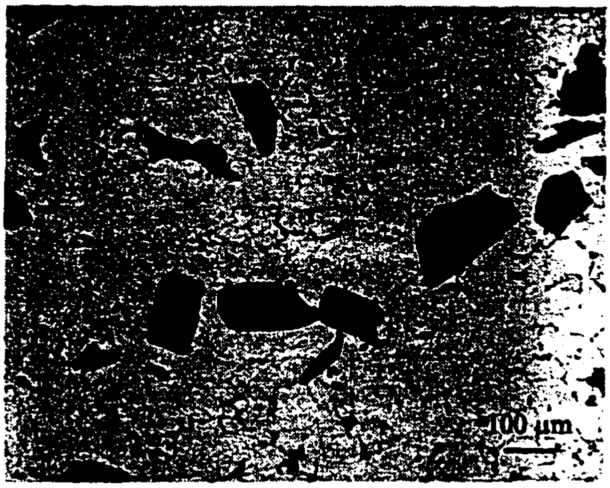

(c)

Fig. 2 (continued)

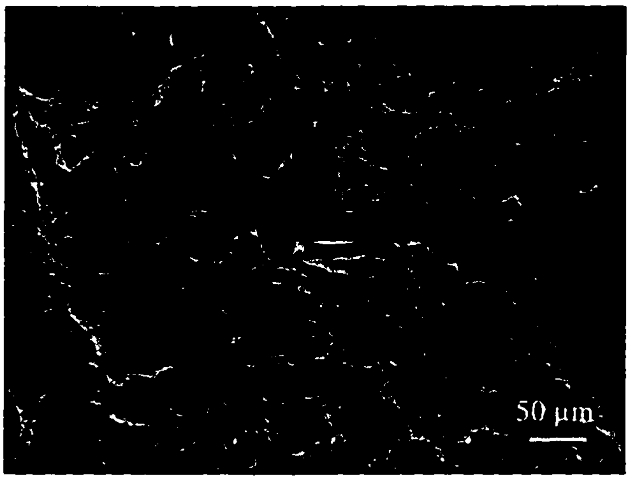

Fig. 3-Micrograph of the fracture surface for Cu8 reinforced with 142 µm SiC.

Table I:Tensile Properties for Alloy 201 and Alloy 201 Matrix Composites

Material	Aging Time at 160°C (Hrs.)	0.1% Offset Yield Strength (MPa)	Ultimate Tensile Strength (MPa)	Elongation to Failure (%)	Strain Hardening Exponent
Alloy 201	0	140	281	10	0.222
	1	193	275	2.5	0.124
	14	299	334	1.3	0.06
Alloy 201 + 9 vol.% 23 µm SiC	0	156	265	4.7	0.155
	1	172	236	3.5	0.102
	14	297	312	0.3	0.05
Alloy 201 + 9 vol.% 63 µm SiC	0	158	246	4.6	0.145
	1	196	240	1.7	0.085
	14	283	291	0.3	0.04
Alloy 201 + 9 vol.% 142 µm SiC	0	150	252	5.9	0.143
	1	196	217	1.5	0.064
	14	260	265	0.3	0.03

tensile properties of Cu7, Cu8, and these copper-based matrices reinforced with 23 µm, 63 µm, and 142 µm SiC particulate were measured after sintering. The tensile property data are presented in Table II.

The ultimate tensile strength (UTS) and elongation to fracture of the composites were lower than those in the unreinforced matrix alloy for the aluminum system. The addition of 9 vol.% SiC particles increased the 0.1% offset

Table II: Tensile Properties for Copper Alloys and Copper Matrix Composites

Materials	0.1% Offset Yield Strength (MPa)	Ultimate Tensile Strength (MPa)	Elongation to Failure (%)	Strain Harden Exponent
Cu7	218	257	1	0.1
Cu7 + 23 µm SiC	240	262	0.5	0.09
Cu7 + 63 µm SiC	219	241	0.6	0.08
Cu7 + 142 µm SiC	205	233	0.8	0.074
Cu8	280	326	1	0.065
Cu8 + 23 µm SiC	318	346	0.5	0.053

yield strength of composites with all three particle sizes, which is in contrast to the results in the same materials after 1 hour and 14 hours of aging at 160 °C.[1] The higher UTS in unreinforced matrix alloy is due to the greater elongation to fracture compared to the composites, even though the 0.1% offset yield strength is lower. The yield strength, UTS, and elongation of the composite materials were not a strong function of particle size in the as-solutionized composites, which differs from those in comparable data in age-hardened materials.[1]

The mechanical properties of the Al-based materials were strongly influenced by heat treatment. The 14-hour aged composites have the highest 0.1 pct offset yield strength, followed by the 1-hour aged and then the solutionized composites for all three particle sizes. The solutionized composites have the highest elongation to fracture, followed by the 1-hour aged and the 14-hour aged composites. The 14-hour aged composites have the highest UTS. The solutionized composites have higher UTS than the 1-hour aged composites, which is due to the higher elongation to fracture in the solutionized composites.

In the copper-based materials, UTS of the composites were lower than those of the matrix alloys except for the case of the 23 µm SiC-reinforced composites. Elongations to fracture of the composites were lower than those of the unreinforced matrix alloys. The addition of 9 vol.% SiC particles increased the 0.1% offset yield strength of composites except for the case of the 142 µm SiC composites. The yield strength and UTS of the composite materials were strongly affected by reinforcement particle size, especially in the case of high strength matrix (Cu8) composites. The composites containing the smallest particles exhibited the highest 0.1 pct offset yield strength and UTS, which is consistent with the results of aluminum matrix composites. Also, the effects of matrix strength on the yield strength and UTS are significant. The higher the matrix strength, the higher the 0.1 pct offset yield strength and UTS, which is consistent with the results of aluminum matrix composites. However, the elongation to fracture was not significantly affected by particle size and matrix strength, which differs from the results of the aluminum matrix composites.

Number Frequency of Cracked Particles

The number frequencies of cracked particles, F_{No}, as a function of plastic strain for as-solutionized alloy 201 reinforced with 9 vol.% of 23 µm, 63 µm, and 142 µm SiC are shown in Figure 4. For each particle size, F_{No} for each number of cracks per particle (from one crack to three cracks) was measured separately as strain varied. The Student t-statistic test showed that a strong correlation between F_{No} and local strain exists since the hypothesis that the slope[1] = 0 can be rejected with a 0.05 level of significance. The F_{No} values increase as local strain increases, and a linear regression was used, which is confirmed to be a statistically valid fit by testing the correlation coefficient with a 0.05 level of significance. These best fit lines are shown in Figure 4. The slopes of best fit lines (up to two cracks in each particle) for the solutionized composites and the age hardened composites are shown in Figure 5.

The data contained in Figure 4 demonstrate that larger SiC particles are more likely to be cracked than smaller

---

[1] The slope is the change in the mean of F_{No} corresponding to a unit increase in the local strain.

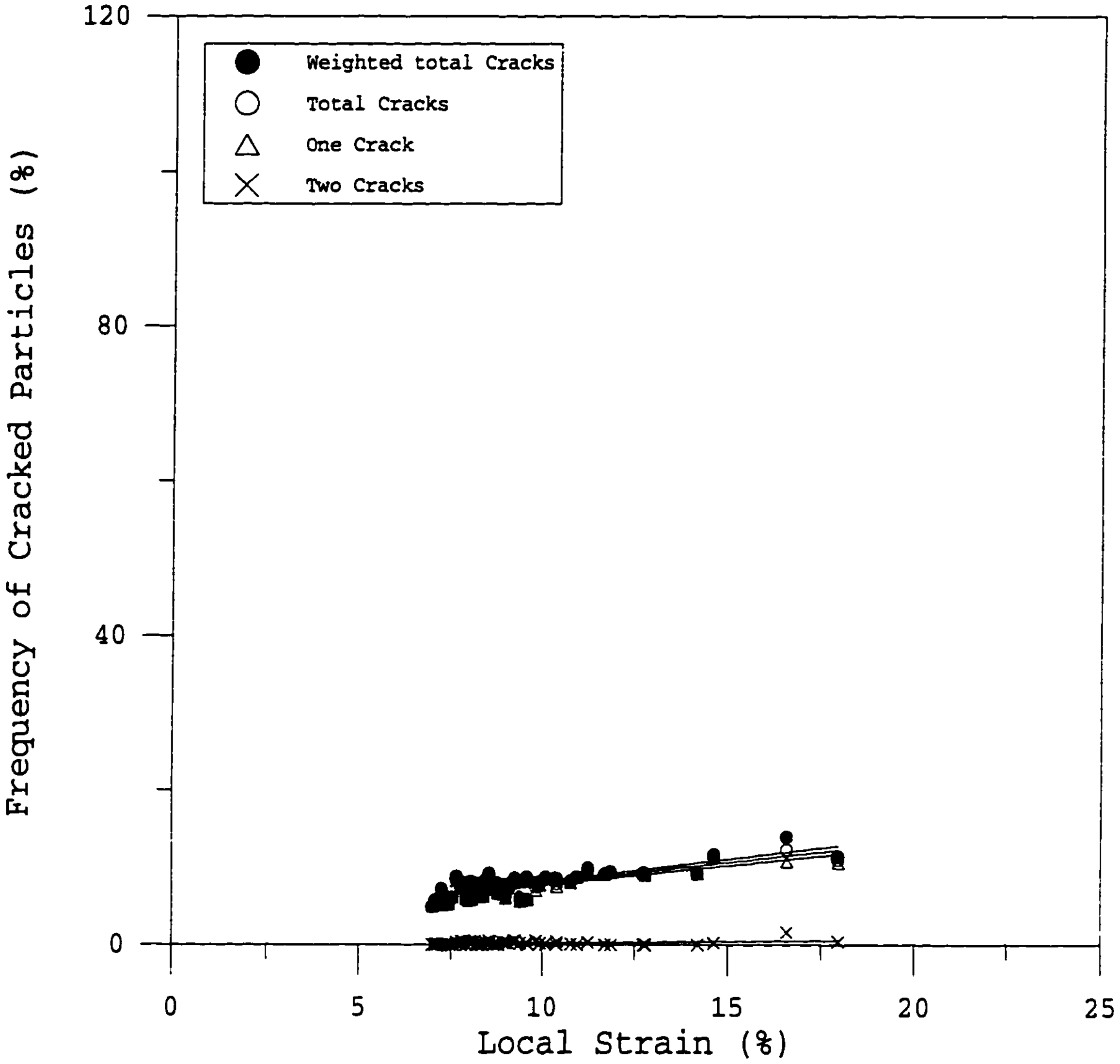

(a)

Fig. 4-F_{No} as a function of local strain for alloy 201 reinforced with 9 vol pct of (a) 23 μm, (b) 63 μm, and (c) 142 μm SiC solutionized. The solid lines are best fit lines.

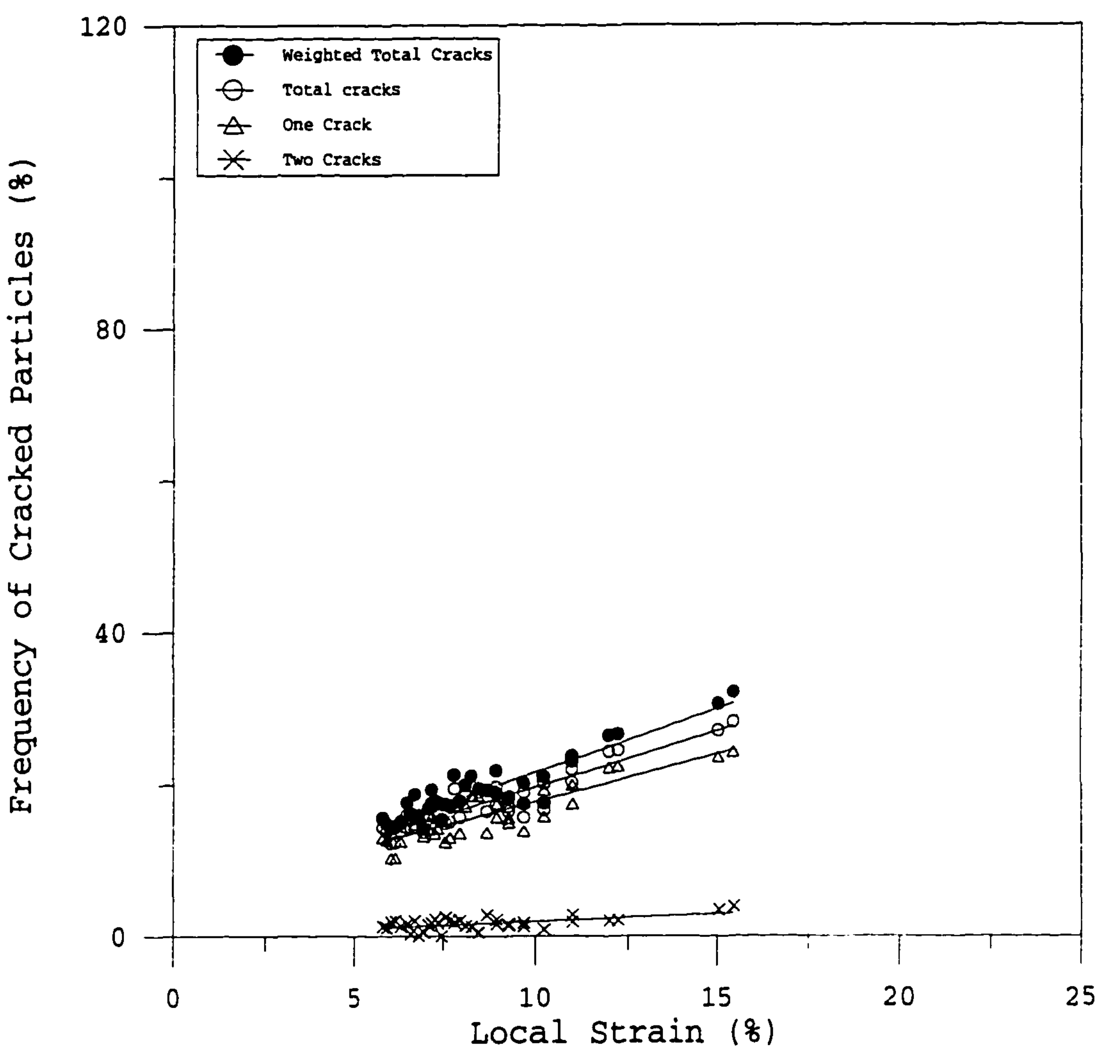

(b)

Fig. 4 (continued)

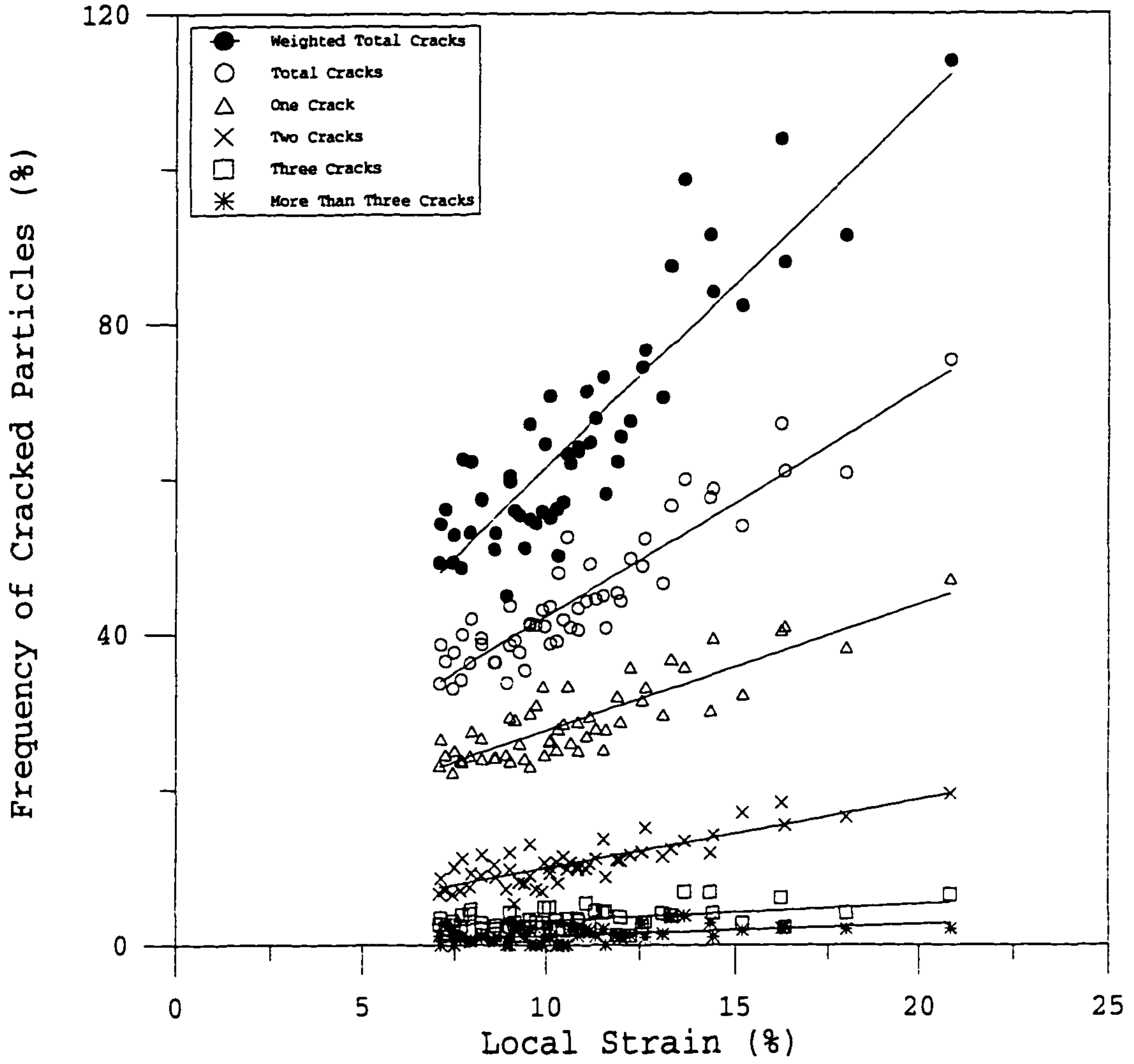

(c)

Fig. 4 (continued)

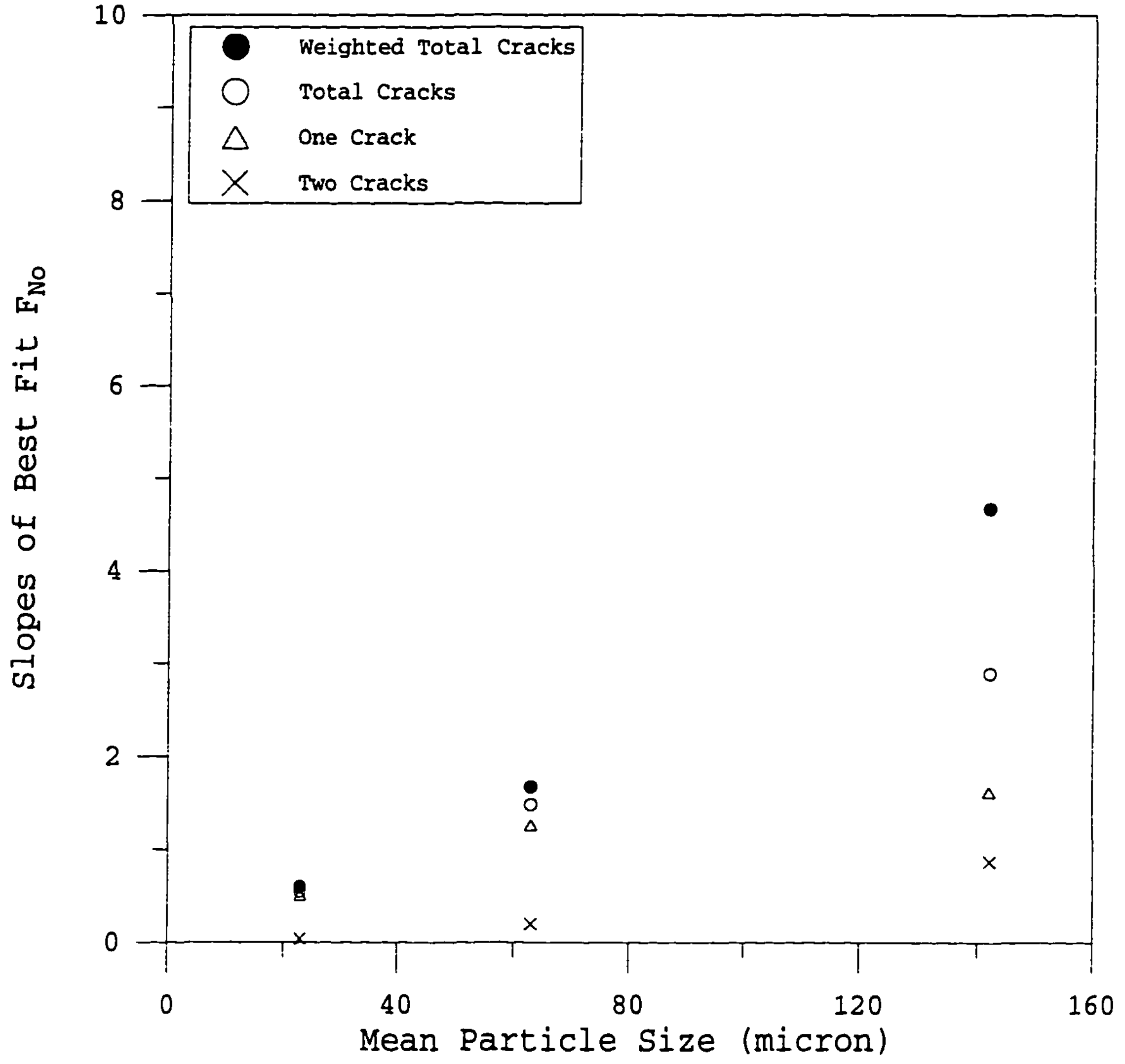

(a)

Fig. 5-The slopes of the best fit F_{No} as a function of mean particle size for alloy 201 reinforced with 9 vol pct SiC particles (a) solutionized, (b) aged for 1 hour, and (c) aged for 14 hours at 160 °C.

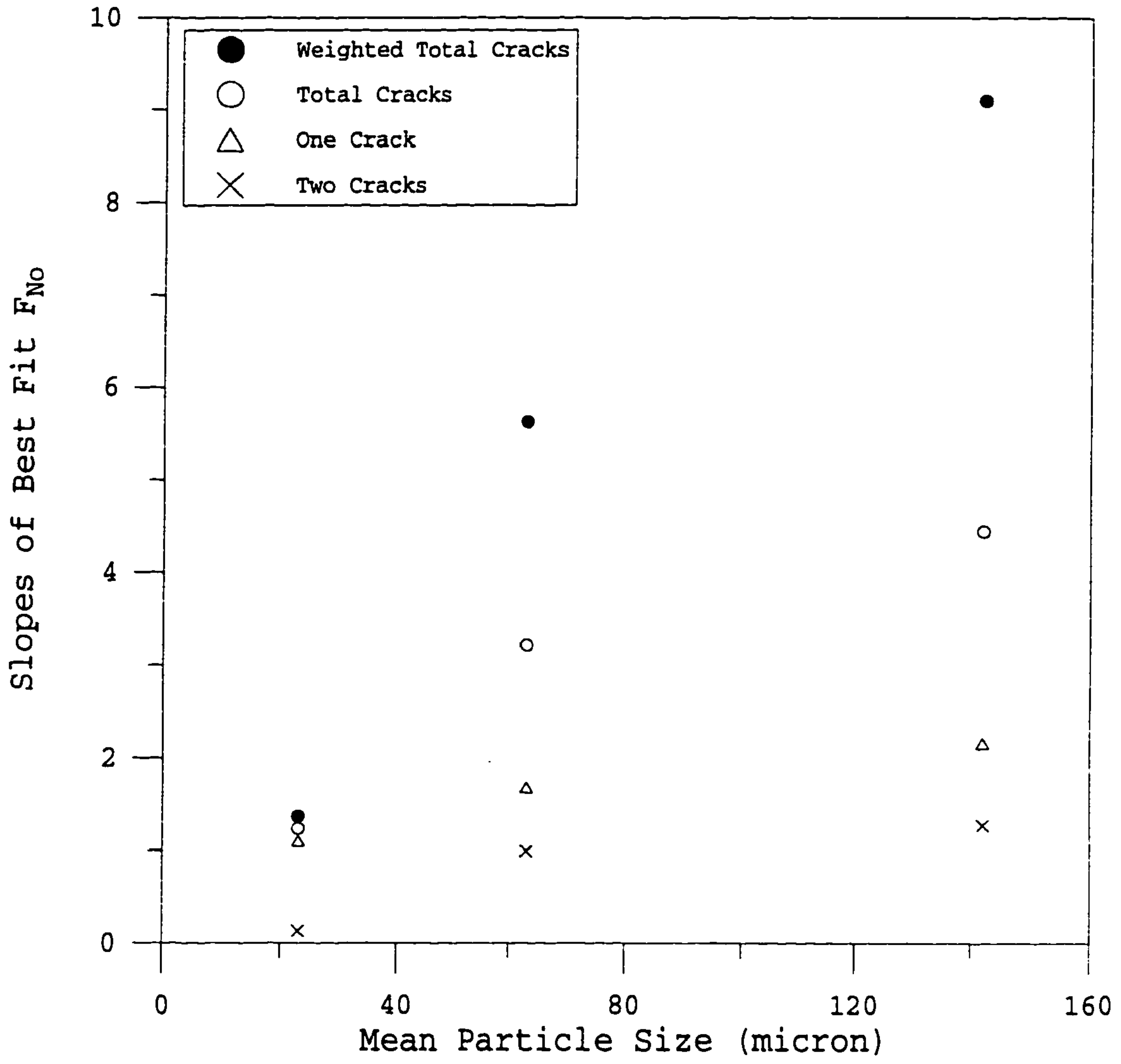

(b)

Fig. 5 (continued)

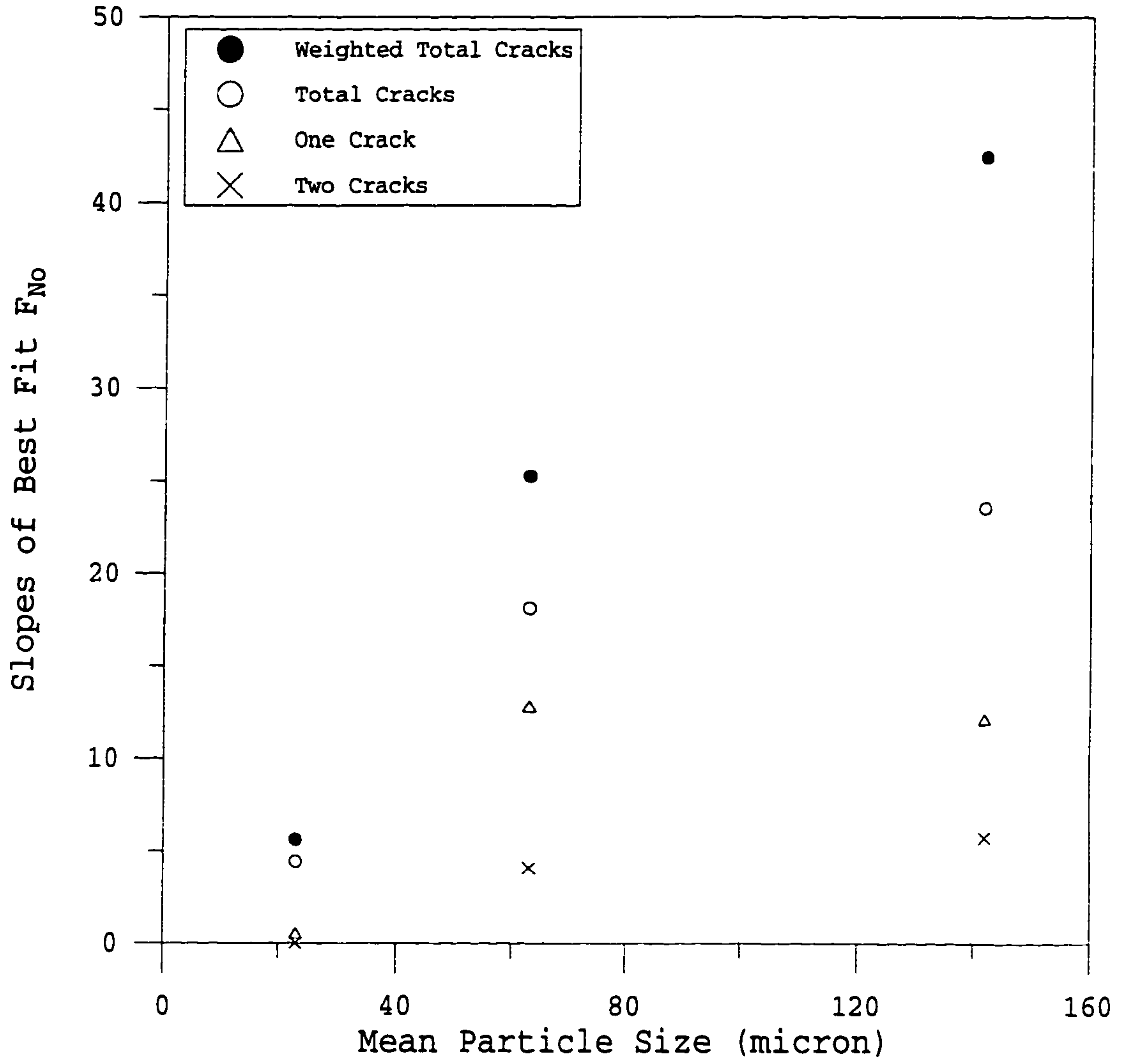

(c)

Fig. 5 (continued)

particles at a given strain for each number of cracks (*i.e.*, weighted total cracks,[2] total cracks,[3] one crack, two cracks, *etc.*), which is similar to the results of the age hardened 201 matrix composites. This effect can be clearly seen in these figures by considering the higher percentage of large particles cracked at a given strain and the higher slopes of the best fit lines in larger particle reinforced composites, which is confirmed to be statistically significant by the comparison of slopes for each number of cracks using the Student *t*-statistics.

The number frequency of cracked particles at a given strain and particle size increases as matrix strength increases (Figure 5). This change is reflected in increases in the slopes of the best-fit lines for each number of cracks, which was confirmed to be statistically significant by using Student's t-statistics with a 0.05 level of significance.

The number frequency of cracked particles, F_{No}, as a function of strain for Cu7 and Cu8 reinforced with 9 vol.% of 23 µm, 63 µm, and 142 µm SiC are shown in Figure 6. The values

---

2 The "weighted total cracks" is defined as the sum of the F_{No} values for each number of cracks multiplied by the corresponding number of the cracks, in which the effect of the multiple cracks is considered. Therefore, the weighted total cracks can be greater than 100%.

3 "Total cracks" is defined as the sum of the F_{No} values for each number of cracks. The maximum total cracks are equal to or less than 100%.

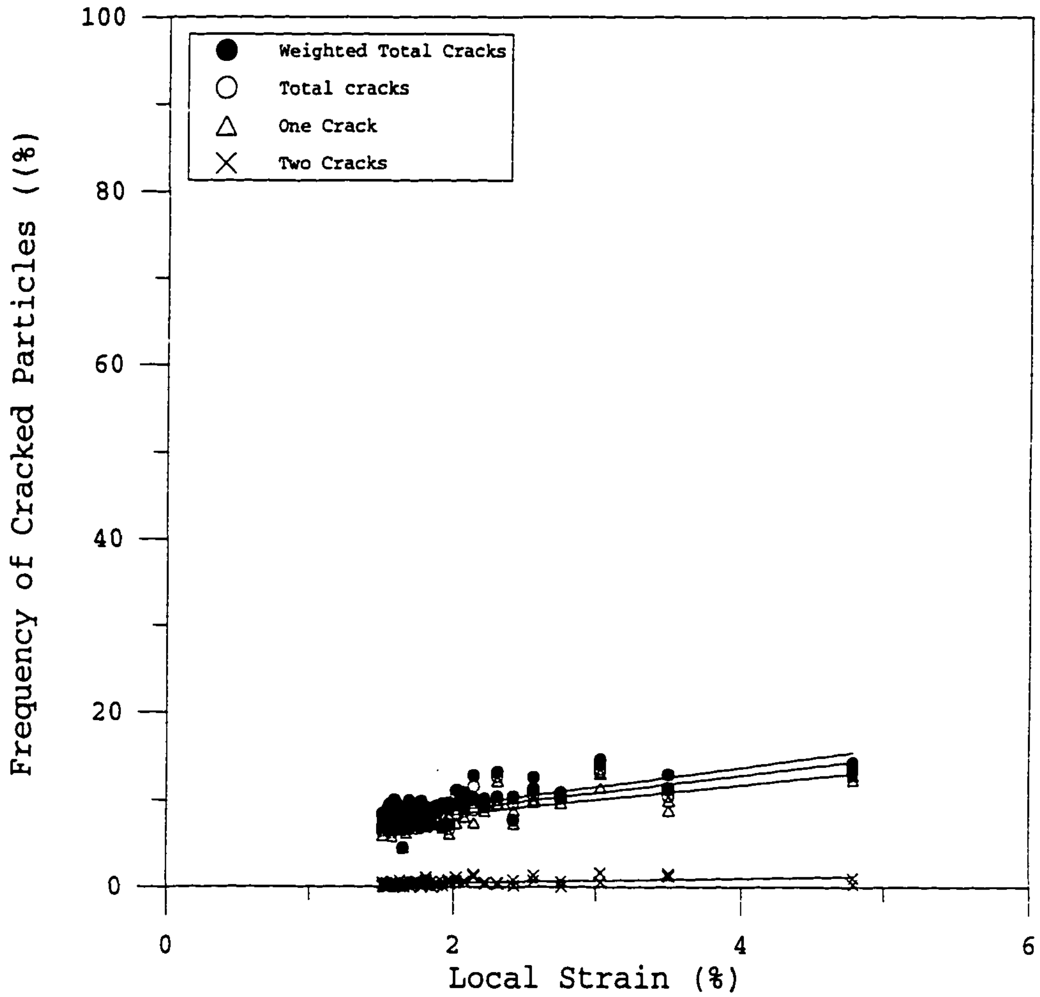

(a)

Fig. 6-F_{No} as a function of local strain for copper-based matrix reinforced with 9 vol pct of (a) 23 µm, (b) 63 µm, and (c) 142 µm SiC for Cu7 matrix composites and (d) 23 µm, (e) 63 µm, and (f) 142 µm SiC for Cu8 matrix composites. The solid lines are best fit lines.

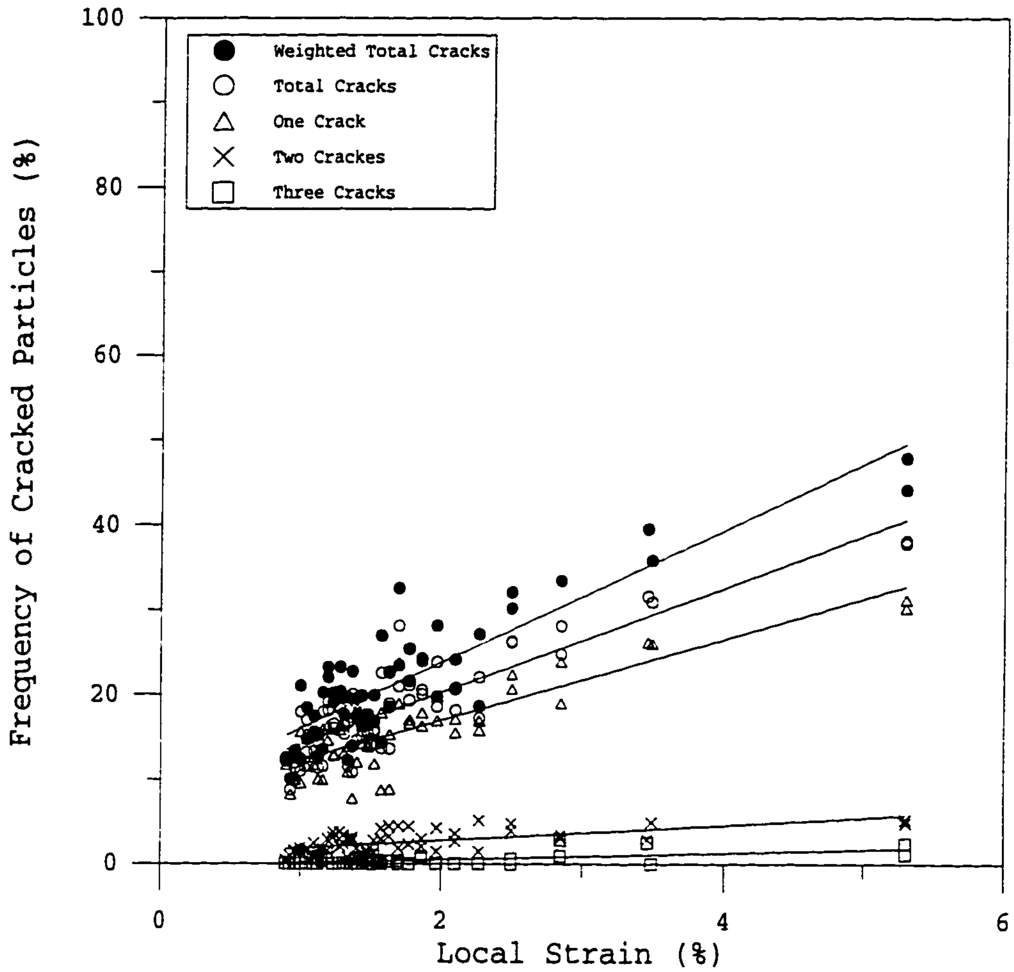

(b)

Fig. 6 (continued)

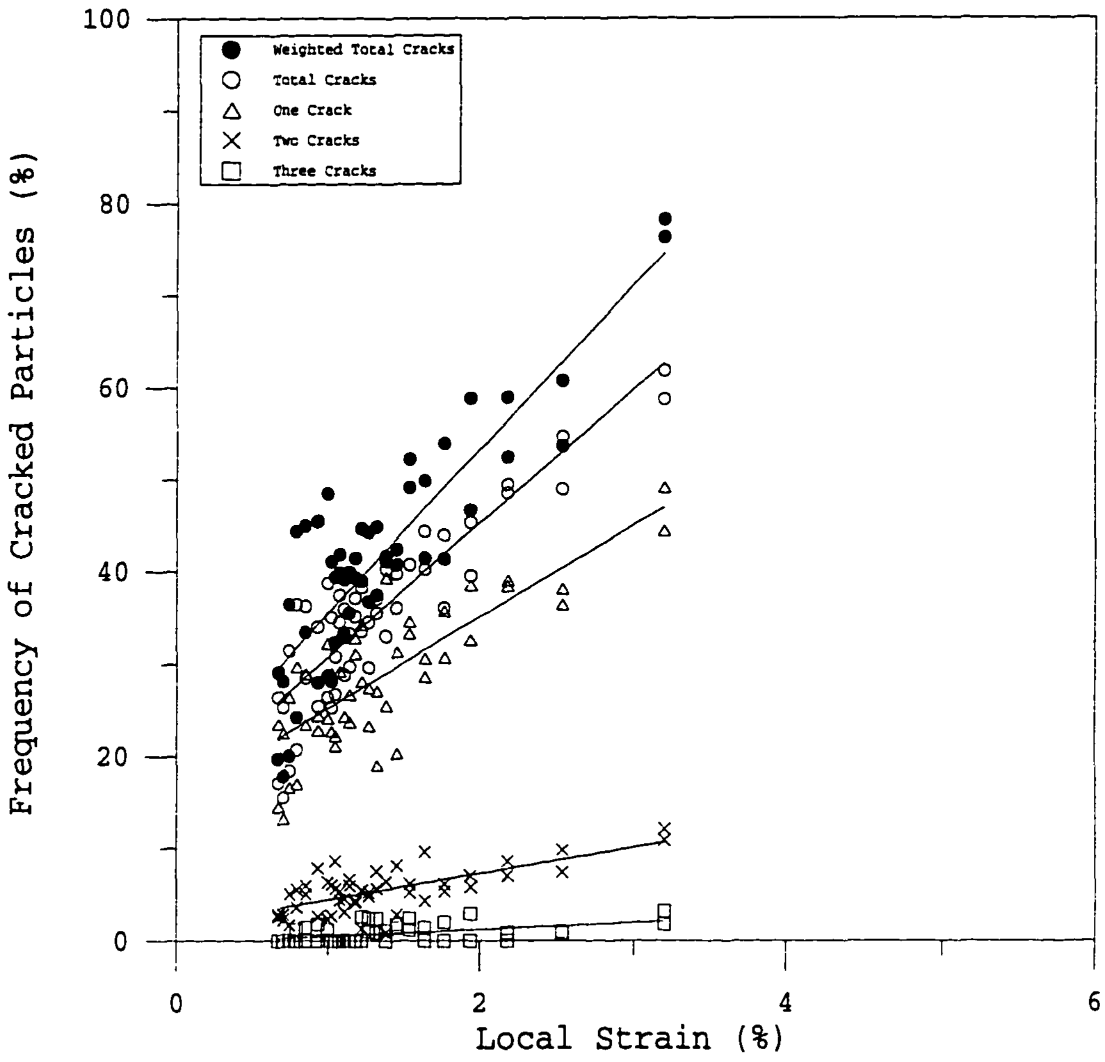

(c)

Fig. 6 (continued)

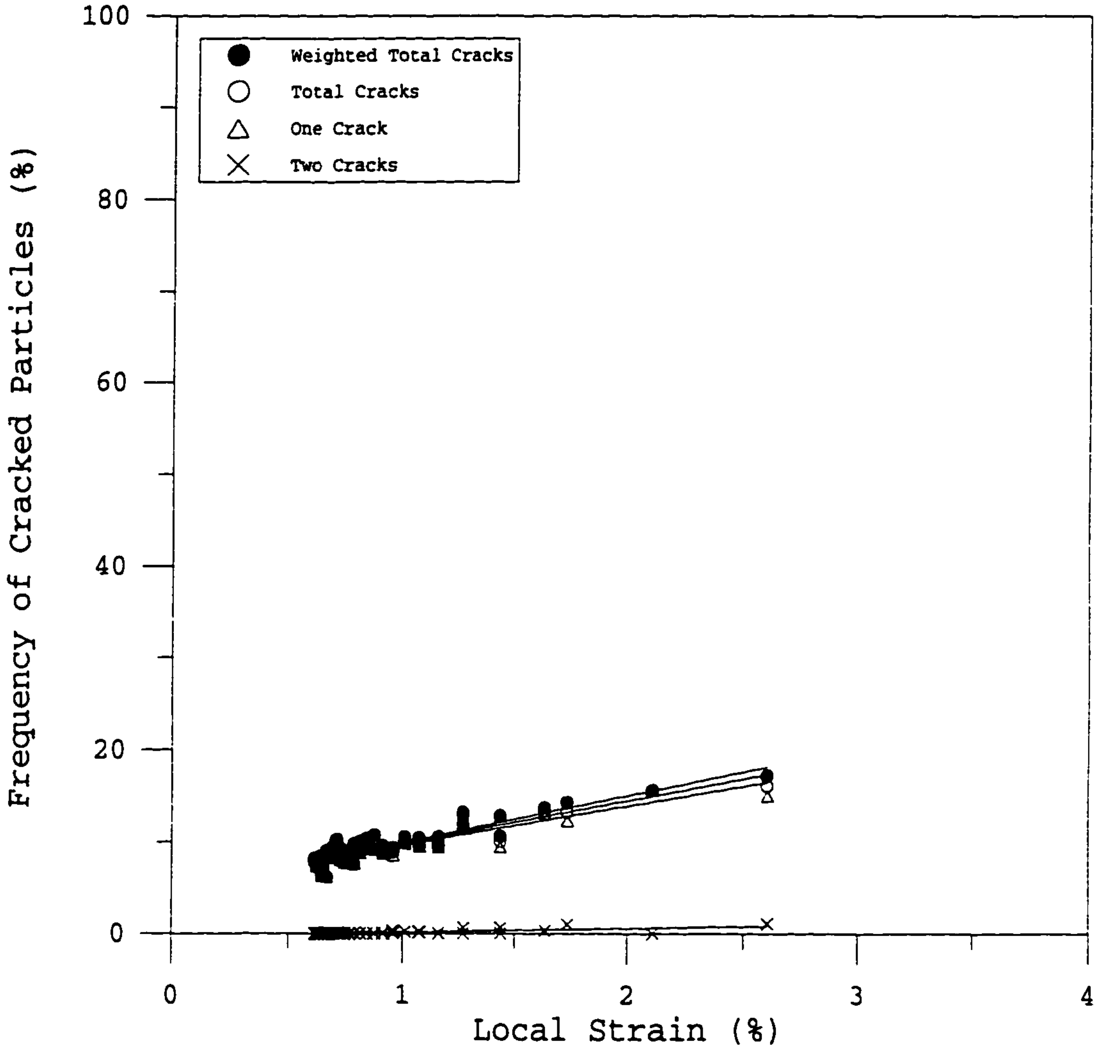

(d)

Fig. 6 (continued)

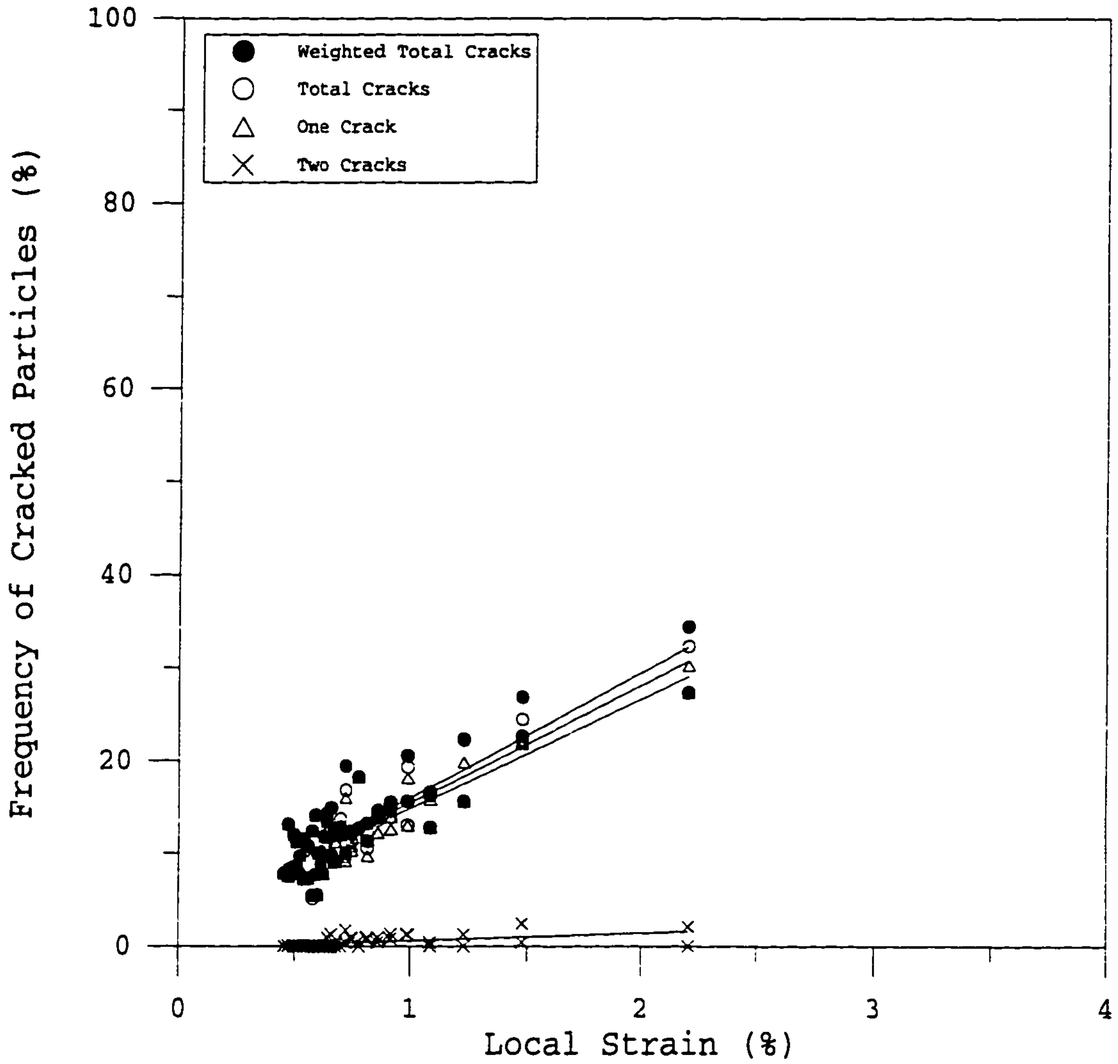

(e)

Fig. 6 (continued)

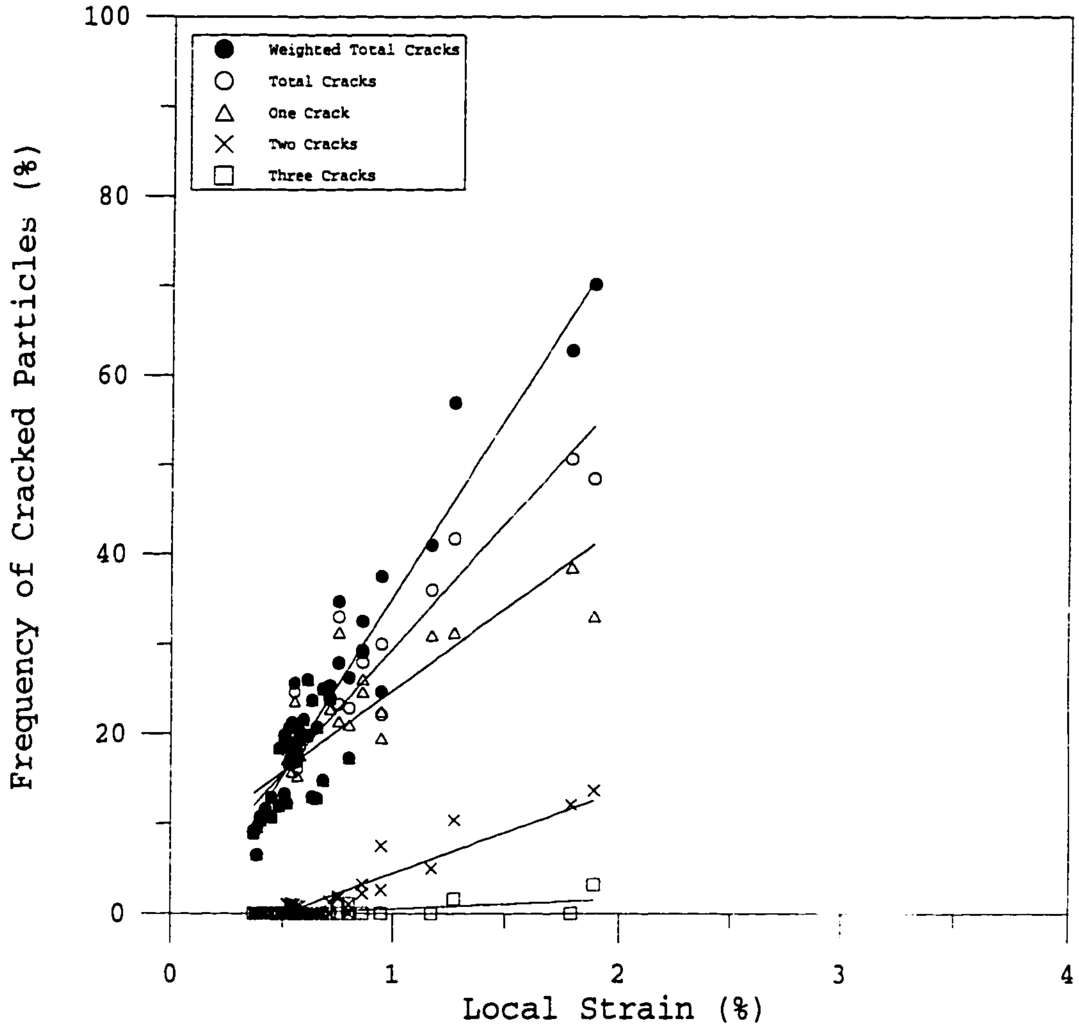

(f)

Fig. 6 (continued)

of F_{No} increase approximately linearly as plastic strain increases. It is apparent that increasing the matrix strength increases the number frequency of cracked particles at a given strain and particle size, which are shown in the summary plots (Figure 7) of the slopes of best fit lines. The larger SiC particles are more likely to be cracked than the smaller particles at a given strain and aging treatment. These results are consistent with the results from the aluminum system. (The same statistic analyses were applied to the data from the copper systems.)

S_V Measurements

The results of the new surface area created by particle cracking per volume, S_V, as a function of strain for solutionized alloy 201 reinforced with 9 vol.% of 23 µm, 63 µm, and 142 µm SiC are shown in Figure 8. S_V increases approximately linearly as local plastic strain increases. A linear regression was used, which was confirmed to be a statistically valid fit by testing the correlation coefficient with a 0.05 level of significance. The slopes and y-intercepts of the linear regressions with 95% confidence intervals were calculated and are also shown in Figure 8, where the envelopes indicate these error bounds. Also, the slopes of best fit lines for the solutionized and the age-hardened composites are summarized in Figure 9.

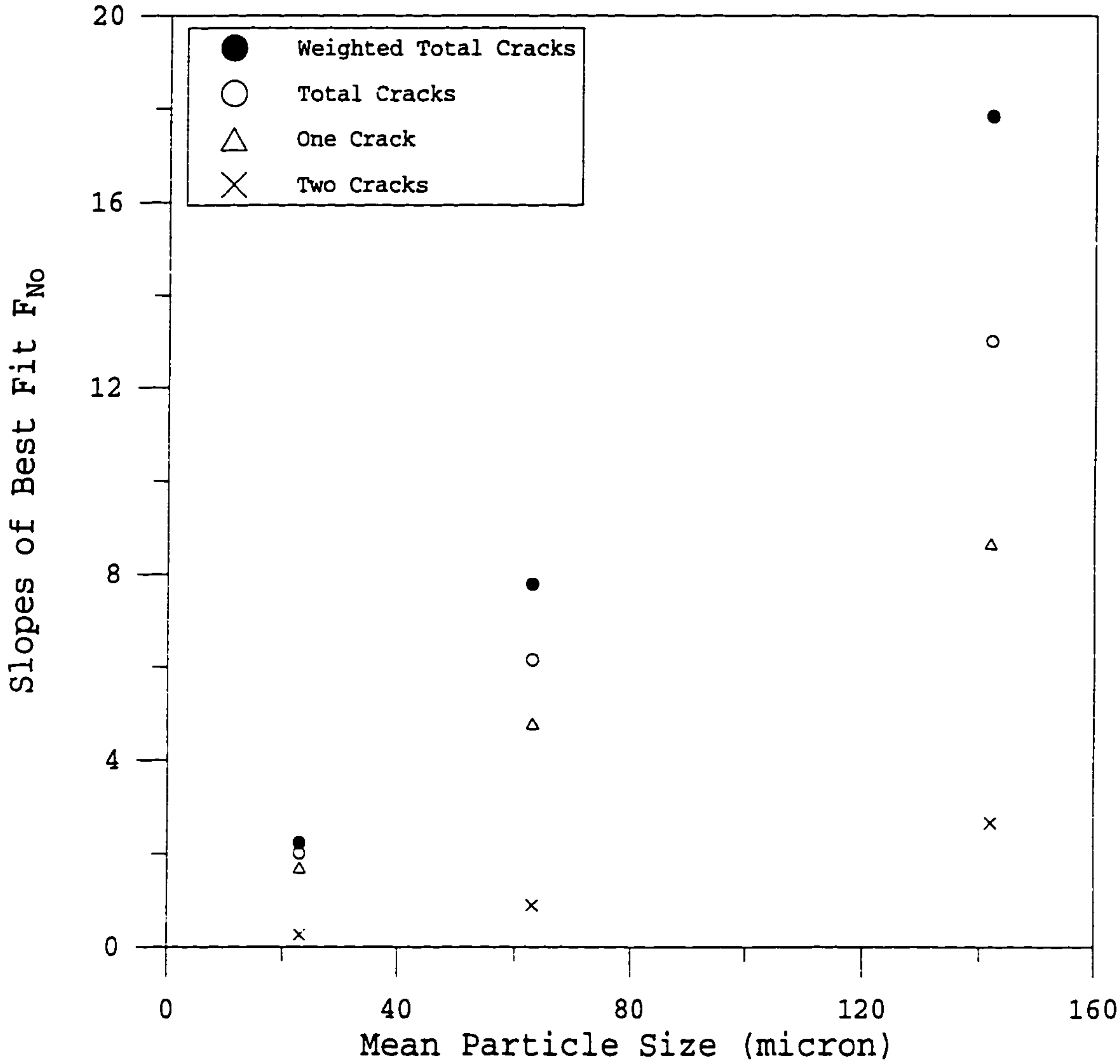

(a)

Fig. 7-The slopes of the best fit F_{No} as a function of mean particle size for copper-based matrix reinforced with 9 vol pct SiC particle (a) Cu7 matrix composites and (b) Cu8 matrix composites.

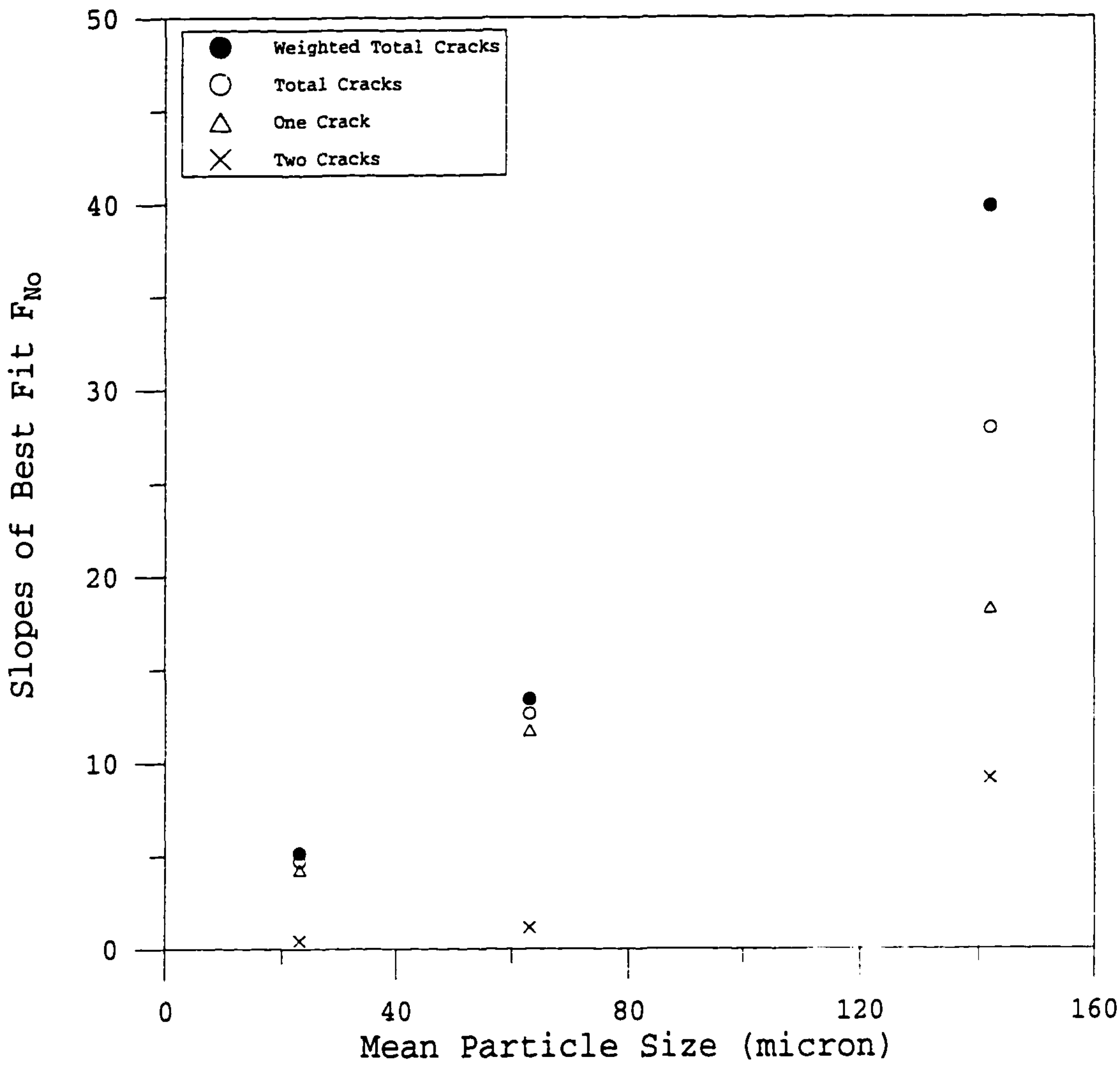

(b)

Fig. 7 (continued)

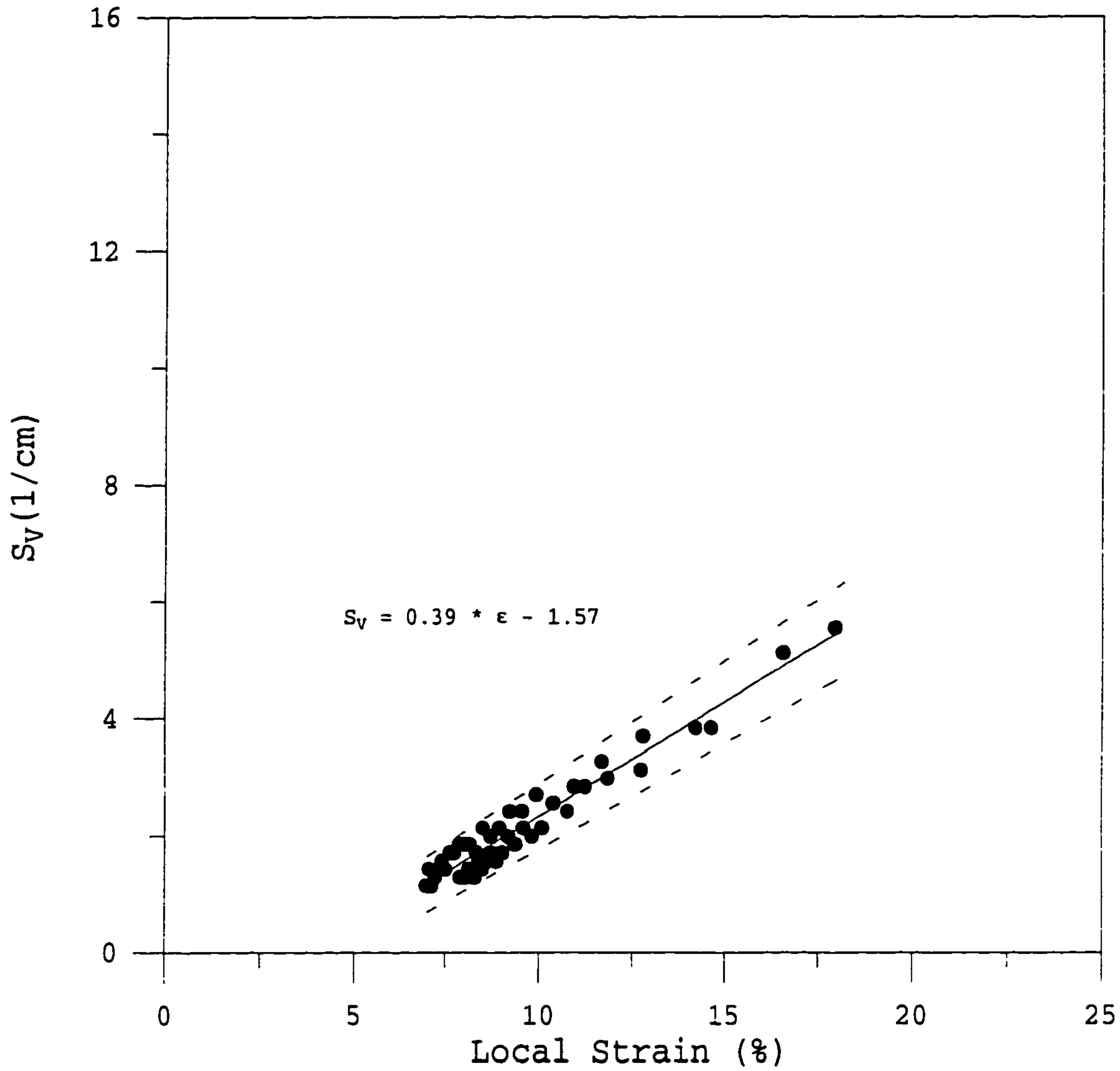

(a)

Fig. 8-S_v as a function of local strain for alloy 201 reinforced with 9 vol pct of (a) 23 μm, (b) 63 μm, and (c) 142 μm SiC solutionized. The solid lines are the best fit lines. The dotted lines represent upper and lower error bounds.

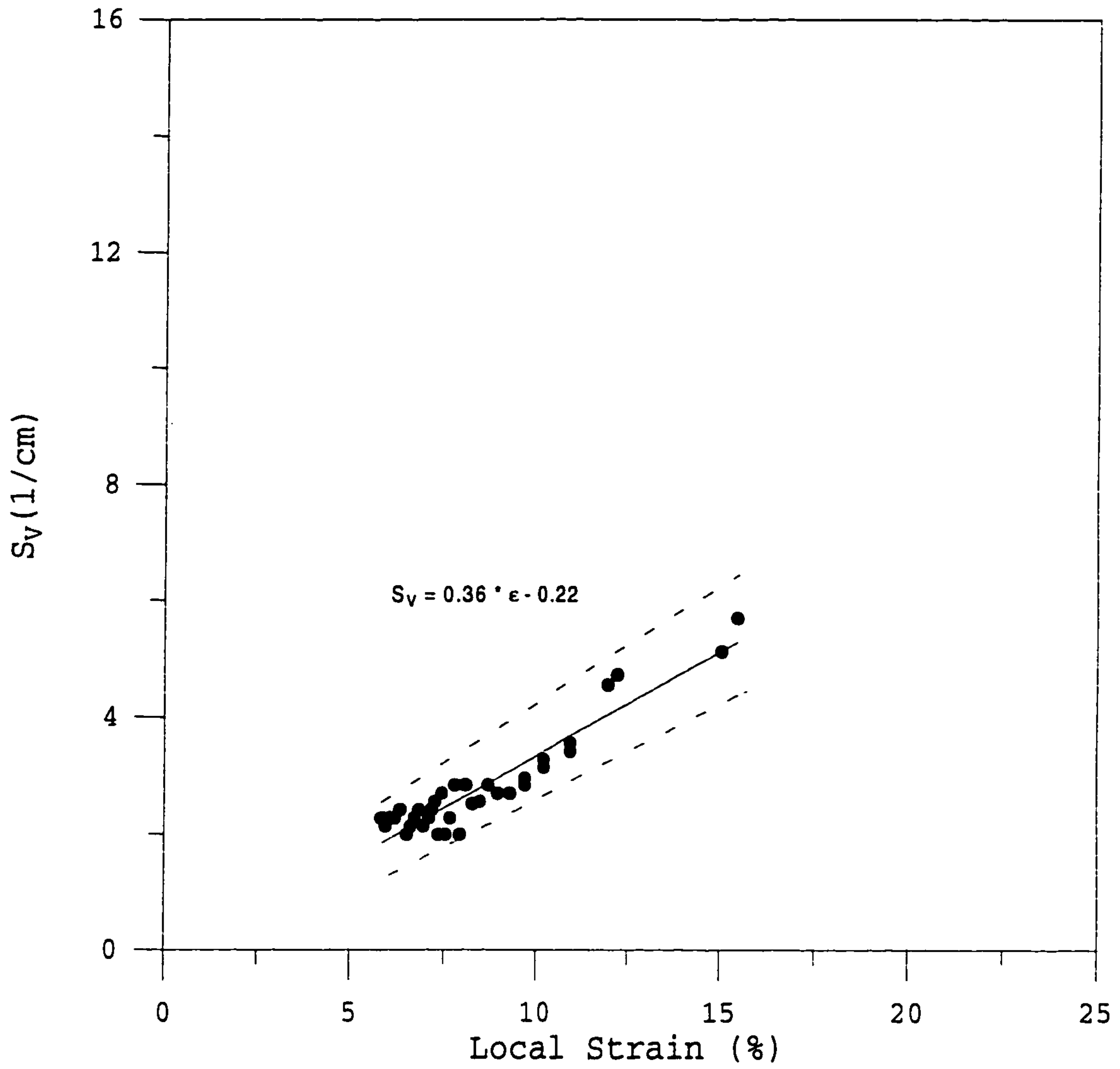

(b)

Fig. 8 (continued)

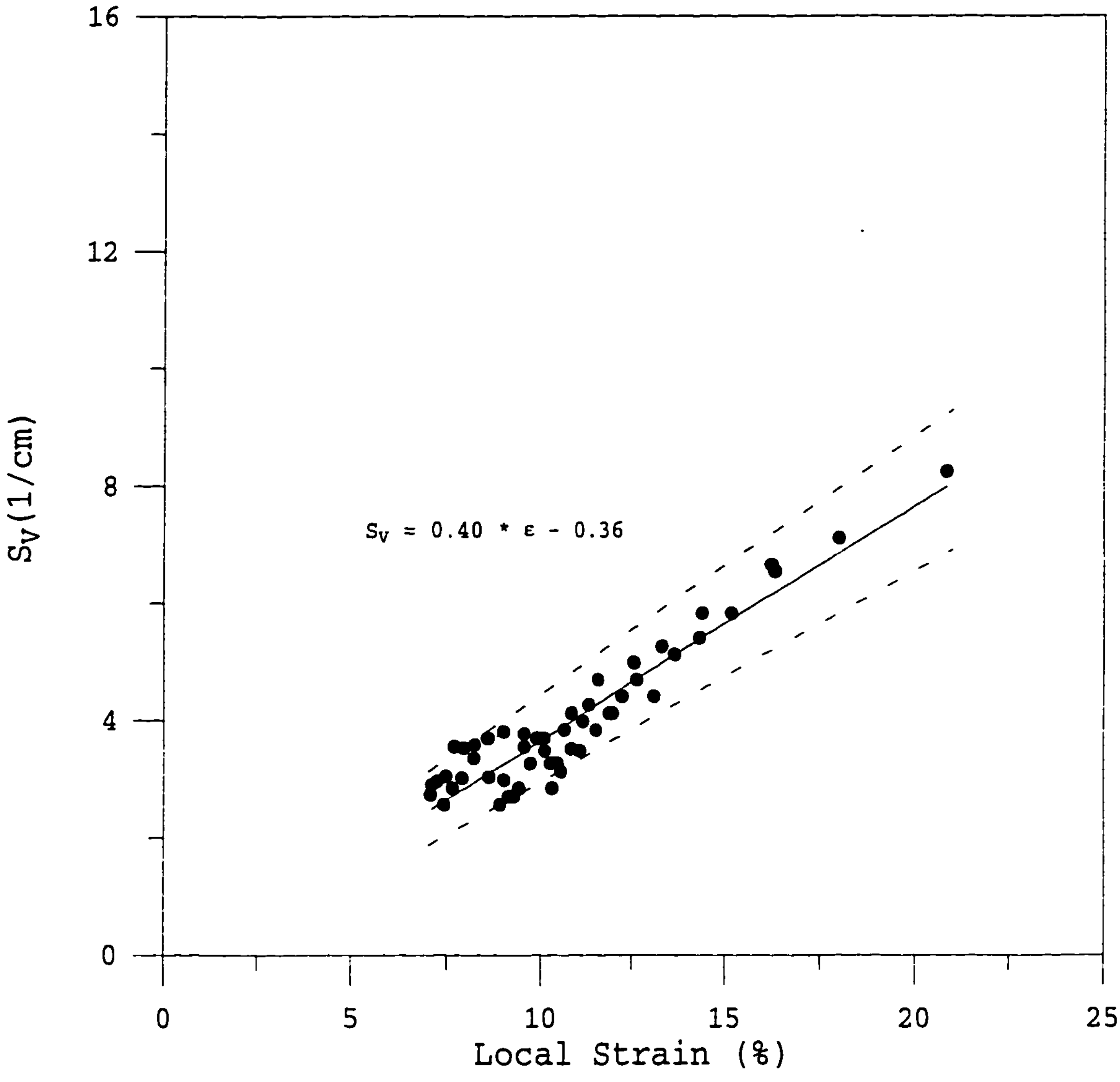

(c)

Fig. 8 (continued)

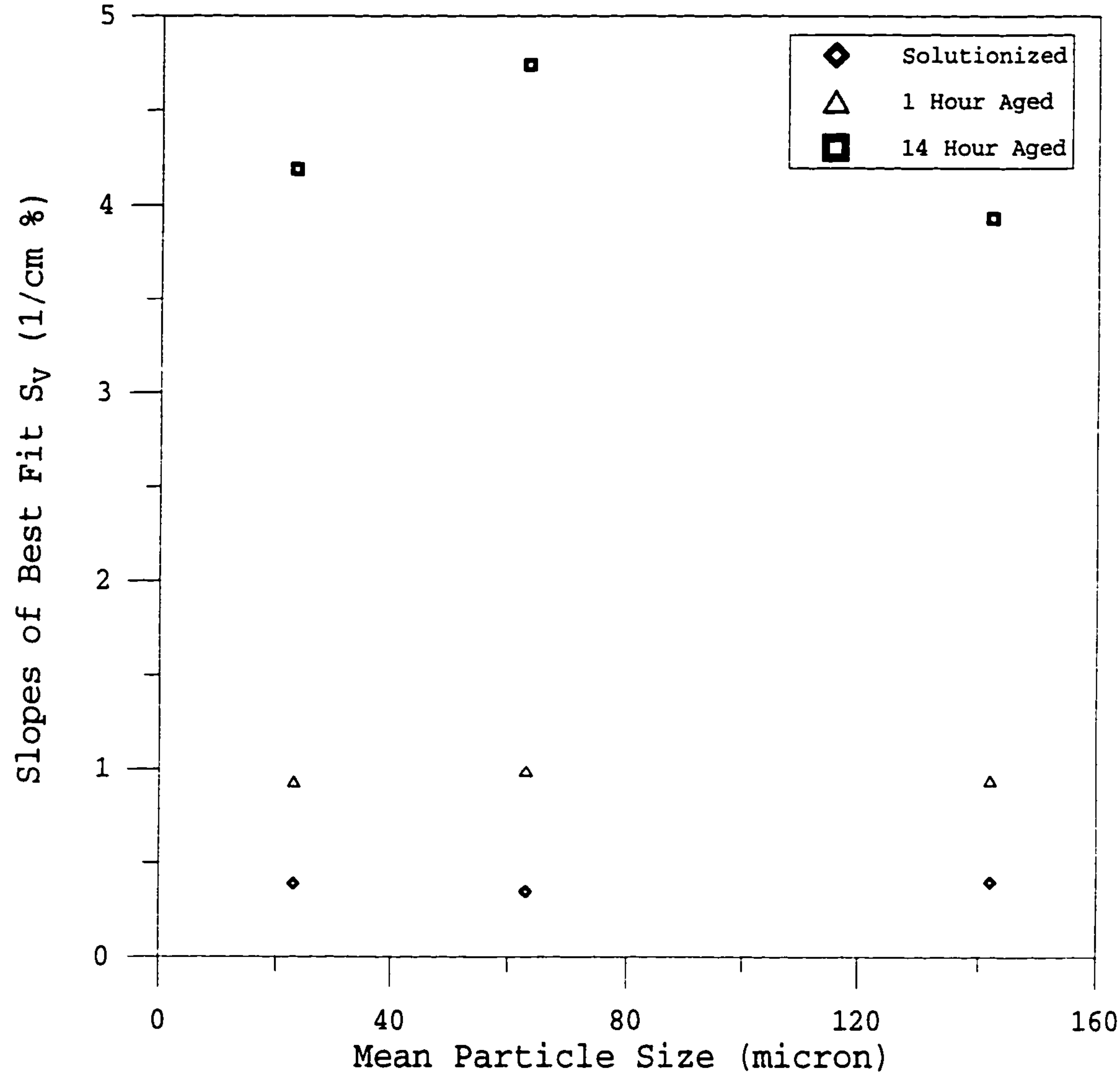

Fig. 9-The slopes of the best fit S_v as a function of mean particle size for alloy 201 reinforced with 9 vol pct SiC particles.

Particle size does not appear to affect the slopes of S_V, which is consistent with the results reported previously.[1] The Student t-statistic test indicated that there was no significant slope difference among the three particle sizes. The data on particle size and crack surface area are in contrast to the effect of particle size on the number frequency of the cracked particles, where the larger the particle size, the higher the number frequency of the cracked particles. These apparently contradictory observations are the result of the effect of particle size on particle number at a constant volume fraction and the surface area created by each crack. (At constant volume fraction and assuming spherical particles, a decrease in diameter by factor of n, number of particle increases by factor of n^3.)

The new surface area per unit volume, S_V, at a given strain and particle size increases as matrix strength increases, as can be seen by comparing the data from as-solutionized composites with the data from the age-hardened composites (Figure 9). This effect is also reflected in increases in the slopes of the best-fit lines, which is confirmed to be statistically significant using the Student t-statistic test with a 0.05 level of significance.

The results of the new surface area created by particle cracking per volume, S_V, as a function of strain for Cu7 and Cu8 reinforced with 9 vol.% of 23 μm, 63 μm, and 142 μm SiC are shown in Figure 10. S_V increases approximately linearly as local strain increases. It is apparent that increasing the matrix strength increases the new surface area per volume, S_V, at a given strain and particle size and also increases the slopes of the best fit lines.

The effect of particle size on the slopes of S_V differs for SiC reinforced Cu7 and Cu8 matrix composites. Particle size does not affect the slopes of S_V for SiC reinforced Cu7 matrix composites. (The Student *t*-statistic test indicates that there were no significant slope differences among the three particle sizes.) However, a statistically significant difference between the slopes was observed, between 142 μm and 63 μm as well as between 142 μm and 23 μm SiC reinforced Cu8 matrix composites. These results are the same as those observed in the aluminum-based composites. For the composites with a relatively low yield strength, particle size does not significantly influence the S_v slopes, whereas the effect of particle size on the S_v slopes was significant in the composites with high yield strength (such as 14 hour aged aluminum matrix composites and Cu8 matrix composites).

DISCUSSION

The results of this study and those from other Al matrix composite studies[1-6] indicate that composite failure frequently takes place by a ductile mechanism, which involves the nucleation, growth, and coalescence of voids at or near

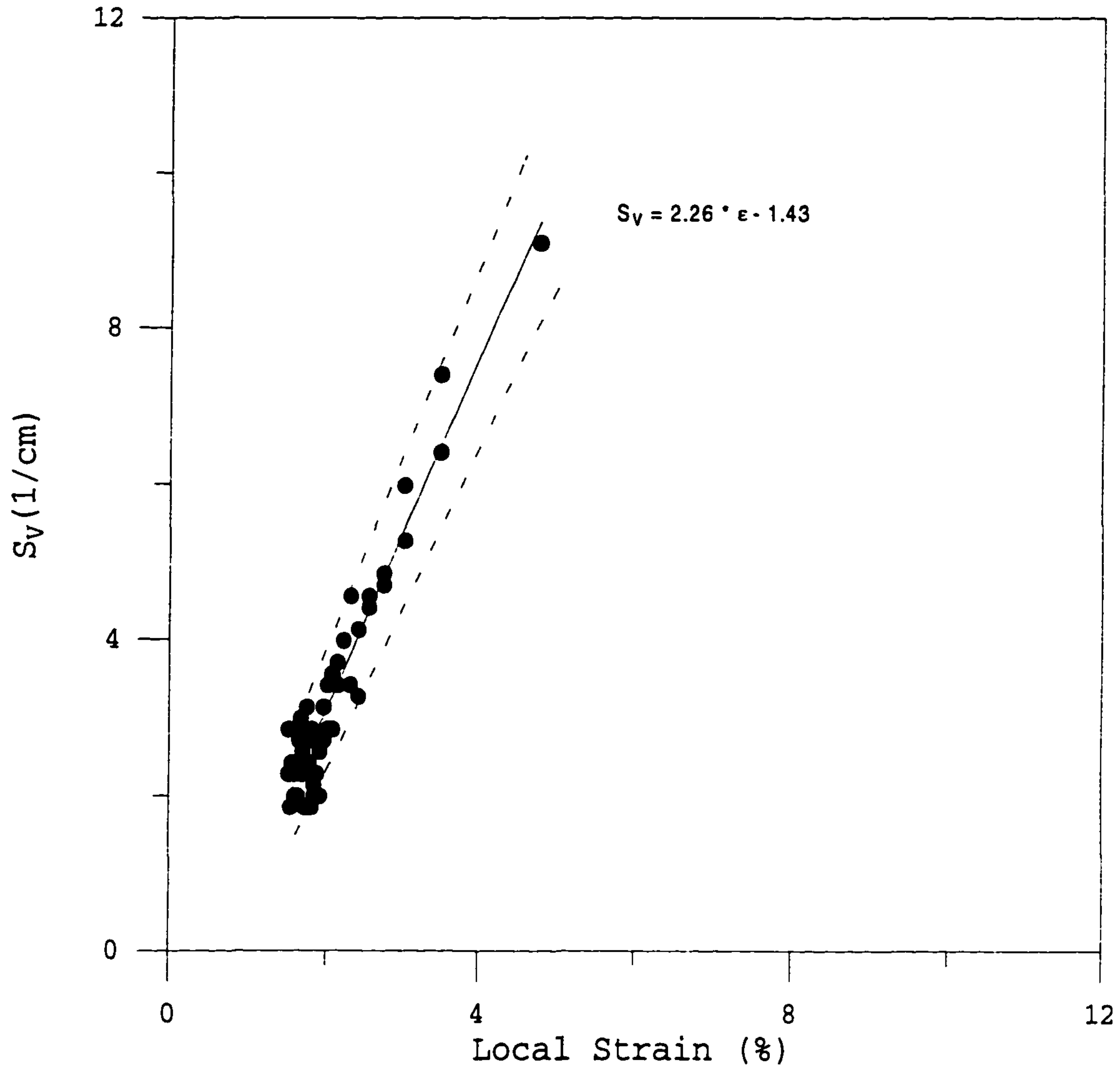

(a)

Fig. 10-S_V as a function of local strain for copper-based matrix reinforced with 9 vol pct of (a) 23 µm, (b) 63 µm, and (c) 142 µm SiC for Cu7 matrix composites and (d) 23 µm, (e) 63 µm, and (f) 142 µm SiC for Cu8 matrix composites.

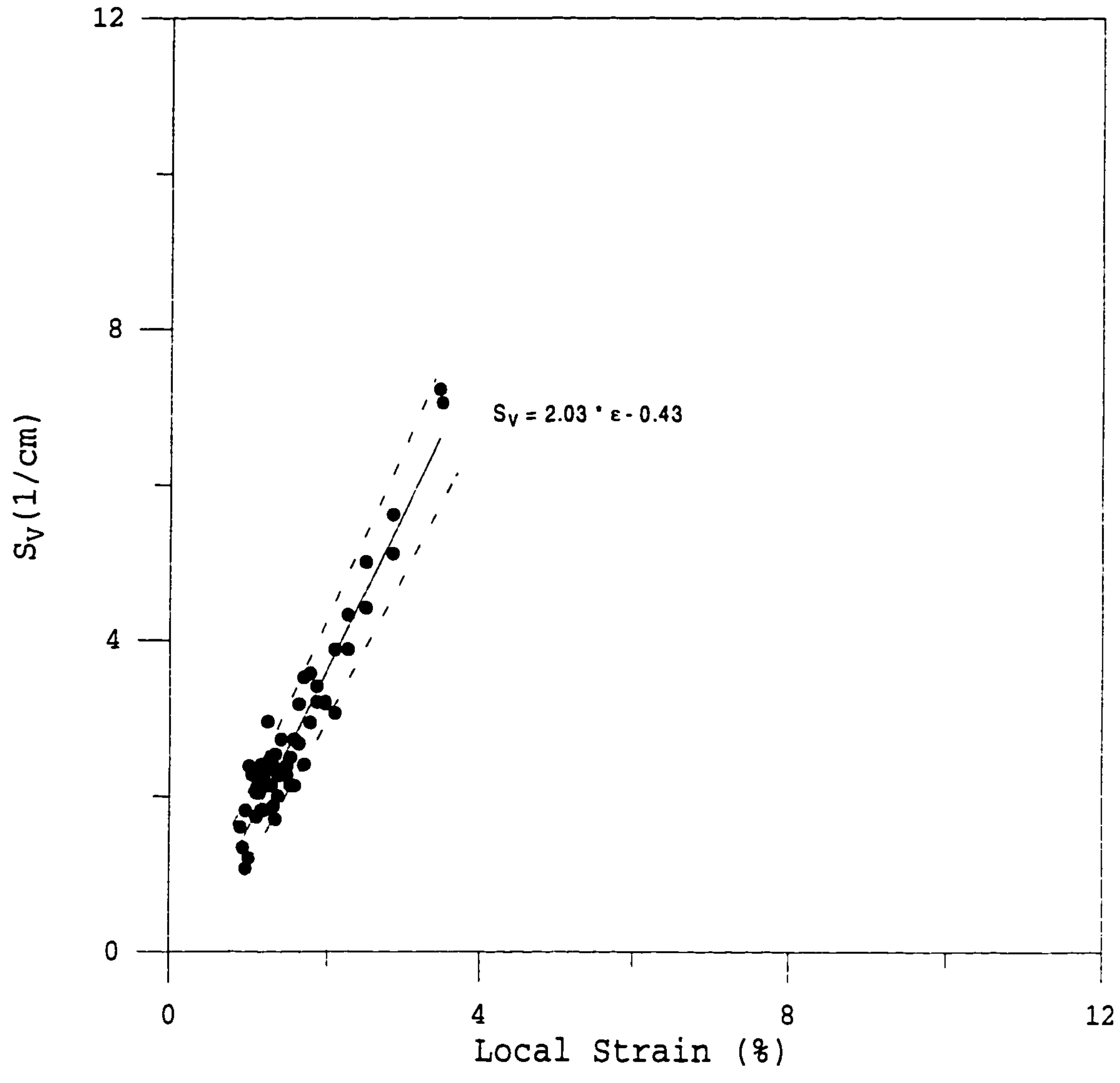

(b)

Fig. 10 (continued)

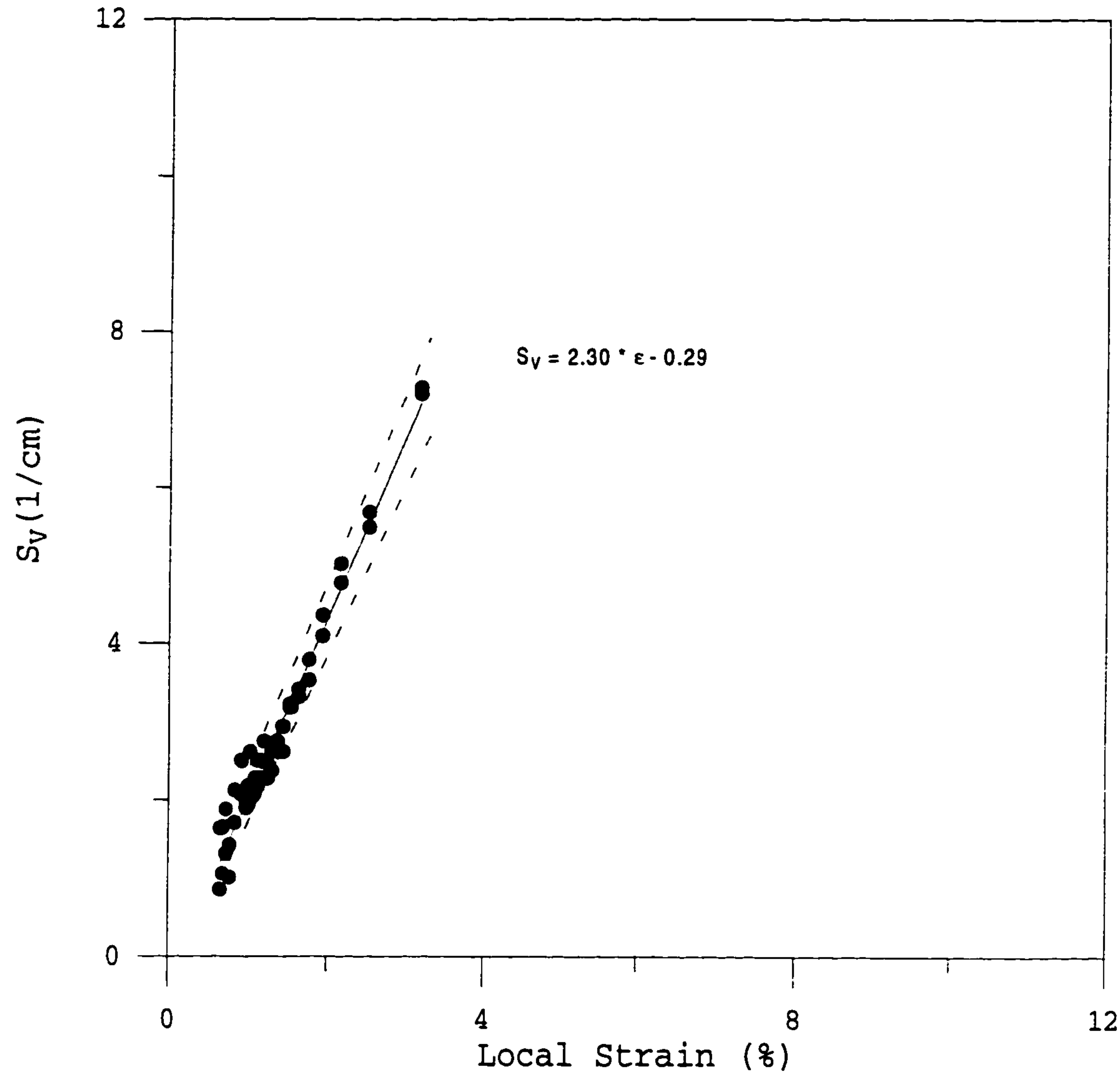

(c)

Fig. 10 (continued)

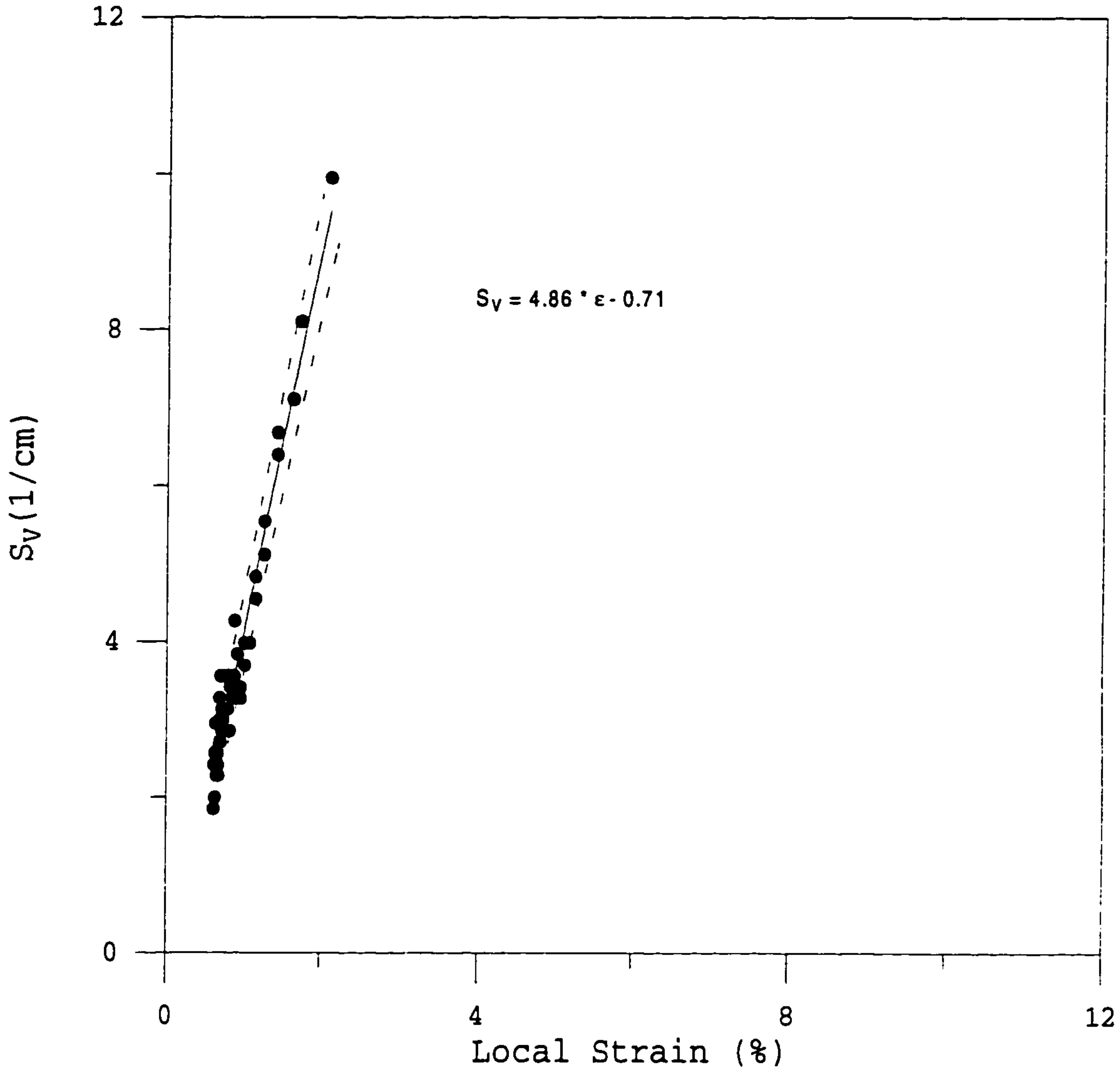

(d)

Fig. 10 (continued)

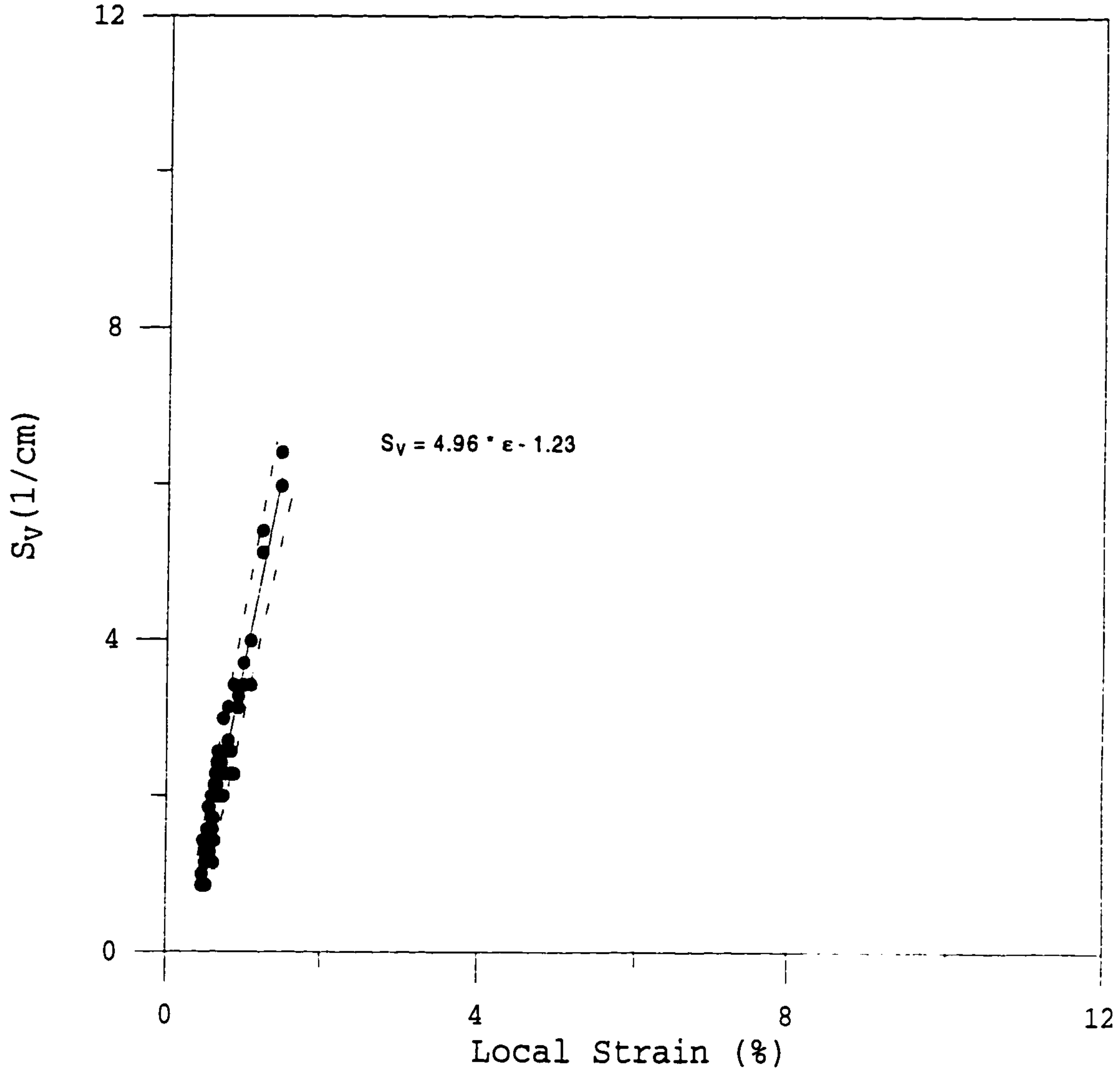

(e)

Fig. 10 (continued)

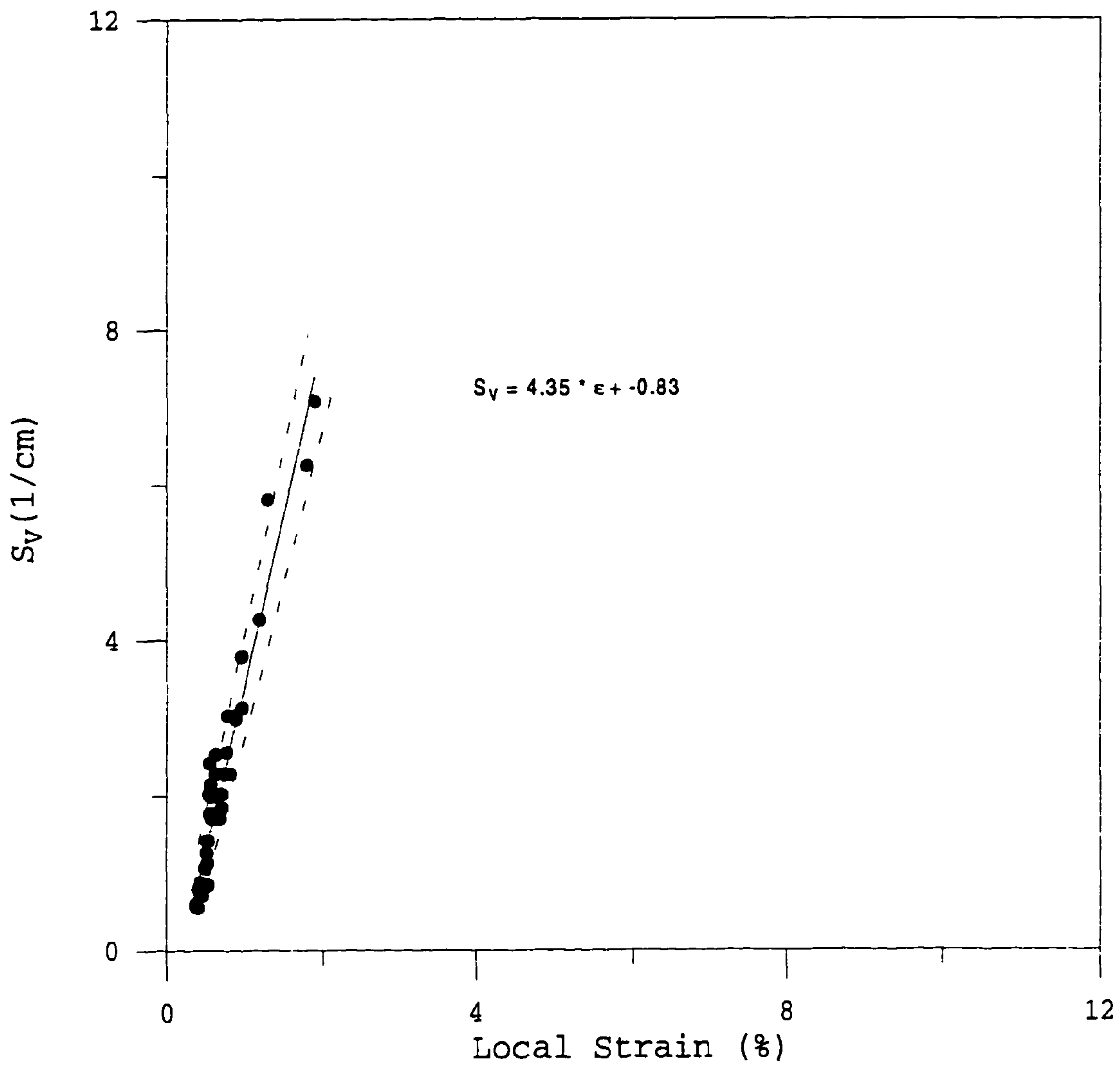

(f)

Fig. 10 (continued)

large cracked SiC reinforcement particles. Similar results have been reported in high strength aluminum alloys and hypereutectoid spheroidized steels, where voids are initiated by the cracking of large second phase particles.[8-11] The number of cracked particles depends on their resistance to cracking (measured by fracture toughness, K_{IC}) and the stress level.

The fracture probability of the SiC particles is a function of stress experienced by SiC particles and the size and location of the surface defects. The size and population of the particle defects are a function of particle size and fabrication method. The larger the particle, the more the surface area and, therefore, the higher the probability of having large defects and a larger total number of defects. The stress necessary to propagate a crack in the particle is also related to the particle size.[10] This relationship is based on the Griffith criteria (the particle will crack, if the elastic strain energy can overcome the energy of the new surface). For a spherical particle, this relationship can be expressed as:

$$\sigma = \frac{1}{k}\left(\frac{2\,E\,\gamma}{D}\right)^{\frac{1}{2}} \qquad [3]$$

where σ is the stress experienced by the particle, k is the stress concentration factor due to the defect in the particle, E is Young's modulus of the particle, γ is the surface energy of the particle material, and D is the particle diameter.

The stress level experienced by the particle primarily depends on the strength of the matrix under the condition of strong interfacial bonding, reinforcement aspect ratio, and the degree of stress concentration due to the presence of the SiC particle. Additional stresses come from the differences in thermal expansion coefficients, elastic modulus, and the incompatible deformation modes of the particle and the matrix.[19] At a given strain, the particles within the low yield strength matrix will experience less stress than those in the high yield strength matrix when interfacial bonding is strong. At a given applied stress, a particle within a low yield strength matrix will experience more stress than those in a high yield strength matrix due to the strain mismatch between the particle and the matrix. The stress level around the particles is increased by the stress concentration within the matrix. The stress concentration factor is only a function of SiC particle size and shape. Load transfer from matrix to reinforcement is achieved by shear loading, which depends largely on the aspect ratio of the particles and matrix shear stress near the interface.

Residual stress also contributes to the local stress around the particle and is particularly significant at low strains.[20] The residual stress state of the Al matrix around the SiC particle is a combination of tension and compression, but the average matrix stress is tensile in nature. In order to crack a particle, the compressive residual stress in the particle must be overcome. Once a composite is strained, additional matrix stresses are developed due to the different elastic moduli of the particle and the matrix as well as transition to plastic deformation of the matrix. This mechanism is likely the primary method for load transfer from the matrix to the particles in the case of composites with small aspect ratio reinforcements. The effect of these factors will be reflected in the particle cracking behavior during the different deformation stages of the composite.

The influence of variations in particle size and matrix properties on the particle fracture behavior during composite deformation has been investigated in this study. Reinforcement particle size is a major parameter that influences particle cracking behavior and the mechanical properties (yield strength, UTS, and elongation to fracture) of the composites. (The average aspect ratio of particles in the direction of loading is on average 1 due to absence of secondary processing in these materials. Therefore, the effect of aspect ratio and alignment on particle cracking can be ignored in this study.) Matrix properties (such as yield strength, Young's modulus, and strain hardening exponent) are also major factors affecting the particle cracking in the composites. Each of these factors will be discussed in detail.

Effect of Particle Size

The effect of particle size on the frequency of cracked particles versus strain behavior can be seen by considering F_{No} values and the slopes of the best fit lines in both aluminum matrix and copper matrix composites (Figures 4-8). The larger SiC particles are more likely to be cracked than smaller ones at a given strain and matrix strength, which is consistent with Eq. [3]. This phenomenon can be interpreted given that reinforcement particles inevitably have defects. The surface area per particle increases with increasing particle size, and the probability of having a defect of a given size increases. Thus, the probability of a defect of critical flaw size being present increases. Composite materials with larger particles exhibit a higher number frequency of cracked particles at a given strain and stress compared to those with smaller particles.

Particle size does not significantly affect the slopes of S_V versus strain in either aluminum matrix or copper matrix composites (Figures 6, 7), which is particularly true for the composites with low matrix yield strength. This result can be understood by considering that the necessary condition for crack propagation through a brittle particle is that the strain energy stored in the particle is sufficient to provide the surface energy of the newly-created crack surface. In this study, the area of the newly-created particle crack surfaces per unit strain was approximately the same for all particle sizes at a constant matrix strength, which indicates that the same amount of strain energy was released by creating a new surface regardless of the particle size.

The effect of particle size on S_V slopes exists in the case of composites with high matrix yield strength (such as 14 hour aged aluminum matrix composites and Cu8 matrix composites) and reinforced with 142 μm SiC. These high strength matrix composites reinforced with 142 μm exhibit significantly low yield strength compared to 63 μm and 23 μm SiC reinforced same matrix composites, which contributes to the low strain energy and, therefore, the small S_v slopes.

The role of stress, as opposed to strain, can be clearly seen from Figure 11, which is data replotted as a function of stress for Cu7 matrix composites in Figure 10. First, the composite stress-strain curves were extended beyond the fracture using the Ramberg-Osgood Eq. [1] and Eq. [2]. The composite stresses for each corresponding local plastic strain were then obtained from the extended stress-strain curves. The S_V values (calculated from the linear regression equations) were then plotted as a function of composite stress. The results in Figure 11 indicate that a higher applied stress is necessary to crack the fine SiC particles and to create the same amount of surface area, which is true for both aluminum and copper matrix composites. From Eq. [3], the stress

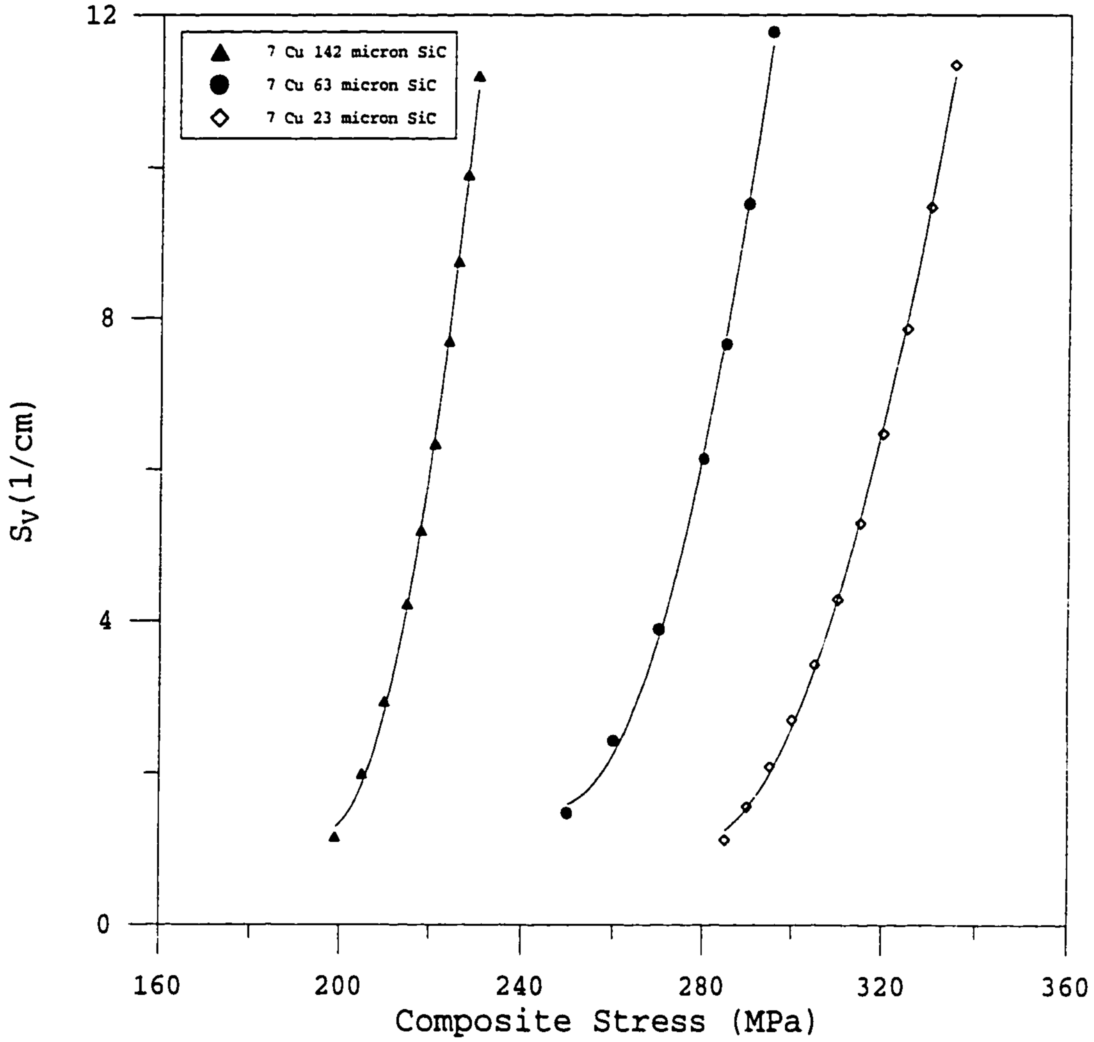

Fig. 11-S_v as a function of composite stress for cu7 matrix reinforced with 9 vol pct of 23 μm, 63 μm, and 142 μm SiC particles.

required to crack a fine particle is higher than that to crack a large particle. It should be noted that the high stress in the composite reinforced with small particles does not necessarily indicate that a small particle experiences higher stress than a large one, and it is difficult to directly prove whether a large or a small particle carries a greater load. The high stress in the composite reinforced with small particles is likely due to the effects of residual stress, grain size strengthening, substructure strengthening, and work hardening (micromechanical models) in addition to the load carried by particles (continuum models).[21] Particle cracking evidently indicates that particles do carry significant load during composite deformation. However, the effect of reinforcement size is predominantly reflected by the change of the matrix microstructure.

Effect of Matrix Properties

Yield Strength and strain-hardening exponent. The matrix yield strength has a significant effect on particle cracking behavior in terms of F_{No} and S_V. The slopes of the best fit lines are higher for the composites with high yield strength matrix in both aluminum and copper matrix composites -- more particles are cracked as local strain increases in the cases of high matrix strength. This result indicates that the particles in high matrix strength materials experience more stress than those in low matrix strength materials at a given strain, as would be expected. According to the relationship between fracture toughness, the applied stress, and the defect size, the critical defect size decreases as the applied stress increases. Since the critical defect size decreases, the fraction of particles having defects of that critical size increases. Thus, a higher number frequency of cracked particles and more surface areas created by particle cracking would be expected in composites with a high strength matrix, as has been previously reported.[1-4]

The cracked particles were concentrated near the fracture surface, which is seen in both S_V and F_{No} measurements. An example of a new surface area created by particle cracking, S_V, as a function of the distance from the fracture surface for 201 alloy reinforced with 142 μm SiC with different matrix yield strength is shown in Figure 12. The amount of cracked particles approaches a constant value when the distance from the fracture surface is beyond 2, 4, and 4 mm for 14-hour aged, 1-hour aged, and solutionized composites, respectively. The S_V value is approximately 7-8 cm^2/cm^3 near the fracture surface for all heat treatments, and drops to approximately 3 cm^2/cm^3 at 1, 4, and 7 mm from the fracture surface for 14-hour aged, 1-hour aged, and solutionized composites, respectively. The nearly constant value of S_V at the fracture surface indicates that once the amount of crack surface area reached a critical value (which corresponds to 50 to 60 pct of 142 μm

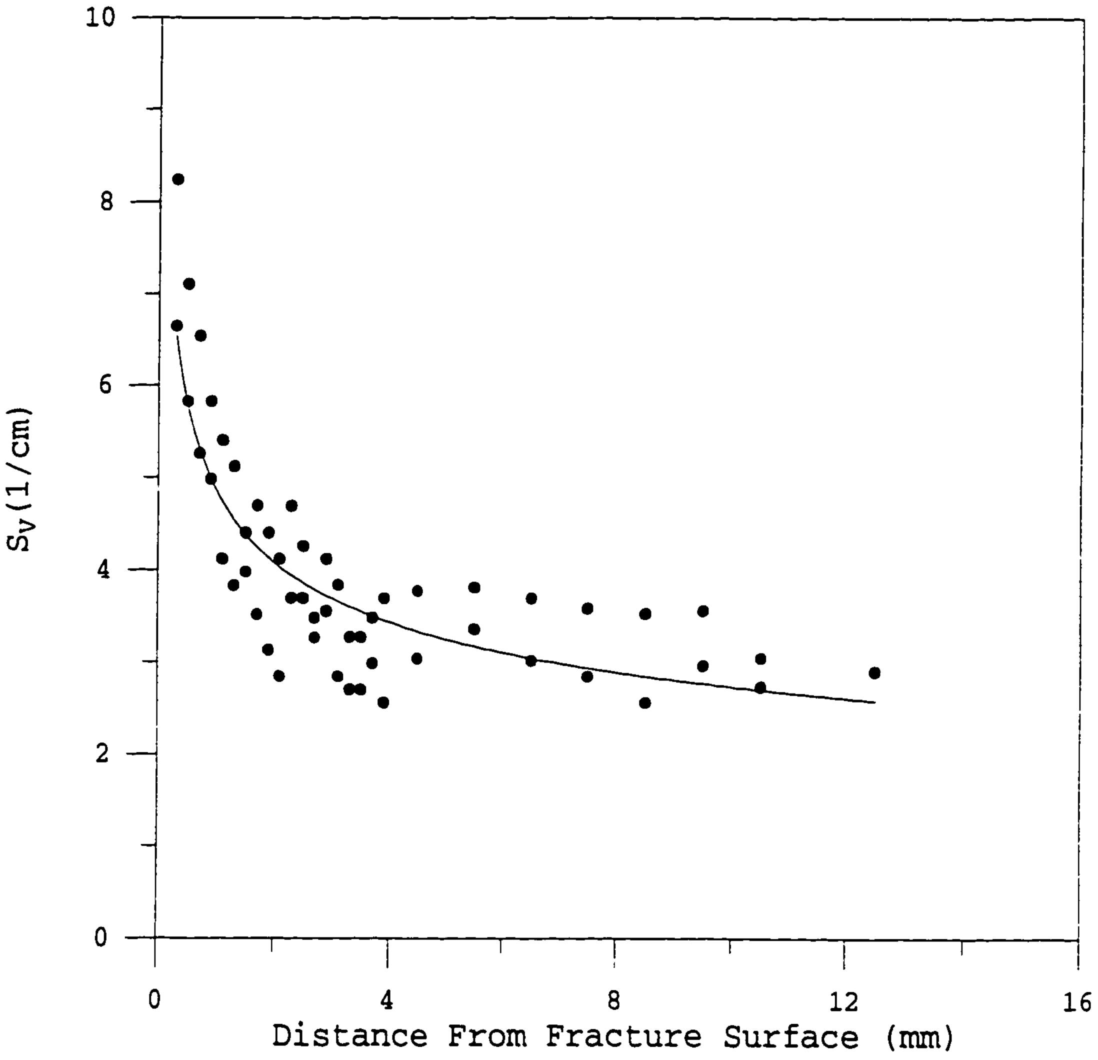

(a)

Fig. 12-S_v as a function of distance from fracture surface for alloy 201 reinforced with 9 vol pct of 142 µm SiC (a) solutionized, (b) aged for 1 hour, and (c) aged for 14 hours.

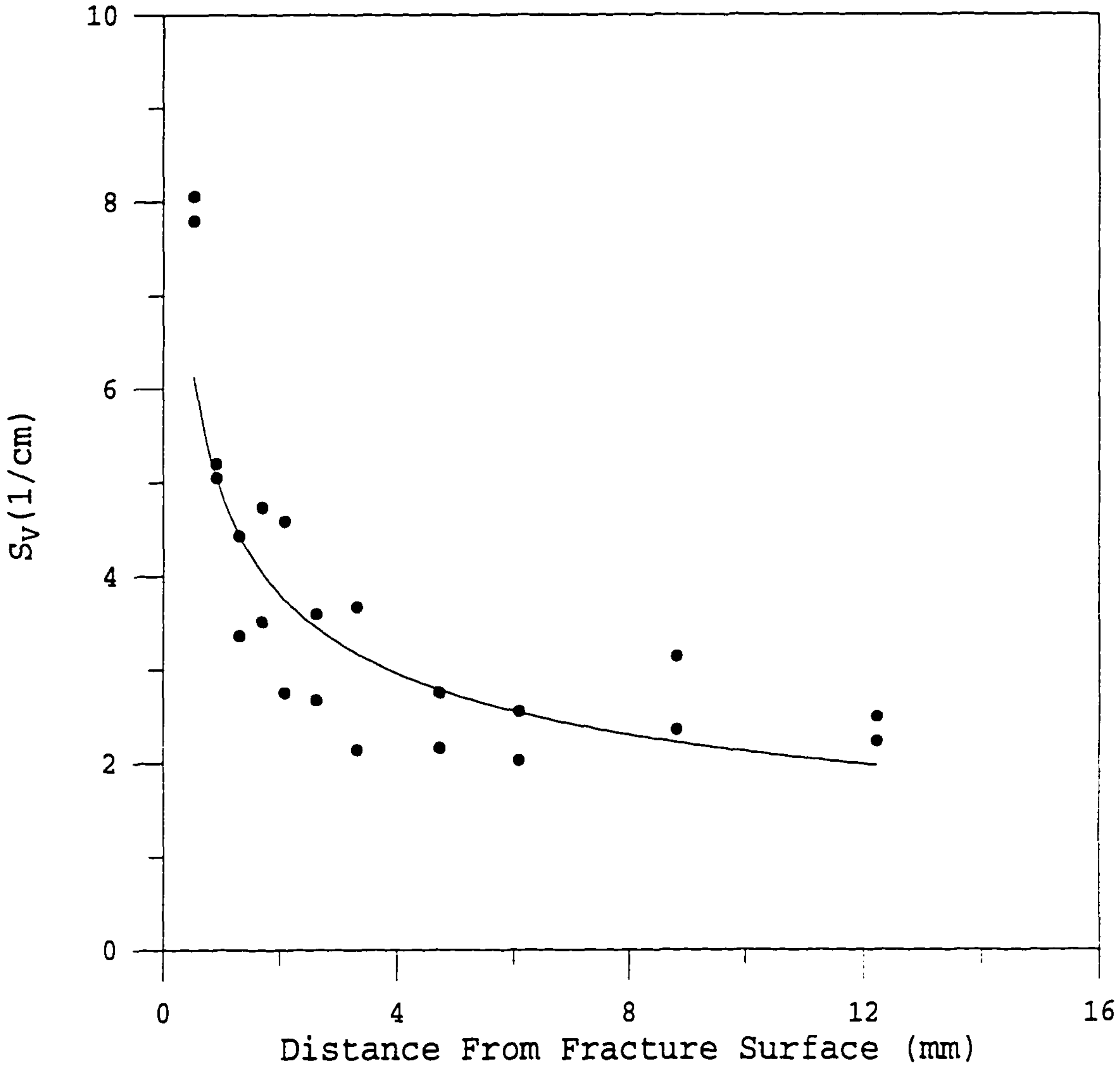

(b)

Fig. 12 (continued)

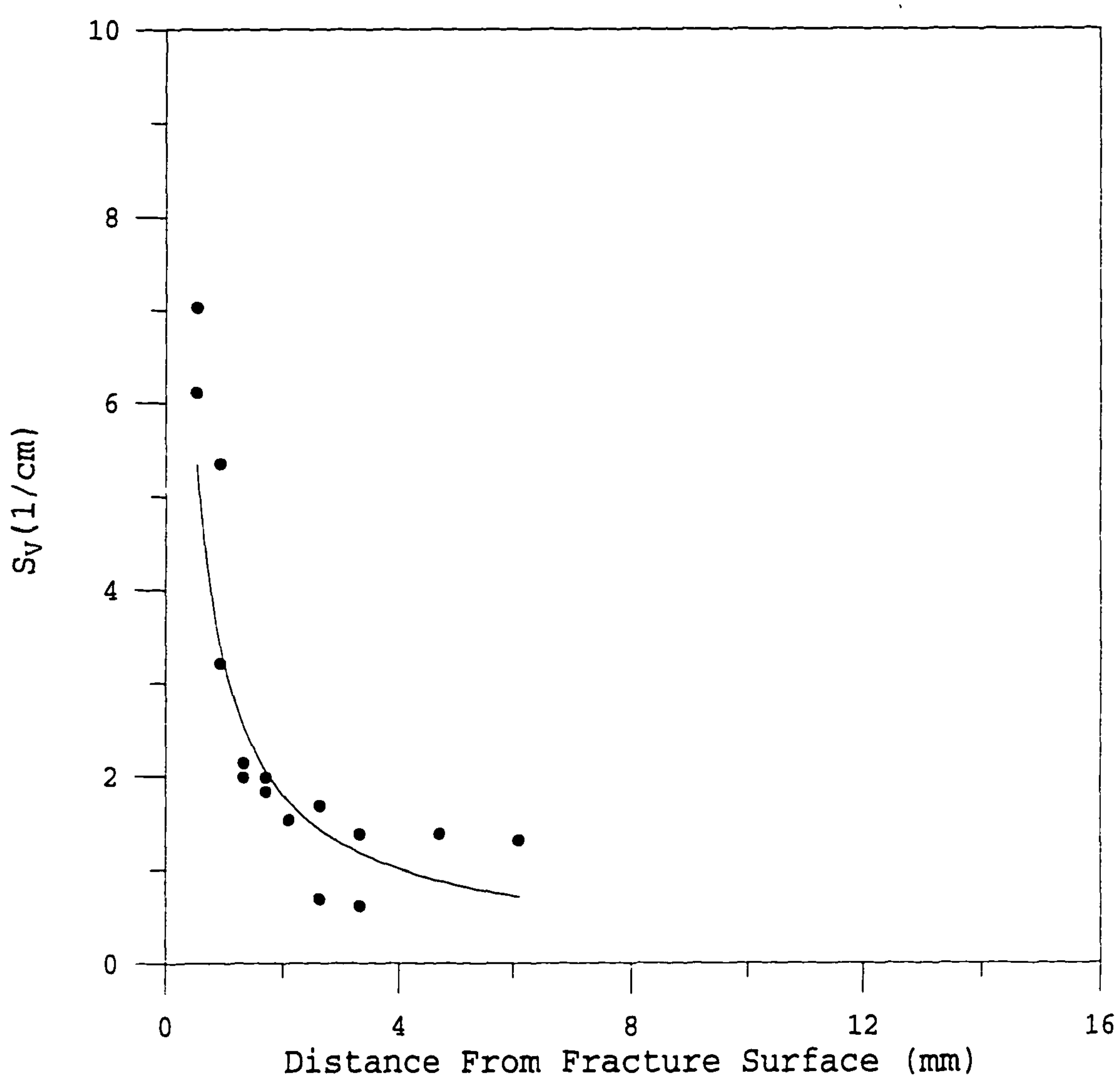

(c)

Fig. 12 (continued)

SiC particles), the voids associated with cracked particles grew, coalesced, and led to composite failure. The composites reinforced with the other two particle sizes exhibit a similar trend. Thus, the localization of particle cracking may be attributed to the capacity of the matrix to strain-harden.[6] The particles in the composite with a high strain-hardening matrix (such as solutionized or naturally aged tempers materials) will crack homogeneously until just prior to fracture. The particles in the composites with a low strain-hardening matrix (such as peak aged) will exhibit localization of particle cracking earlier during deformation.[6, 12]

The localization of particle cracking can be considered in terms of strain localization in the composite. Local strains as a function of distance from the fracture surface for 201 alloy reinforced with 142 μm SiC with different matrix yield strengths are shown in Figure 13. The minimum strain, the maximum strain, and the strain localization varied for these three composites. The minimum strain, which is the strain far from the fracture surface, and the maximum strain, which is the strain at the fracture surface, are lowest for 14- hour aged composite, followed by the 1-hour aged, and then the solutionized composites. The strain localization, which is reflected by the distance from the fracture surface when the strain level approaches the minimum strain, decreases (approximately 12, 6, and 3 mm) in the order of solutionized,

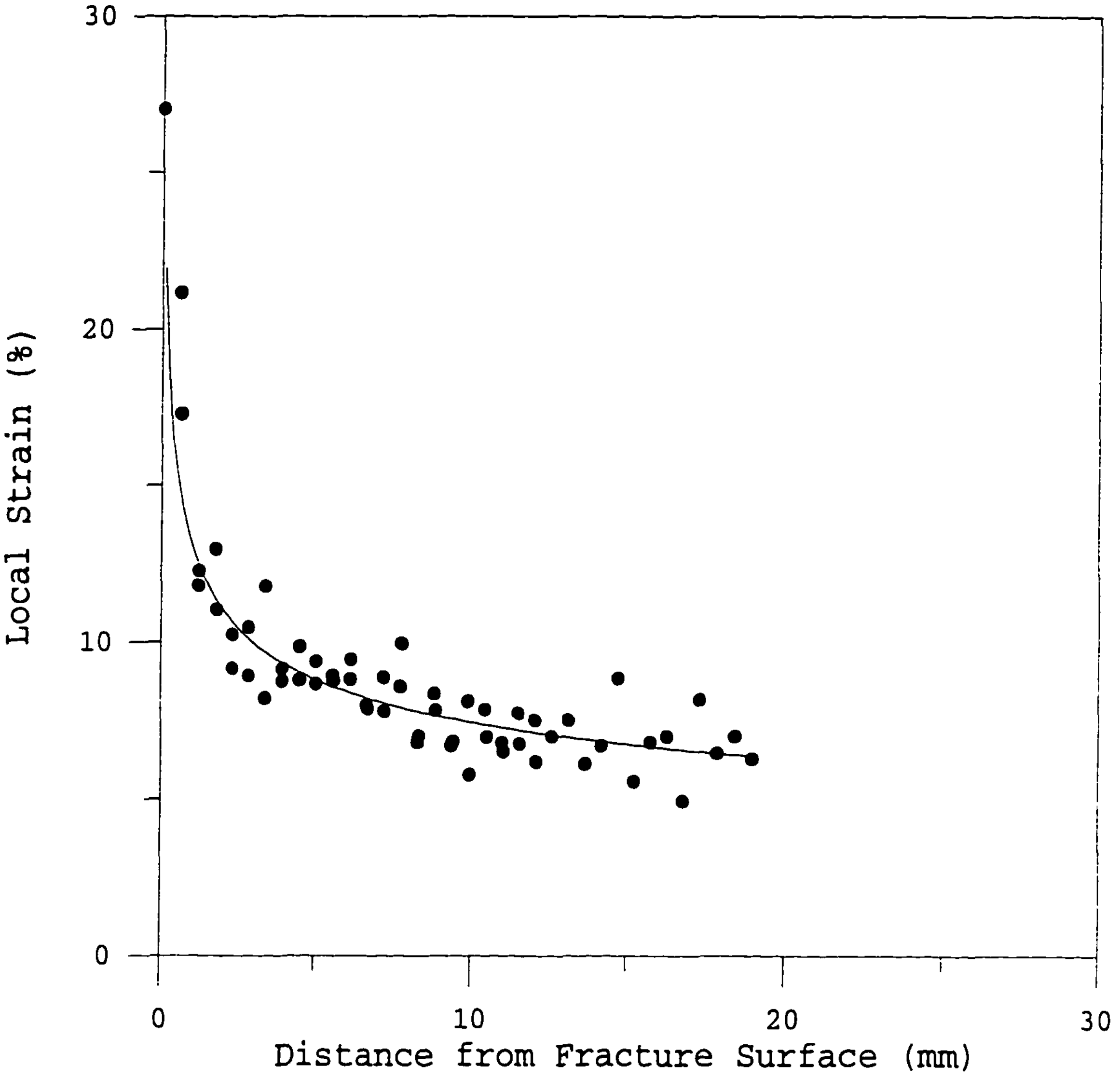

(a)

Fig. 13-Local plastic strain as a function of distance from fracture surface for alloy 201 reinforced with 9 vol pct of 142 µm SiC (a) solutionized, (b) aged for 1 hour, and (c) aged for 14 hours.

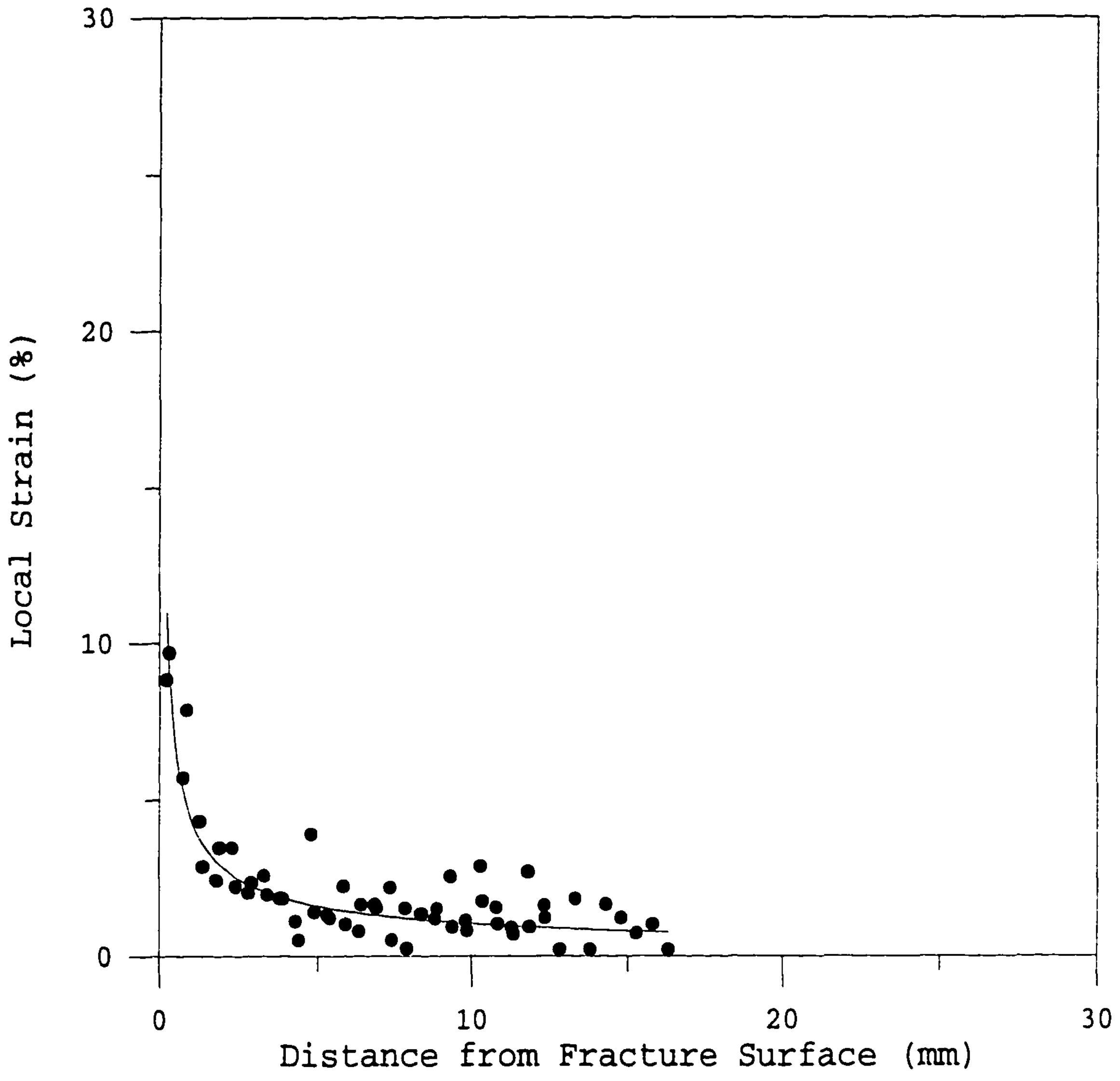

(b)

Fig. 13 (continued)

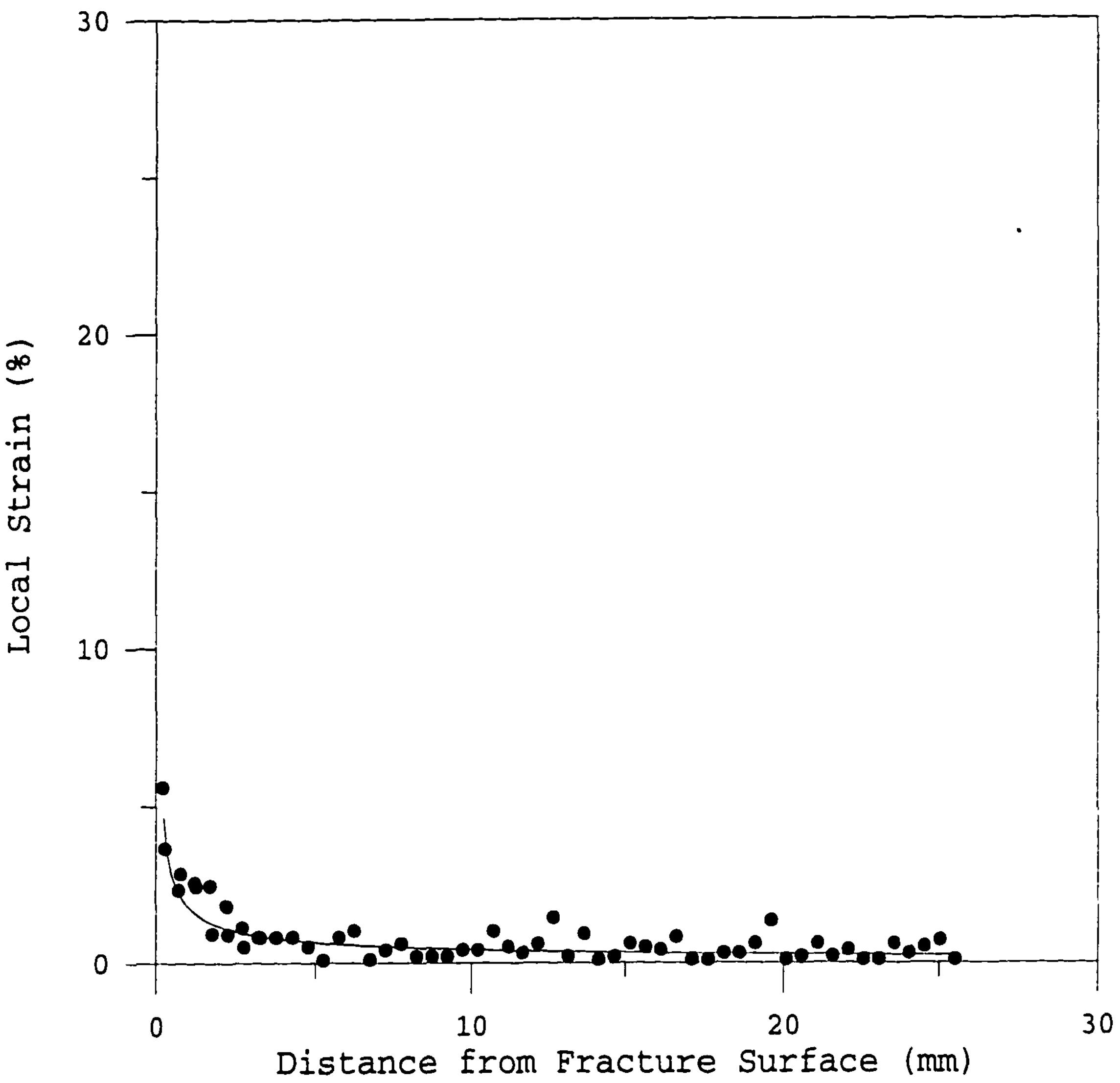

(c)

Fig. 13 (continued)

1-hour aged, and 14-hour aged composites, respectively. The age-hardened composites exhibited more strain localization than solutionized composites. The higher strain localization in peak-aged composites is a likely contributor to the higher localization of particle cracking in these composites.

Strain-hardening capacity and strain localization are directly related to the strain hardening exponent, n, which can be obtained from Ramberg-Osgood Eq. [1] and Eq. [2]. The values of n were fit from the stress-strain curves and are listed in Tables I and II. In general, the higher the yield strength, the lower the strain hardening exponent for both matrix and composite. The strain hardening exponent is smaller in the composites, decreasing with increasing reinforcement size, which is in agreement with other results.[12] The composites with a high strain-hardening exponent (such as the solutionized composites), which have high strain hardening capacity, exhibit low strain localization and, therefore, low localization of particle cracking.

The effect of matrix properties on particle cracking behavior is also shown in S_V as a function of strain (Figure 8c), which is a combination of Figures 9a and 10a. The S_V increase rate (the slope of best fit line) largely depends on the strain localization in terms of the difference between the maximum strain and minimum strain and, therefore, the matrix yield strength. The y-intercepts of the best fit lines depend on the Young's modulus, which will be discussed later in detail, matrix yield strength, and the particle size.

The slopes of the best fit lines of S_V as a function of composite yield strength for aluminum matrix and copper matrix composites are summarized in Figure 14. The slopes of S_V increase as composite yield strength increases for both matrix composite systems with an approximately linear relationship. The data from composites with different particle sizes and matrix alloys fit in the same linear relationship, which projects back to zero slope of S_V at approximately 150 MPa composite yield stress. This result indicates that S_V would not be a function of strain if composite yield stress is below a constant (150 MPa in this case).

The investigation of copper matrix composites in addition to aluminum matrix composites further broadens the range of the yield strength and strain-hardening, and, therefore, a more global picture of matrix effect on particle cracking behavior in MMCs can be developed. The experimental results ensure that slopes of S_V strongly depend on the strain localization and, therefore, the matrix yield strength, regardless of the matrix system. A similar trend was found in the other aluminum matrix composites.[4] The significant difference between the aluminum and the copper matrix composites lies in the Young's modulus, which does not

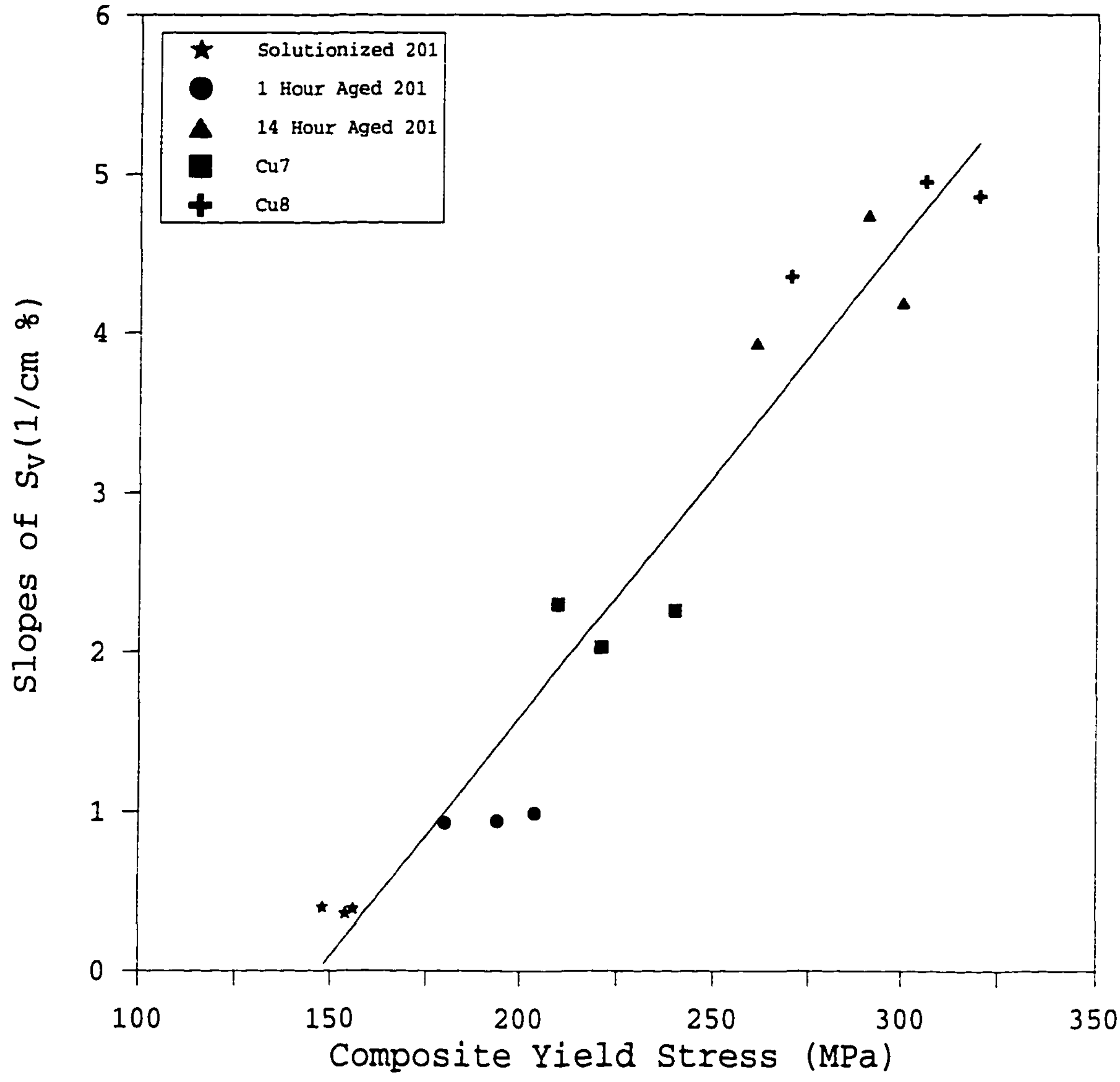

Fig. 14-The slopes of S_V as a function of composite yield stress for alloy 201 (solutionized, aged for 1 hour, and aged for 14 hours), Cu7, and Cu8 matrix reinforced with 9 vol pct of 23 μm, 63 μm, and 142 μm SiC particles.

significantly affect the S_v slopes. (The effect of Young's modulus on particle cracking will be discussed in detail later.)

The slopes of the best fit lines of F_{No} as a function of composite yield strength for different particle sizes and matrix systems are also summarized in Figure 15. (The slopes of F_{No} for weighted total cracks, total cracks, one crack, two cracks, etc. have the similar trend in terms of effects of particle size and matrix strength. Therefore, the representative slopes of F_{No} (total cracks) were plotted in Figure 15.) The slopes of F_{No} increase as composite yield strength increases for different particle sizes and matrix systems. The slopes of F_{No} are also a function of particle size; the larger the particle size, the higher the slopes of F_{No}. This effect is more significant as composite yield strength increases.

The data of S_V for two copper matrices reinforced with 63 µm SiC were replotted as a function of applied stress in order to examine the effect of matrix yield strength on particle cracking behavior. As shown in Figure 16, a greater applied stress would be necessary to create the same amount of new surface by particle cracking within the high strength matrix composites, which is true for both aluminum matrix and copper matrix composites. A similar result was reported in other aluminum matrix composites.[12] At a given applied stress, the

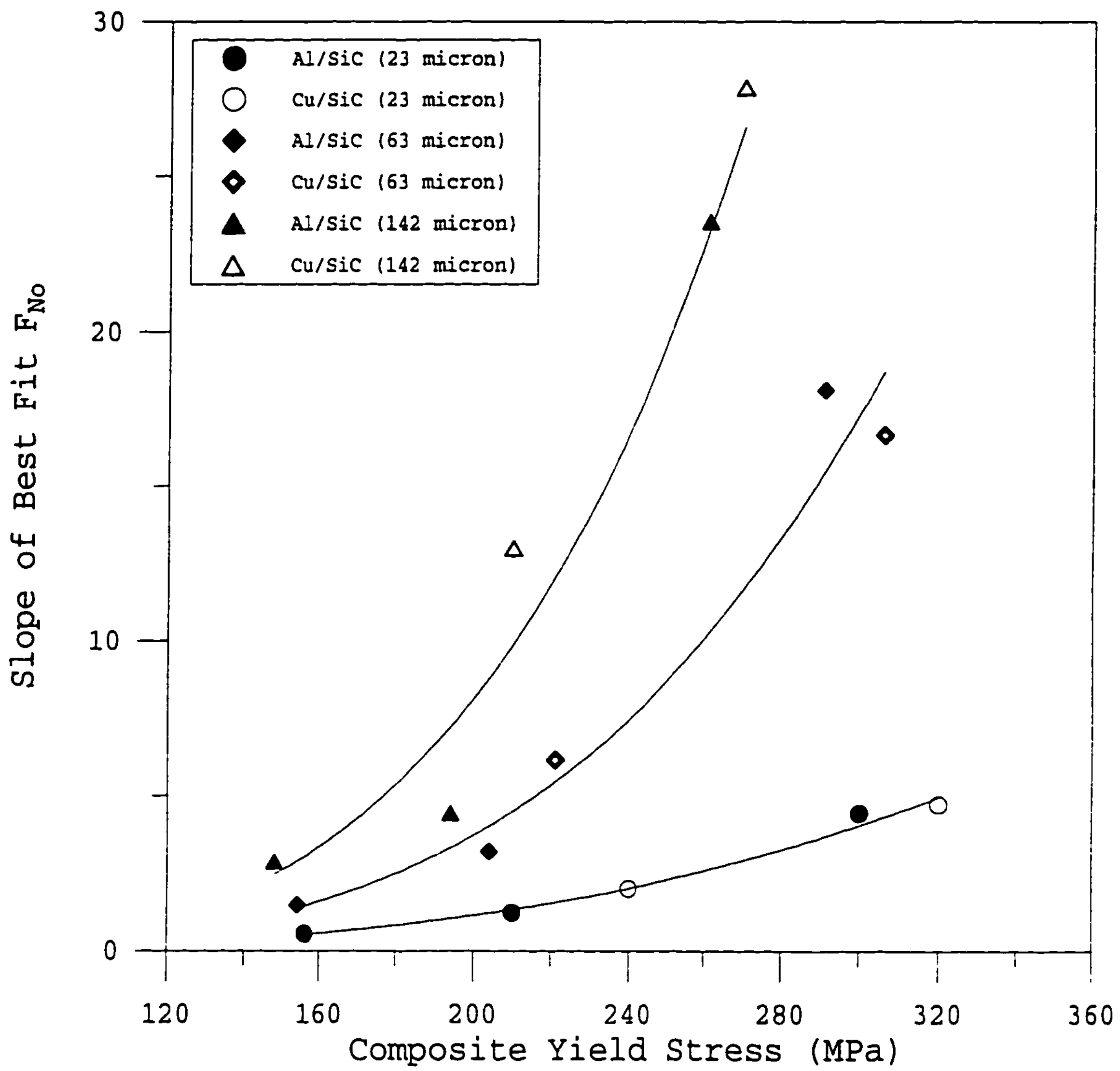

Fig. 15-The slopes of F_{No} (total cracks) as a function of composite yield stress for alloy 201 (solutionized, aged for 1 hour, and aged for 14 hours), Cu7, and Cu8 matrix reinforced with 9 vol pct of 23 μm, 63 μm, and 142 μm SiC particles.

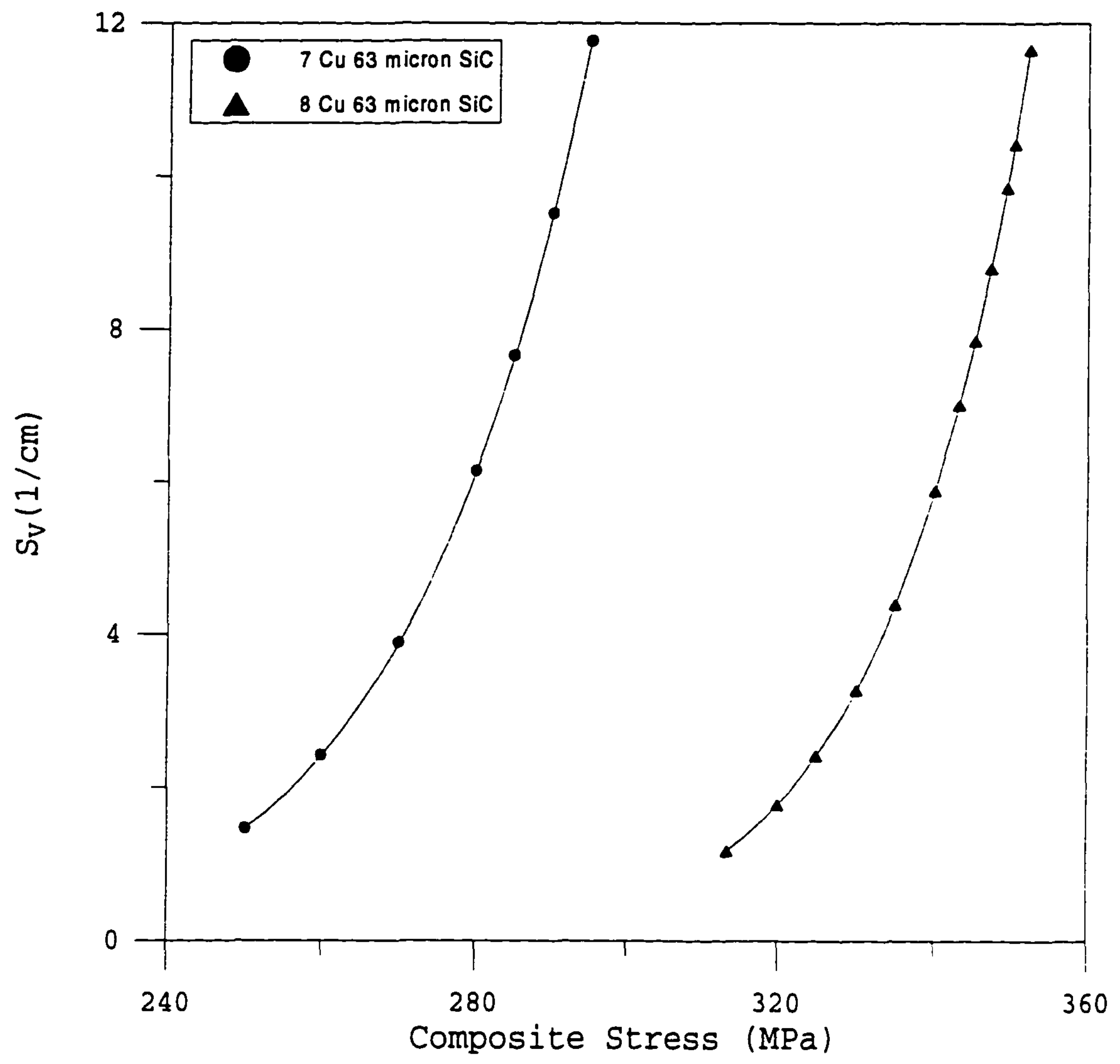

Fig. 16-S_v as a function of composite stress for Cu7 and Cu8 reinforced with 9 vol pct of 63 μm SiC particles.

high strength matrix composites will be in the low strain (Figure 17). The load transfer due to the misfit strain between matrix and particles makes particles experience less stress in the case of high matrix strength composites than those in the case of low matrix strength composites. Since both composites experience the same stress, the matrix in the case of the high strength matrix composites will carry more load, which is likely the reason for the less strengthening in a high strength matrix composite.[22, 23]

Young's Modulus. There is a significant difference between Young's modulus of aluminum and copper alloys. However, it is difficult to identify the effect of Young's modulus on the particle cracking behavior directly from the relationships of S_V and F_{No} as a function of strain. The positive, non-zero y-intercept for the best fit line of S_V vs. strain implies that elastic deformation causes particle cracking if sufficient stress is experienced by the particle. To test this hypothesis, tensile specimens were loaded to their yield points in order to examine the effect of matrix Young's modulus on particle cracking behavior. S_V and F_{No} were measured on the longitudinally sectioned surface. Since deformation is macroscopically uniform in the elastic region and there were no systematic variations of measured S_V and F_{No} values along the gage length, S_V and F_{No} values will be

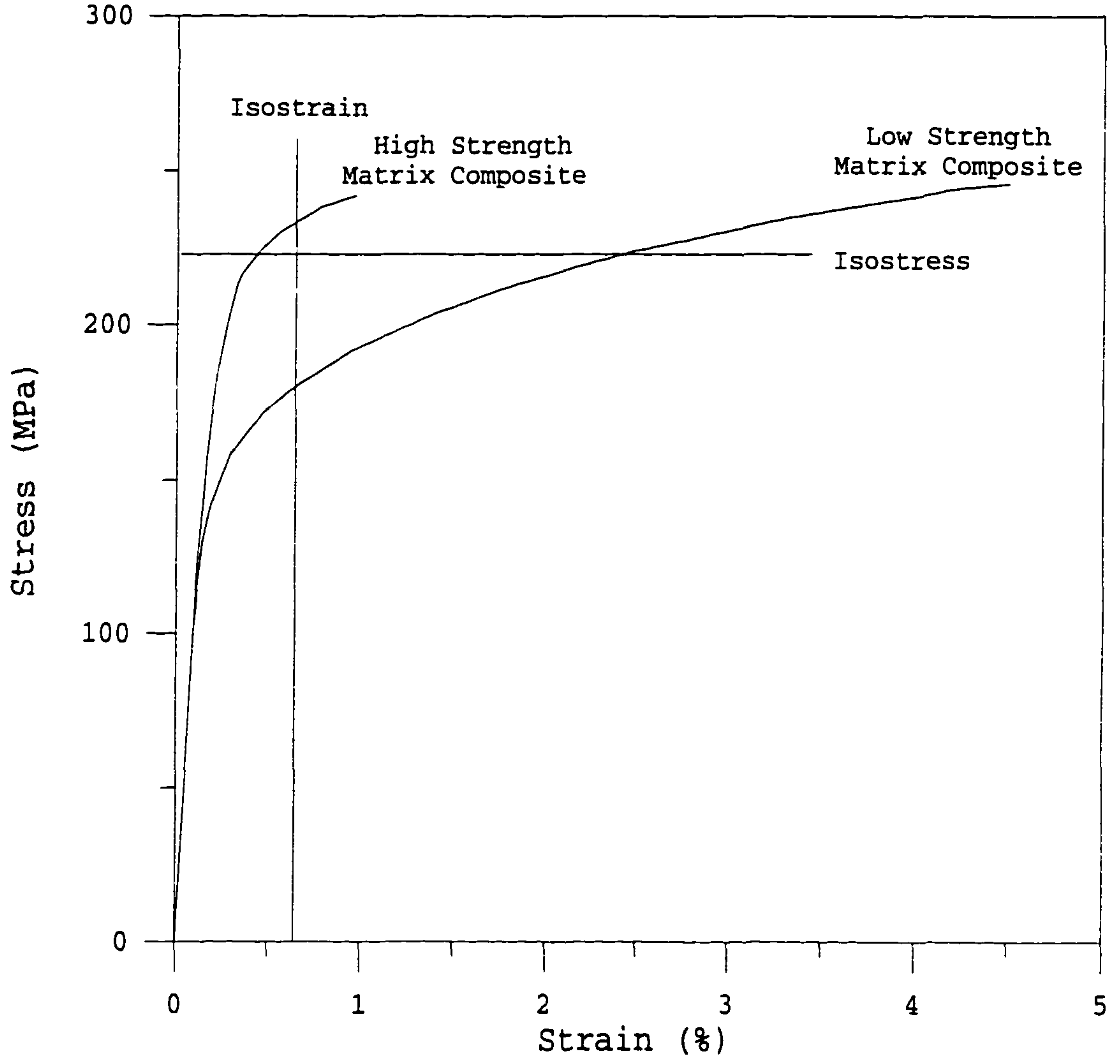

Fig. 17-The stress-strain curves for composites with high matrix strength and low matrix strength.

presented as a average value rather than as a function of position.

The values of S_V and F_{No} as a function of applied stress for aluminum matrix composites reinforced with 63 μm and 142 μm SiC are shown in Figure 18. Both S_V and F_{No} increase as the applied stress increases due to difference of the matrix yield strength. The *t*-test showed that there was a statistically significant difference between solutionized and 14-hour aged composites reinforced with 63 μm and 142 μm SiC for both S_V and F_{No}. The results indicated that even though a small amount of particle cracked during elastic deformation, particularly in the case of solutionized composites, the elastic deformation contributed to the particle cracking, which is in agreement with other observations.[24, 25] The degree of particle cracking due to elastic deformation is small compared to that due to plastic strains. However, it is in the same order of magnitude as that observed at low plastic strain. The effect of particle cracking due to elastic deformation on the composite properties is evident and is likely significant in the cases of low plastic deformation, such as high cycle fatigue.

The values of S_V and F_{No} as a function of applied stress for copper matrix composites reinforced with 63 μm and 142 μm SiC are also shown in Figure 18. The trend is similar as in the case of aluminum matrix composites. The comparison was

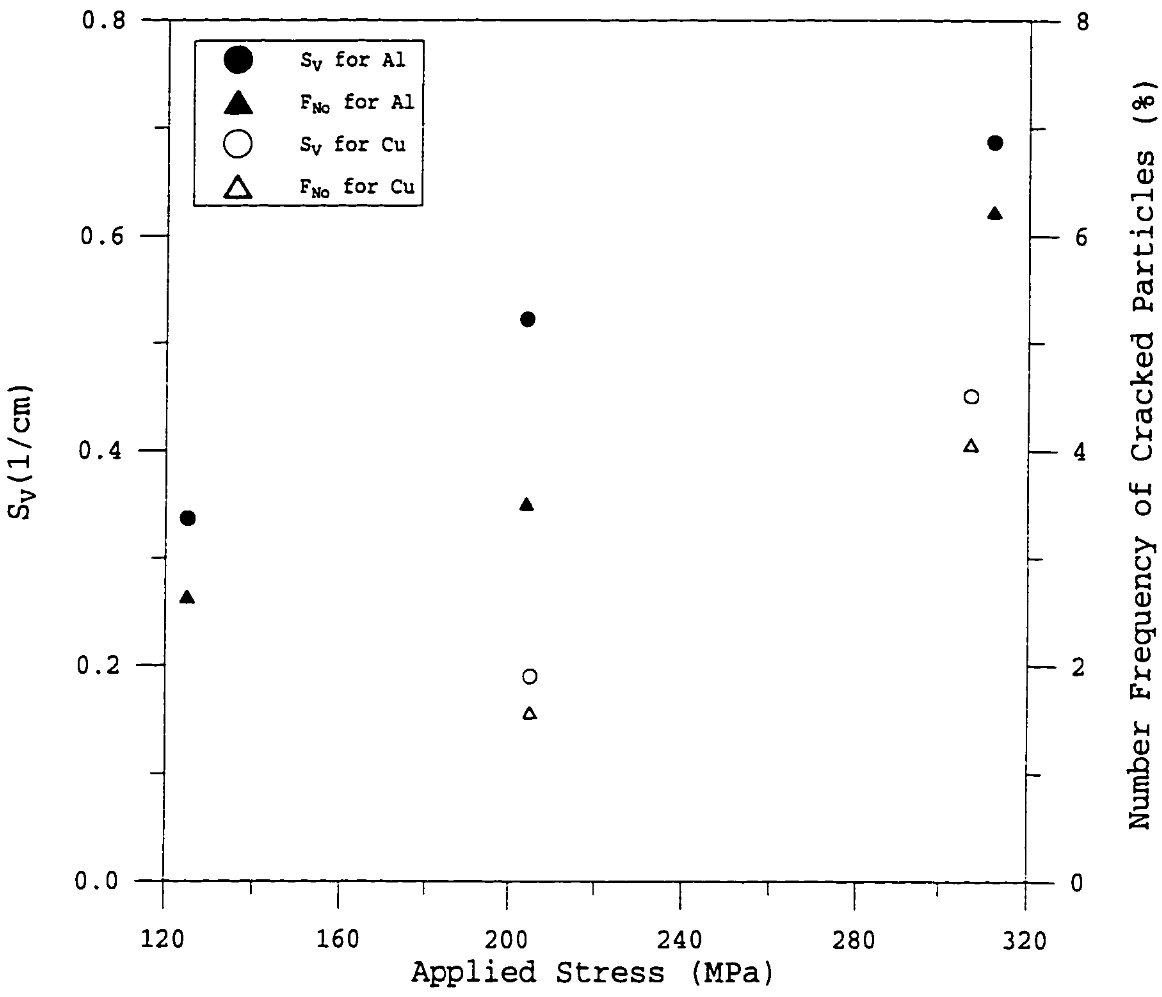

(a)

Fig. 18-S_V and F_{No} as a function of applied stress (under yield stress) for alloy 201 and copper-based alloy reinforced with 9 vol pct of (a) 63 μm and (b) 142 μm SiC particles.

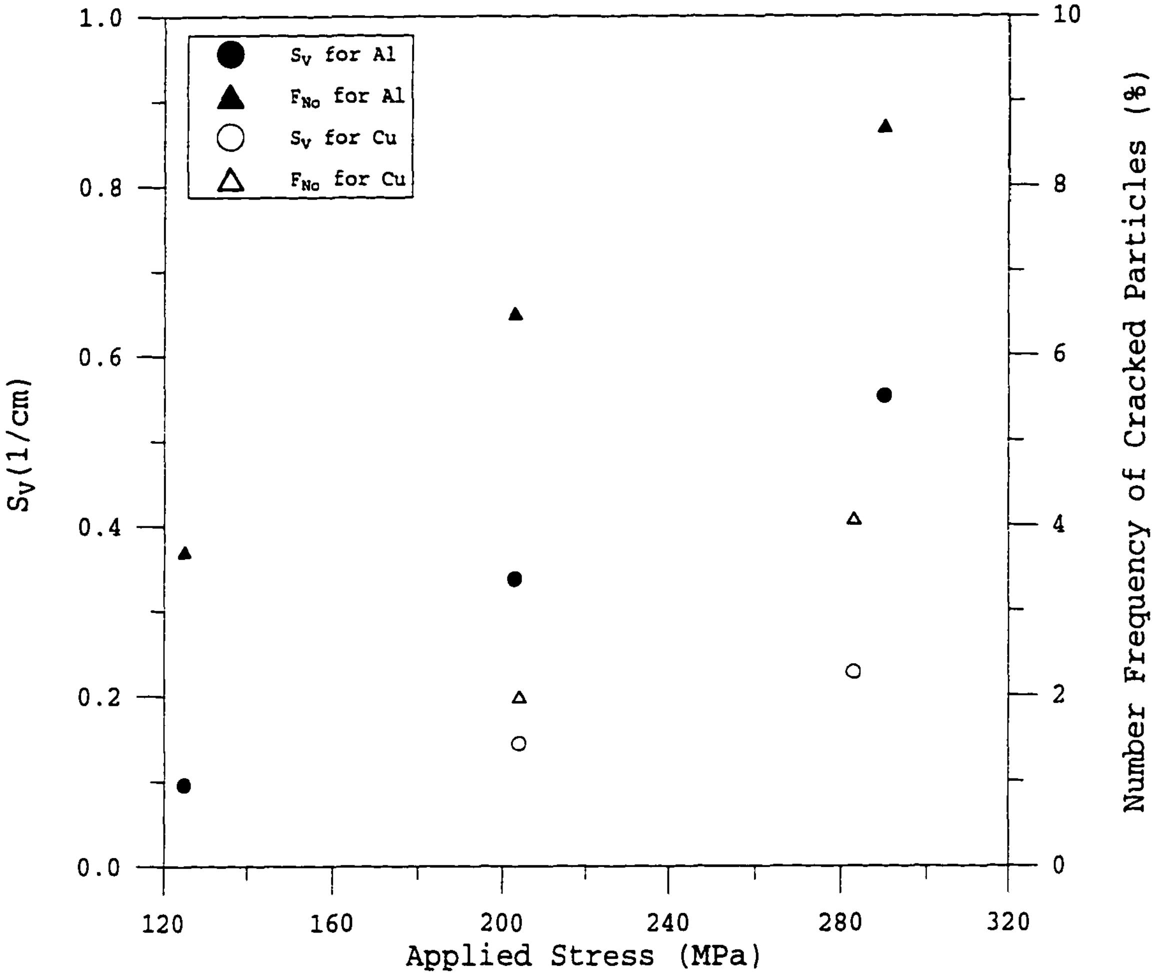

(b)

Fig. 18 (continued)

made between aluminum and copper matrix composites. The *t*-statistic test indicates that there is a statistically significant difference between aluminum matrix and copper matrix composites for S_V and F_{No} at a given applied stress and particle size. When analyzing the effect of matrix Young's modulus, residual stress should also be taken into consideration since the residual stress contributes to the local stress around SiC particles, which is particularly significant at low strain. The copper matrix has smaller thermal expansion coefficient (~17 × 10^{-6} /°C) than the aluminum matrix (~23 × 10^{-6} /°C). Thus, the residual stress in the copper matrix composites will be expected to be less than that in the aluminum matrix composites. The SiC particles within the copper matrix composites will experience less residual compression and, therefore, less inhibition to particle cracking. This argument further reduces the observed effect of matrix Young's modulus on particle cracking behavior. For a given applied stress, fewer particles will be cracked in the composites with high matrix Young's modulus due to the higher load carried by matrix and, therefore, the lower load carried by particles. Alternatively, it would be expected that more particles are cracked in the composites with high matrix Young's modulus at a given strain during elastic deformation.

SUMMARY

(1) The cracking of SiC particles during composite deformation in Al- and Cu-based MMCs was quantitatively measured as a function of particle size and matrix strength. The measurement was undertaken in the sample interior rather than the surface.

(2) The two measured fracture features, S_V and F_{No}, were found to be approximately linear as a function of local strain.

(3) The slopes of S_V vs. strain were not significantly affected by particle size, whereas the F_{No} slope values were. The large particles tend to have a higher degree of crack than do the small ones at a given strain and stress.

(4) The slopes of S_V and F_{No} were strongly dependent upon the strain localization and, therefore, the matrix yield strength. The higher the matrix yield strength, the higher the slopes of S_V and F_{No} for both aluminum and copper matrix systems.

(5) The results of this study indicate that particle cracking is controlled by both strain and stress.

(6) The investigation of copper matrix composites showed that matrix Young's modulus did affect the particle cracking in the elastic region, although the effect was too small to be observed in the plastic region. For a given stress, fewer particles would be cracked in the composites with high matrix

Young's modulus. This result further indicates that particles crack during elastic deformation of composite and that the effect of matrix Young's modulus on particle cracking may be substantial in the case of low plastic deformation.

ACKNOWLEDGMENT

The support of the Alabama NSF-EPSCoR Composites Program is gratefully acknowledged.

REFERENCES

1. B. Wang, G.M. Janowski, and B.P. Patterson: *Metall. Trans. A*, 1995, vol. 26A, pp. 2457-67.

2. J. Llorca, A. Martin, J. Ruiz, and M. Elices: *Metall. Trans. A*, 1993, vol. 24A, pp. 1575-88.

3. P.M. Singh and J. J. Lewandowski: *Metall. Trans. A*, 1993, vol. 24A, pp. 2531-43.

4. J. Llorca and P. Poza: *Mater. Sci. Eng.*, 1994, vol. A185, pp. 25-37.

5. M.J. Hadianfard, J. Healy, and Y.W. Mai: *J. Mater. Sci.*, 1994, vol. 29, pp. 2321-27.

6. P. Poza and J. Llorca: *Metall. Trans. A*, 1995, vol. 26A, pp. 3131-41.

7. C.P. You, A.W. Thompson, and I.M. Bernstein: *Scripta Metall.*, 1987, vol. 21, pp. 181-85.

8. R.H. Van Stone, R.H. Merchant, and J.R. Low, Jr.: *Fatigue and Fracture Toughness-Cryogenic Behavior, ASTM STP 556*, American Society for Testing and Materials, Philadelphia, PA, 1994, pp. 93-124.

9. D. Broek: *Eng. Frac. Mechanics*, 1973, vol. 5, pp. 55-66.

10. J. Gurland and J. Plateau: *J. Trans., Am. Soc. Metals*, 1963, vol. 56, pp. 442-54.

11. D.R. Lesuer, C.K. Syn, and O.D. Sherby: *Acta Metall. Mater.*, 1995, vol. 43, pp. 3827-35.

12. D.J. Lloyd: *Acta Metall. Mater.*, 1991, vol. 39, pp. 59-71.

13. Y. Brechet, J.D. Embury, S. Tao, and L. Luo: *Acta Metall. Mater.*, 1991, vol. 39, pp. 1781-86.

14. P.M. Mummery and B. Derby: *J. Mater. Sci.*, 1994, vol. 29, pp. 5615-24.

15. A.G. Evans, J.W. Hutchinson, and R.M. McMeeking: *Scripta Metall.*, 1991, vol. 25, pp. 3-8.

16. D.J. Lloyd: *International Materials Reviews*, 1994, vol. 39, pp. 1-23.

17. G.M. Janowski: *Ph.D. Dissertation*, Michigan Technological University, 1988.

18. ASM Metals Handbook, 10th Edition, vol. 3, *Alloy Phase Diagrams*, pp. 3.12.

19. S.F. Corbin and D.S. Wilkinson: *Acta Metall. Mater.*, 1994, vol. 42, pp. 1329-35.

20. S.F. Corbin and D.S. Wilkinson: *Acta Metall. Mater.*, 1994, vol. 42, pp. 1319-27.

21. F.J. Humphreys, A. Basu, and M.R. Djazeb: *In Proc. 12th Risφ Int. Symp. on Metal Matrix Composites - Processing, Microstructure and Properties*, N. Hansen, D. Juul Jensen, T. Leffers, H. Lilholt, T. Lorentzen, A.S. Pedersen, O.B. Pedersen and B. Ralph, eds., Risφ National Laboratory, Denmark, 1991, pp. 51-66.

22. G.M. Janowski and B.J. Pletka: *Mater. Sci. Eng.*, 1990, vol. A129, pp. 65-76.

23. M. Manoharan and J.J. Lewandowski: *Acta Metall.*, 1990, vol. 38, pp. 489-96.

24. R. DaSilva, D. Caldemaison, and T. Brethau: *in Mechanical and Physical Behavior of Metallic and Ceramic Composites*, S.I. Anderson, H. Lilholt and O.B. Pederson, eds., Risφ National Laboratory, Denmark, 1988, pp. 333-38.

25. F.J. Humphreys: *in Proceedings of EMAG-MICRO89*, IOP Publishing Ltd., Bristol, UK, 1990, pp. 465-68.

A TECHNIQUE FOR SPUTTER COATING OF CERAMIC REINFORCEMENT PARTICLES

B. WANG, Z, JI, F.T. ZIMONE, G.M. JANOWSKI, and J.M. RIGSBEE

Submitted to International Conference on Metallurgical Coating and Thin Film. Also will be published in Surface and Coating Technology.

ABSTRACT

The reinforcement/matrix interface is a key factor in determining the properties of composite materials. The microstructure and, therefore, the properties of interfaces are determined by composition and composite processing. Coatings applied to the reinforcement phase will change the composition near the interface and may yield the desired interface properties. In this study, a technique for sputter coating ceramic powders was developed and used to coat large SiC particles (mean size of 142 µm) with copper. The copper coating was found to be face-centered cubic and uniform in thickness on the level of SEM/EDS. These particles were mixed with Cu powder and sintered to form a Cu-matrix composite material. Although the copper coating did not significantly improve the interfacial bonding in these materials, the success in coating ceramic particles suggests that this approach may be useful in other composite systems.

INTRODUCTION

The reinforcement/matrix interface is one of the critical factors in determining the properties of a composite material.[1,2] A strong interface is necessary to transfer load from the matrix to the reinforcing phase, which is a requirement in many particle- and fiber-reinforced composites. The properties of the interface are determined by the composite processing methods (time, temperature, and pressure), the composition and nature of the phases in contact, and the interface geometry. The composition at the interface will be modified by applying a coating to the reinforcing phase, which can alter the thermodynamics or kinetics of interface evolution. A successful example of improved interface bonding is a Ni or Cu coating on non-metallic fibers in low melting alloy matrix composites (such as Al). The improved wetting of the liquid alloys when the Ni or Cu coating was present increases the interfacial bonding.[3] Thus, it is possible to control the properties of a composite material by coating the reinforcement phase.

It is difficult to achieve a uniform coating on a discontinuous reinforcing phase of a metal-matrix composite (MMC) since (1) most are nonconductive and (2) the smallest dimension is typically less than 150 µm (and often less than 10 µm), which precludes mechanical manipulation of individual whiskers, platelets, or particles. Sputter deposition is one way to apply a coating to a non-conductive material. However, several problems remain, specifically the introduction of the reinforcement into a high-vacuum system and the exposure of all sides of the reinforcement to the sputter source. The former obstacle is due to the transport of the reinforcement during the pumping sequence, which results in contamination of the chamber and ingestion into the vacuum pump(s) in the worst case.

This paper will describe a technique for sputter coating relatively large SiC particles, approximately 142 μm in diameter. These particles are to be used as the reinforcement for Cu-based composites processed by solid-state sintering. Previous experiments have shown that the bond strength was insufficient and the particles debonded for the as-received particles. As-received, acid-cleaned, and Cu-coated SiC particles will be analyzed by x-ray and SEM/EDS both before and after composite sintering. The effect of coating on interface behavior will be addressed.

PROCEDURE

The sputter coating system used in this study is a model Discovery 24 manufactured by Denton Vacuum, Incorporated. This unit utilizes a rotary pump for roughing and a cryo-pump for high vacuum. A copper target was utilized; its composition is shown in Table I. The base pressure of this system is below 10^{-5} Pa (10^{-7} torr), and the working pressure is approximately 1 Pa (10^{-2} torr). The dc cathode power used in this study was operated at 700 watts, which yields a deposition rate of approximately 1.9 nm/s of Cu on a flat substrate.

The turbulence caused by rapidly evacuating or backfilling the deposition chamber may cause transport of the light powder

Table I: Composition of Copper Target

Ag	Bi	Pb	O	Other	Cu
500 ppm	< 10 ppm	< 50 ppm	400 ppm	< 300 ppm	99.9%

particles, which will contaminate the vacuum vessel and, in the worst case, damage the vacuum components. Reducing the gas flow rate during the initial stages of pumping, so-called "soft-roughing," has been previously shown to reduce the chamber turbulence.[4] One manner to accomplish soft-roughing is to place a flow-actuated check valve between the chamber and rotary pump. This device, which is available and marketed by HPS, a division of MKS Instruments, Incorporated under the name "Auto-Soft", is shown in Figure 1. The Auto-Soft nearly isolates the chamber from the pump during the initial stages of rough pumping, but gradually opens as the gas flow rate (and system pressure) decreases. However, the time to reach 1 Pa ($\approx 10^{-2}$ torr) increased from about 3 minutes without the flow-actuated check valve to about 10 minutes with it. An examination of the chamber showed no evidence of particle contamination after a complete pumping cycle.

Exposing all sides of particles and achieving a relatively uniform coating is a primary requirement for successful particle coating. Continuous particle tumbling is one way that all sides of a particle can be exposed to the sputtered flux. A schematic of the physical layout that was used in this study is shown in Figure 2. The turntable, shown in Figure 3, was purchased from Ernest F. Fullam, Incorporated. A petri dish was set at a pre-set angle, α, and rotated, which resulted in particle tumbling due to gravity. The rotation speed was controlled by an external

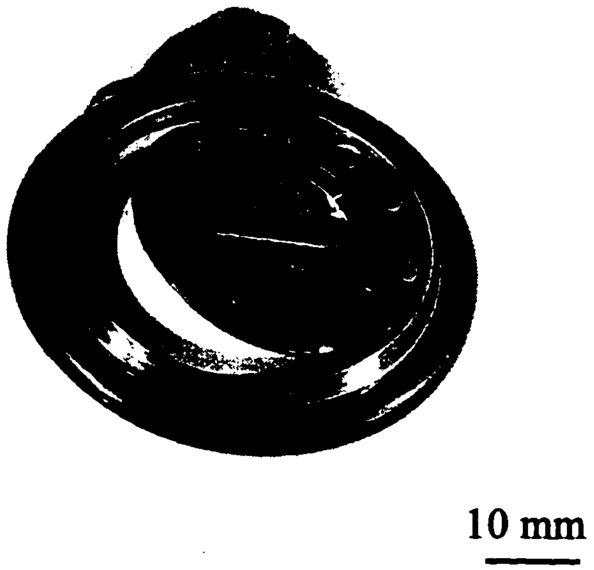

Fig. 1-The Auto-Soft closes very quickly at the beginning of pumping and opens gradually during roughing.

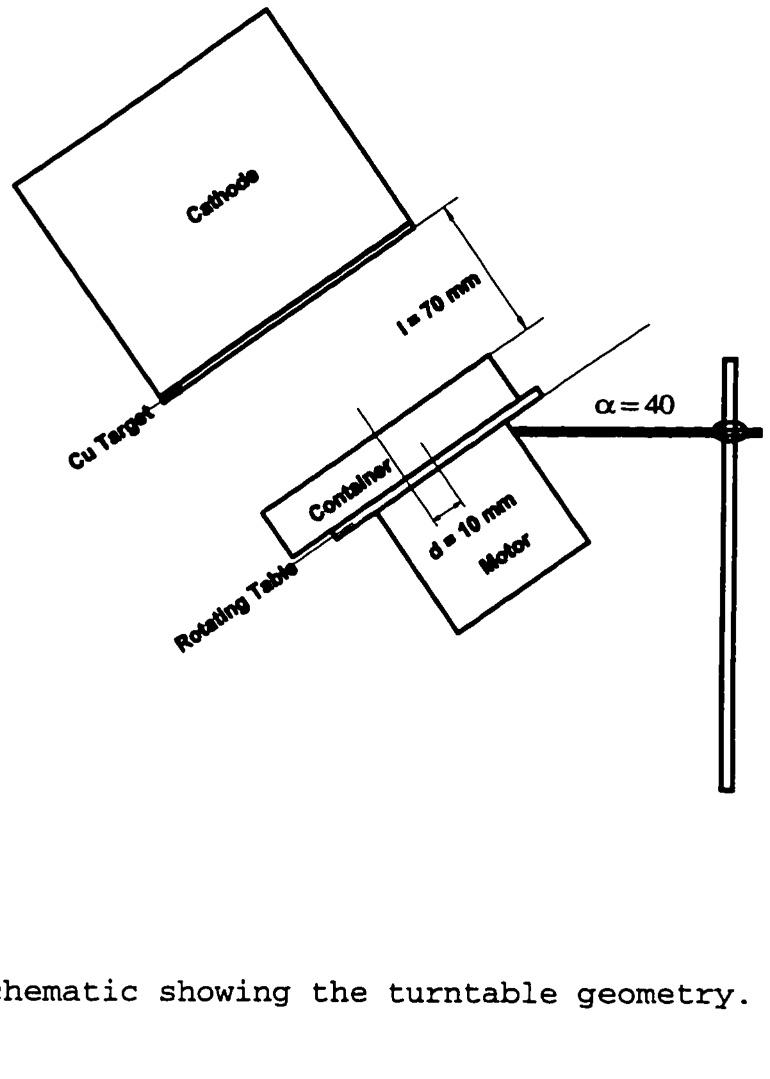

Fig.2-Schematic showing the turntable geometry.

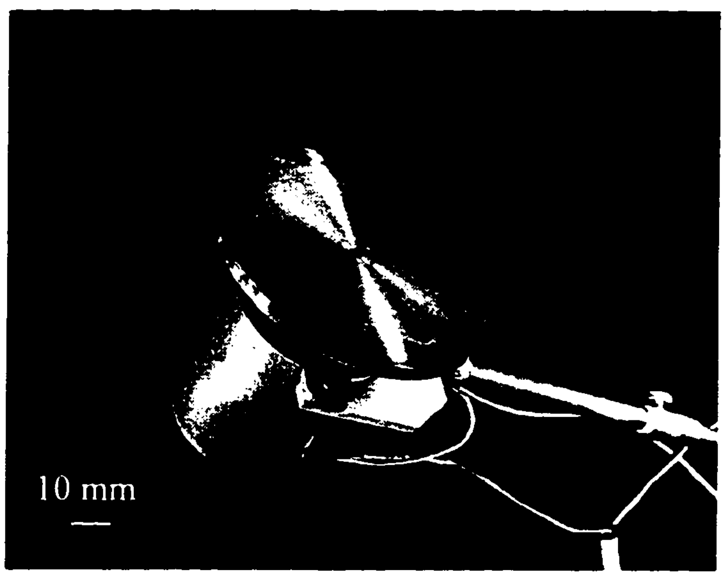

Fig. 3-The rotor provides 360° rotation at a pre-set angle.

rheostat, and the tilt angle was set when loading the powder. The tumbling of the particles depends on the smoothness of the container surface, the speed of rotation, the distance between the center of the container and the center of the rotating table, d, (Figure 3), as well as particle shape, size, and density. The increasingly attractive forces between coated particles and between coated particles and the container surface eventually stop the tumbling, which precludes the application of a thick coating. Further investigation is necessary to reduce or eliminate this limitation.

The silicon carbide particles were 120 grit commercial grinding media obtained from Leco Corporation; the density of SiC is 3.17 g/cm^3. The as-received SiC particle size ranged from 35 µm to 170 µm, with a mean size of 142 µm. The as-received particles were treated with stirred hydrofluoric acid (HF) for 46 hours, rinsed in distilled water, and dried; these particles will be referred to as "HF-treated".

The SiC particles, before and after sputter coating, were characterized by x-ray diffraction, scanning electron microscopy (SEM), and energy dispersive spectroscopy (SEM/EDS). The Cu-based composites were fabricated by sintering, which entails powder mixing, cold compacting, and sintering. The composite powders were produced by blending 9 vol.% of 142 µm SiC particles with copper powder. The SiC particles were either as-received, as-received with Cu coating, or HF-treated with Cu coating. After compacting in a standard powder tensile test specimen die, the specimens were sintered at 995 °C ± 3° C for 1 hour under a high vacuum (between 10^{-2} and 10^{-4} Pa). Tensile tests were then carried out using a servo-hydraulic testing machine and an initial strain rate of 2.67×10^{-4}/s.

RESULTS AND DISCUSSION

Uncoated SiC Powders

The surface of the uncoated SiC particles has a large number of spots, as large as 2 µm, in the secondary electron micrograph (Figure 4). EDS analysis indicates that there is oxygen in these areas in addition to Si; oxygen was not detected in areas away from these spots. Based on this observation and free energy considerations, these small aspersions on the SiC surfaces are likely silicon oxide. The size of these oxide particles is less than the emission volume for characteristic x-rays, which precludes an accurate analysis.

SiC particles were treated in HF based upon the assumption that the surface particles were silica and, therefore, soluble in HF. After cleaning, the surfaces were clean and smooth (Figure 5) and had only a few large spots (approximately 2 µm). There is a silicon peak in the EDS spectra, but no detectable oxygen on these large spots. It is likely that the silica particles dissolved, and that the large particles found on the SiC surfaces after cleaning are organic contaminants. It is also possible that the largest of the silica particles did not have

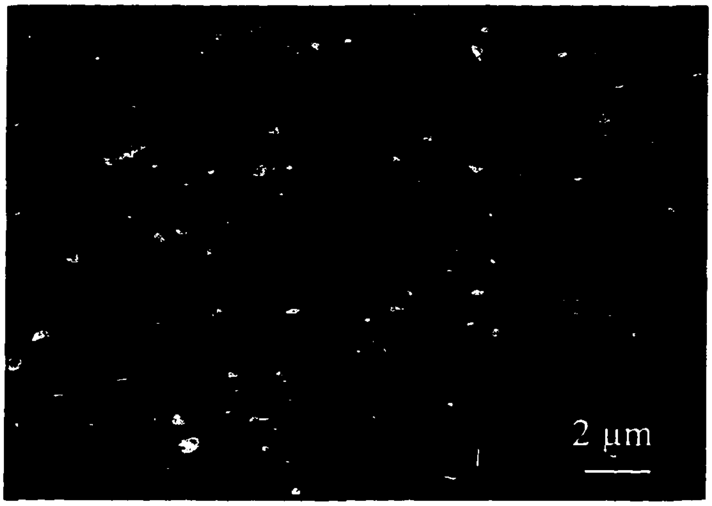

Fig. 4-Secondary electron micrograph showing the surface of as-received SiC particles.

Fig. 5-Secondary electron micrograph showing the surface of HF-treated SiC particles.

sufficient time to dissolve, although the absence of oxygen in the spectra makes this less likely.

Coated SiC Particles

The as-received and coated SiC particles were examined using x-ray diffraction to determine if a thin coating could be detected with x-ray diffraction and, if so, to determine the crystal structure of the copper coating. Although the predominance of the peaks in the coated specimen were from SiC, very low intensity Cu peaks, consistent with a face-centered cubic crystal structure, were present. The small intensity of the Cu peaks was due to the very thin coating on the particles.

The copper coating is apparently fairly uniform over the surface of both the as-received and HF-treated SiC particles based upon EDS analysis of ten different areas. A typical micrograph from the surface of as-received, Cu-coated SiC particles is shown in Figure 6, which is similar to the surface of as-received SiC particles (Figure 4). However, the intensity of the Cu characteristic x-rays is higher in the regions of the silica aspersions. This result is likely due to the greater surface area of these regions. (Since the silica particles are smaller than the emission volume, their entire surface is excited, which gives an apparent increase in the Cu intensity.)

Fracture Observations

The fracture surfaces of copper matrix composites reinforced with as-received SiC; as-received, Cu-coated SiC; and

Fig. 6-Secondary electron micrograph showing the surface of as-received SiC after copper coating.

HF-treated, Cu-coated SiC particles all exhibited large amounts of particle debonding, which is indicative of a weak interface. In all three cases, there are two distinct features on the surface of the SiC particles (the darkest region), which appear as bright spherical particles and dark irregular regions in a secondary electron image. Figure 7 is a micrograph of the particle surface of as-received SiC after coating and sintering. These spherical particles are found to be rich in Cu, O, and Si and are located on the top of the dark phases. The darker regions are rich in Si and O, which is likely silica, with a very small amount of copper. Some of spherical particles are very rich in Cu with small amounts of oxygen and silicon, which suggests that copper tends to separate from silica, forms spherical particles to reduce the surface energy, and subsequently leaves silica behind. The small amount of oxygen on the spherical particles is likely associated with either copper or silicon. In the darkest regions, there is silicon and very little copper, but no detectable oxygen.

The difference in the particle surfaces of the uncoated and copper-coated SiC particles lies in the amount of spherical particles; a large amount of spherical particles was found only in specimens with copper-coated SiC particles. Since the spherical particles result from the separation of physically bonded copper and SiO_2 or SiC during sintering, there is no reason to expect these spherical particles in the case of as-

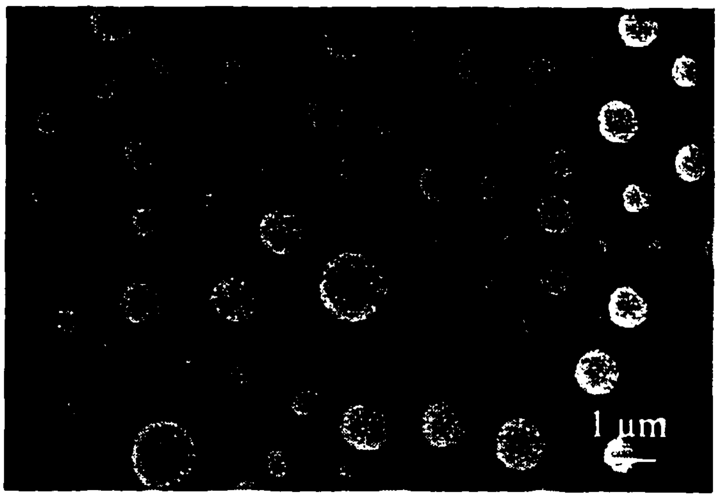

Fig. 7-Secondary electron micrograph showing the surface of as-received SiC after copper coating and after composite fabrication.

received SiC particles. The particle surface of two copper-coated SiC particles (as-received and HF treated) differs in the amount of the darker phase; a lesser amount of dark phases is found in HF treated SiC due to the less initial SiO_2.

The experimental results show that the copper coating on SiC particles did not improve the interfacial bonding in this composite material. This result may be due to insufficient coating thickness, a weak bond between the coating and SiC, or inherently poor bond strength between Cu and SiC under these processing conditions.

SUMMARY

A technique for uniformly sputter coating ceramic reinforcement particles was developed. This technique is very effective for relatively large ceramic particles since the particles tumble well and is applicable to either large or dense particles. If the particles can tumble and particle contamination of the vacuum system can be eliminated, this technique is also suitable for small and light particles. Although the copper coating did not significantly improve the interfacial bonding in these copper-matrix composites, the results suggest that this coating process is applicable to other particulate reinforced composite systems where interfacial chemistry may play a more critical role.

ACKNOWLEDGMENT

The support of the Alabama NSF-EPSCoR Composites Program is gratefully acknowledged.

REFERENCES

1. W.H. Hunt, Jr.: *Interfaces in Metal-Matrix Composites,* A. K. Dhingra and S. G. Fishman, eds., Metallurgical Society of AIME, 1986, pp. 3-25.

2. A.P. Majidi, J. Yang, and T. Chou: *Interfaces in Metal-Matrix Composites*, A. K. Dhingra and S. G. Fishman, eds., Metallurgical Society of AIME, 1986, pp. 27-44.

3. K.C. Russell, J. A. Cornie, and S-Y. Oh: *Interfaces in Metal-Matrix Composites*, A. K. Dhingra and S. G. Fishman, eds., Metallurgical Society of AIME, 1986, pp. 61-91.

4 J.F. O'Hanlon: *J. Vac. Sci. Technol.*, 1987, A5(4), pp. 2067-72.

SUMMARY

(1) A method was developed to quantify particle cracking behavior as a function of local strain in the sample interior rather than the exterior. The effect of particle size and matrix properties on particle cracking behavior during deformation in Al- and Cu-based metal-matrix composites (MMCs) was quantitatively measured.

(2) The two measured fracture features, S_V and F_{No}, were found to be approximately linear as a function of local strain.

(3) The slope of S_V was not significantly affected by particle size, whereas the F_{No} value was. The composite materials reinforced with large particles exhibited a high percentage of cracked particle.

(4) The slopes of S_V and F_{No} were strongly dependent upon the matrix yield strength. The higher the matrix yield strength, the higher the slopes of S_V and F_{No}, which fit into the same trend for both aluminum and copper matrix systems.

(5) Particle cracking occurs during elastic deformation. The matrix Young's modulus was found to affect the particle cracking behavior. For a given stress, fewer particles crack

in composites with higher matrix Young's modulus. This effect may be critical in the case of low plastic deformation.

(6) Multiple cracks in a single particle were observed more frequently in composites reinforced with large particles. The probability of a particle cracking a second time was less than the probability of it cracking the first time. This relationship was affected by both matrix strength and particle size.

(7) The results of this study indicate that particle cracking is controlled by both strain and stress.

(8) A technique for uniformly sputter coating ceramic reinforcement particles was developed, which is very effective for relatively large ceramic particles. This technique is also applicable to small and light particles if (1) the particle can tumble well and (2) particle contamination of the vacuum system can be eliminated.

(9) Although the copper coating did not significantly improve the interfacial bonding in these copper matrix composites, the success in coating ceramic particles suggests that this approach may be useful in other composite systems where interfacial chemistry may play a more critical role.

REFERENCES

1. C.Y. Barlow: *In Proc. 12th Risϕ Int. Symp. on Metal Matrix Composites - Processing, Microstructure and Properties*, N. Hansen, D. Juul Jensen, T. Leffers, H. Lilholt, T. Lorentzen, A.S. Pedersen, O.B. Pedersen, and B. Ralph, eds., Risϕ National Laboratory, Denmark, 1991, pp. 1-15.

2. D.J. Lloyd: *International Materials Reviews*, 1994, vol. 39, pp. 1-23.

3. D.J. Lloyd: *Acta Metall. Mater.*, 1991, vol. 39, pp. 59-71.

4. J. Llorca, A. Martin, J. Ruiz, and M. Elices: *Metall. Trans. A*, 1993, vol. 24A, pp. 1575-88.

5. P.M. Singh and J. J. Lewandowski: *Metall. Trans. A*, 1993, vol. 24A, pp. 2531-43.

6. Jian Ku Shang, Weikang Yu, and R.O. Ritchie: *Mater. Sci. Eng.*, 1988, vol. A102, pp. 181-92.

7. Y. Flom and R.J. Arsenault: *6th International Conf. on Composite Materials/Second European Conf. on Composite Materials (ICCM VI/ECCM2)*, F.L. Matthews, N.R. Buskell, J.M. Hodgkinson, and J. Morton, eds., Elsevier Applied Science, London and New York, 1987, vol.2, pp. 2189-98.

8. B.J. Weng, S.T. Chang, and J.S. Shiau: *Scripta Metall.*, 1992, vol. 27, pp. 1127-32.

9. J.J. Lewandowski, D.S. Liu, and C. Liu: *Scripta Metall.*, 1991, vol. 25, pp. 21-26.

10. J. Yang, C. Cady, M.S. Hu, F. Zok, R. Mehrabian, and A.G. Evans: *Acta Metall.*, 1990, vol. 38, pp. 2613-19.

11. Y. Brechet, J.D. Embury, S. Tao, and L. Luo: *Acta Metall. Mater.*, 1991, vol. 39, pp. 1781-86.

12. M. Manoharan and J.J. Lewandowski: *Acta Metall.*, 1990, vol. 38, pp. 489-96.

13. J.J. Lewandowski, C. Liu, and W.H. Hunt, Jr.: *Mater. Sci. Eng.*, 1989, vol. A107, pp. 241-55.

14. C.P. You, A.W. Thompson, and I.M. Bernstein: *Scripta Metall.*, 1987, vol. 21, pp. 181-85.

15. Young-Hwan Kim, Sunghak Lee, and N.J. Kim: *Metall. Trans. A*, 1992, vol. 23A, pp. 2589-96.

16. Zhirui Wang and R.J. Zhang: *Metall. Trans. A*, 1991, vol. 22A, pp. 1585-93.

17. A.K. Vasudevan, O. Richmond, F. Zok, and J.D. Embary: *Mater. Sci. Eng.*, 1989, vol. A107, pp. 63-69.

18. D.S. Liu, M. Manoharan, and J.J. Lewandowski: *Metall. Trans. A*, 1989, vol. 20A, pp. 2409-17.

19. C.S. Lee, Y.H. Kim, T. Lim, and K.S. Han: *Scripta Metall.*, 1991, vol. 25, pp. 613-18.

20. D.L. Davidson: *Metall. Trans. A*, 1991, vol. 22A, pp. 113-23.

21. S.R. Nutt: in "*Interfaces in Metal Matrix Composites*," The Metallurgical Society of AIME, Metals Park, OH, 1986, pp. 157-67.

22. W.H. Hunt, Jr., J.R. Brockenbrough, and P.E. Magnusen: *Scripta Metall.*, 1991, vol. 25, pp. 15-20.

23. G.M. Janowski and B.J. Pletka: *Mater. Sci. Eng.*, 1990, vol. A129, pp. 65-76.

24. B. Wang, G.M. Janowski, and B.P. Patterson: *Metall. Trans. A*, 1995, vol. 26A, pp. 2457-67.

25. S.V. Kamat, J.P. Hirth, and R. Mehrabian: *Acta Metall. Mater.*, 1989, vol.37, pp. 2395-02.

26. F.H. Samuel and A.M. Samuel: *Metall. Trans.* A, 1994, vol. 25A, pp. 2247-63.

27. J. Llorca and P. Poza: *Mater. Sci. Eng.*, 1994, vol. A185, pp. 25-37.

28. M.J. Hadianfard, J. Healy, and Y.W. Mai: *J. Mater. Sci.*, 1994, vol. 29, pp. 2321-27.

29. P. Poza and J. Llorca: *Metall. Trans. A*, 1995, vol. 26A, pp. 3131-41.

30. R.W. Hertzberg: *Deformation and Fracture Mechanics of Engineering Materials*, 1st ed., John Wiley & Sons Inc., New York, NY, 1976, pp. 335-48.

31. R.D. Goolsby and L.K. Austin: *Advances in Fracture Research*, 1st ed., ICF-7 Conf. Proceedings, K. Salama, K. Raui-Chander, D.M.R. Taplin, and P. Rama-Rao, eds., Pergamon Press, Oxford, UK, 1989, vol. 4, pp. 2423-35.

32. P.K. Mirchandani: *Ph.D. Dissertation*, Michigan Technological University, 1987.

33. T.J. Downes and J.E. King: *In Proc. 12th Risφ Int. Symp. on Metal Matrix Composites - Processing, Microstructure and Properties*, N. Hansen, D. Juul Jensen, T. Leffers, H. Lilholt, T. Lorentzen, A.S. Pedersen, O.B. Pedersen, and B. Ralph, eds., Risφ National Laboratory, Denmark, 1991, pp. 305-10.

34. J. Llorca: *Journal DE Physique IV*, 1993, vol. 3 (11), pp. 1793-98.

35. D.S. Liu and J.J. Lewandowski: *Metall. Trans. A*, 1993, vol. 24A, pp. 609-15.

36. D.J. Lloyd: *In Proc. 12th Risφ Int. Symp. on Metal Matrix Composites - Processing, Microstructure and Properties*, N. Hansen, D. Juul Jensen, T. Leffers, H. Lilholt, T. Lorentzen, A.S. Pedersen, O.B. Pedersen, and B. Ralph, eds., Risφ National Laboratory, Denmark, 1991, pp. 81-99.

37. R.W. Davidge: *Mechanical Behavior of Ceramics*, Cambridge University Press, New York, NY, 1979, pp. 31-50.

38. J. Llorca: *Acta Metall. Mater.*, 1995, vol. 43, pp. 181-92.

39. J. Llorca, A. Needleman, and S. Suresh: *Acta Metall. Mater.*, 1991, vol. 39, pp. 2317-35.

40. P. Scarber Jr. and G.M. Janowski: *Proc. of Symp. on Modeling of Composites: Processing and Properties*, S.P. Chen and M.P. Anderson, eds., The Minerals. Metals & Materials Society, Warrendale, PA, 1996, pp. 57-75.

41. G. Bao: *Acta Metall. Mater.*, 1992, vol. 40, pp. 2547-55.

42. J.R. Brockenbrough and F.W. Zok: *Acta Metall. Mater.*, 1995, vol. 43, pp. 11-20.

43. S.F. Corbin and D.S. Wilkinson: *Acta Metall. Mater.*, 1994, vol. 42, pp. 1329-35.

44. S.F. Corbin and D.S. Wilkinson: *Acta Metall. Mater.*, 1994, vol. 42, pp. 1319-27.

45. Y. Zong and B. Derby: *Journal DE Physique IV*, 1993, vol. 3 (11), pp. 1861-66.

46. C.A. Lewis and P.J. Withers: *Acta Metall. Mater.*, 1995, vol. 43, pp. 3685-99.

47. P.M. Mummery and B. Derby: *J. Mater. Sci.*, 1994, vol. 29, pp. 5615-24.

48. ASM Metals Handbook, 10th Edition, 1990, vol. 2, *Properties and Selection: Nonferrous Alloys and Special-Purpose Materials*, pp. 67-68.

49. ASM Metals Handbook, 10th Edition, 1990, vol. 2, *Properties and Selection: Nonferrous Alloys and Special-Purpose Materials*, pp. 386-86.

50. P. Yih and D.D.L. Chung: *Processing and Fabrication of Advanced Materials III*, V.S. Srivatsan and J.J. Moore eds., The Minerals, Metals & Materials Society, 1994, pp. 29-33.

51. P. Yih and D.D.L. Chung: *Advanced Materials: Performance Trough Technology Insertion.* 1993, vol.38. I, pp. 134-37.

52. H. Sun, J.E. Orth, and H.G. Wheat: *JOM*, 1993, 45(9), pp. 36-41.

53. X. Zhang, M. Ying, and C. Wang: *Advances in Composite Materials*, P. Ramakrishnan ed., Bombay, India, 1990, pp. 323-27.

54. W.M. Zhong, G. L'esperance, and M. Suery: *Metall. Trans. A*, 1995, vol. 26A, pp. 2637-49.

55. W.M. Zhong, G. L'esperance, and M. Suery: *Metall. Trans. A*, 1995, vol. 26A, pp. 2625-35.

56. N. Wang, Z. Wang, and G.C. Weatherly: *Metall. Trans. A*, 1992, vol. 23A, pp. 1423-30.

57. ASM Metals Handbook, 10th Edition, 1990, vol. 2, *Alloy Phase Diagrams*, pp. 3.12.

58. I. Miller and J.E. Freund: *Probability and Statistics for Engineers*, 2nd ed., Prentice-Hall Inc., Englewood Cliffs, NJ, 1977, pp. 289-17.

59. A.G. Evans, J.W. Hutchinson, and R.M. McMeeking: *Scripta Metall.*, 1991, vol. 25, pp. 3-8.

GRADUATE SCHOOL
UNIVERSITY OF ALABAMA AT BIRMINGHAM
DISSERTATION APPROVAL FORM

Name of Candidate Bingjie Wang

Major Subject Materials Engineering

Title of Dissertation "An Experimental Study of Particle Cracking in Metal Matrix Composites".

Dissertation Committee:

Gregg Janowski, UAB, **Chairman**

Burton R. Patterson, UAB

J. M. Rigsbee, UAB

Robin Griffin, UAB

John Barnard, UA

Director of Graduate Program Burton R. Patterson

Dean, UAB Graduate School John L. Baker

Date April 18, 1996

PS-1428